UNIVERSIDAD DE LAS AMÉRICAS PUEBLA

School of Engineering

Department of Industrial, Mechanical and Logistics Engineering

Modelling of a Rotary Hammer with the implementation of a Dynamic Eliminator of Vibrations

Thesis that the Student Presents to Complete the Requirements of the UDLAP Honors Program

Roberto Sanz Camacho

ID: 150345

Bachelor's in Mechanical Engineering

Dr. Tadeusz Majewski

San Andrés Cholula, Puebla. **Fall 2018**

Signature Sheet

Thesis that the Student **Roberto Sanz Camacho ID: 150345** Presents to Complete the Requirements of the Honors Program

Thesis Director

_____

Dr. Tadeusz Majewski

Thesis President

_____

Dr. René Ledesma Alonso

Thesis Secretary

_____

Dr. Jorge Arturo Yescas Hernández

ACKNOWLEDGMENTS

El presente trabajo es muestra del esfuerzo y la dedicación puesta en mis estudios a lo largo de una de las mejores etapas de mi vida. Primero que nada, quiero agradecer a Dios por ser mi guía y darme la fortaleza para salir adelante en cada una de las dificultades y problemas de mi carrera.

También, quiero agradecer a mis padres por todo el apoyo que me han dado desde que soy pequeño y por haberme dado la oportunidad de estudiar en esta universidad. Papá, muchas gracias por enseñarme a ser quien soy y por ser mi ejemplo a seguir, gracias por enseñarme a ser una persona honesta y trabajadora y por dar tu máximo esfuerzo para que nosotros siempre tengamos lo mejor. Mamá, muchas gracias por estar ahí para mí las 24 horas del día y 7 días de la semana, gracias por ser mi doctora y atender todas mis preocupaciones. Carmen y Fer, gracias por estar siempre ahí para mí, compartir buenos momentos conmigo y hacerme sonreír. Saben que siempre estaré para ustedes y nunca les fallaré.

Abuelos, muchas gracias por todas las historias y experiencias contadas, por las sonrisas y el cariño que siempre me han mostrado, por mantener a nuestra familia siempre unida sin importar la situación, he aprendido mucho de ustedes. A mis tíos y tías, por siempre estar dispuestos a ayudarme. A mi novia María Fernanda, por aguantarme durante toda mi carrera y hacerme tan feliz durante todos estos años.

De igual forma quiero agradecer a mis profesores y a esta institución por todas las enseñanzas y por ser siempre receptivos a mis preguntas, que seguramente fueron muchas. Especialmente quiero agradecer a mi amigo el Dr. Tadeusz por compartirme sus conocimientos y su dedicación para sacar adelante este proyecto.

Finalmente, doy gracias a mis amigos tanto de la prepa como los que hice a lo largo del camino, por hacer que estos 4 años y medio fueran inolvidables. Gracias a Andrés, Jesús, Ricardo, Maus, Chapa, Gale, Belmont, Grecia, Quiroz, Sergio, Gabs, Chobo, Churro, Guru, Chucho, Miguel, Juan, Adolfo, Pau, Yayo y Xotla; por hacer de esta etapa un recuerdo que llevaré siempre conmigo. Muchas gracias a todos, no lo hubiera logrado sin ustedes.

“To give anything less than your best is to sacrifice the gift”

-Steve Prefontaine

CONTENTS

LIST OF FIGURES

LIST OF TABLES

ABSTRACT

The mathematical modelling of a Dynamic Eliminator of Vibrations is presented. This model is based on two drums that rotate in opposite directions with a speed equal to the excitation frequency of the system. These drums contain the same amount of free elements such as rollers or spheres that translate in a viscous environment and compensate the excitation forces with the action of their centrifugal force. Also, a rotary hammer working principle is modelled with a novel method for the mathematical implementation of the DEV to this system, to determine the possibility of vibrations damping. Several systems of equations are developed and solved numerically using different input parameters. Results of these simulations where vibrations reduction (of 99%) is illustrated, are presented throughout this work, starting from simpler models up to systems with several degrees of freedom.

CHAPTER I – Introduction

1.1 Context of the Research

Vibrations can exist in all the systems that are part of this planet. They are produced in a great variety of conditions that define their intensity, duration, and frequency. These conditions mainly depend on the characteristics of the system itself, the excitation source and the way the vibrations are produced. This means that while some bodies could experience stronger vibrations for a short amount of time, others could suffer imperceptible vibrations for longer periods of time.

In most of the cases, vibrations are an undesirable phenomenon that affects different systems. On the one hand, they can affect mechanical devices and structures, causing fatigue damage, components wear and noise. On the other hand, the human body is harmed by certain levels of vibration that can cause muscular and osteoarticular disorders. For that reason, design engineers have spent great efforts in developing systems that can reduce vibrations to an acceptable level.

One example of this situation is well described by the use of power tools in areas such as construction, woodworking, manufacturing, among others, which produce high levels of vibrations, directly affecting the user; even leading to permanent health issues.

Therefore, companies have developed specialized damping systems that absorb and try to eliminate vibrations produced by power tools, particularly, impact ones. Examples of these technologies have been developed by leading companies of this sector such as spring mechanisms, floating handles, different types of active and dynamic vibration absorbers, etc.

Hence, a Dynamic Eliminator of Vibrations is proposed in this work, based on the theory developed by Dr. Tadeusz Majewski and with the purpose of determining its grade of effectiveness in vibrations damping. This system is mathematically modelled and solved with Matlab software. Additionally, the working principle of a rotary hammer is also modelled with the purpose of evaluating the feasibility of the implementation of a DEV of this kind.

1.2 Research Questions

During the definition of the general scope for this work, some questions arose and were answered as one of the main objectives of this research.

I. Why is it so important to damp vibrations? Which are the main medical issues caused by the exposure to high levels of vibration?

II. How does a Dynamic Eliminator of Vibrations work?

III. What is the working principle of a rotary hammer? How could it be modelled mathematically?

IV. Is it possible to reduce vibrations produced by a rotary hammer with a Dynamic Eliminator of Vibrations? Under which conditions is it possible to accomplish?

1.3 Outline of the Document

This work intends to develop the mathematical model of a Dynamic Eliminator of Vibrations, as well as, explain the mechanics behind this system. In this thesis, the author should determine whether it is possible or not to reduce vibrations produced by a device such as a rotary hammer and under which circumstances this could be accomplished.

A rotary hammer has been chosen from a list of impact tools available for the research with the purpose of having a real life reference and application.

Hence, this thesis is structured in several chapters that include the work done through this entire project and the obtained results at each stage.

After setting the context in chapter I, a brief description of the most common power impact tools and their working principle is given in chapter II; along with the explanation of the vibrations effects on health and the existing damping systems and technologies for their reduction.

Then, the Dynamic Eliminator of Vibrations is presented in chapter III, starting with a simple model based on Lagrange Equations. Additionally, the mechanics of this system are also explained in this section. Afterwards, in chapter IV, the description of the rotary hammer chosen for this work is given. Some measurements of its vibrations production are presented, as well as, two different approaches of the mathematical modelling of this device. The first one is a kinetic model based on algebraic equations that describes the motion of the main components of this system. Then, a dynamic model is proposed based on differential equations with the objective of the further combination with the DEV equations developed in chapter III.

The implementation of the DEV to the rotary hammer is described in chapter V, being analyzed in one and two directions of motion. Finally, in chapter VI, a spring connection between the main body and the chisel, is added to approximate the model to the real complexity of the rotary hammer. This model is also analyzed with and without the implementation of the DEV. It is important to mention that theory, equations and graphical representation of models numerical solution in Matlab are combined throughout this work in an organized manner that helps the reader understand the aims of this project.

CHAPTER II – Power Tools

2.1 Introduction

As explained earlier, this work is going to be focused on the application of a Dynamic Eliminator of Vibrations on impact tools. Accordingly, this section starts with a brief description of this kind of tools and the medical issues that the exposure to these systems vibrations represent for the human body.

2.2 Power tools and their vibrations production

Tools are the means that allow man to do what he cannot do with his bare hands. A power tool is a device that is actuated by an external source or mechanism, such as internal combustion engines, electric motors, and compressed air; that allows the user to perform tasks that he cannot easily do by himself. In particular, the AC motor represented a breaking point for the evolution of power tools.

Tools can be classified in portable or hand tools (such as rotary hammer, drills, impact wrench, etc.) and stationary power tools (e.g. bandsaw, lathe, disc sander, etc.). The main advantage of hand tools is their mobility, whereas stationary tools can provide more precision. A vast percentage of power tools transmit vibrations to the user through the hand-arm system, which could have repercussion on his health (Ideara, 2014). These effects will be discussed later.

Sectors of higher incidence of the usage of this type of tools include construction, metal-mechanical, woodworking, automotive, and agricultural. For construction, there are different types of tools from hand devices to big machines powered by combustion engines. In this sector, pneumatic tools are also commonly used. The main tools used in construction

include jackhammer, rotary hammer drill, impact wrench, asphalt cutter, paving roller, compactor, etc.

In the case of metal-mechanical area, there are stationary tools such as lathe, miter saw and mill for metal machining and portable ones like disc cutter, drill, and grinder. For woodworking, the most common power tools are polisher, disc saw, drill, and sander. For the automotive sector, impact wrenches represent a very useful tool for changing lug nuts and bolts. In agriculture, small combustion engines devices are used for the mechanization of the processes. Some examples are lawn mower, brush cutter and motor hoe, among others (Ideara, 2014).

A brief description of some of these tools is given in Table 1 along with its levels of continuous vibration (average acceleration of vibrations).

Power tool	Description	Level of continuous vibrations [m/s^2]
Jackhammer 	Pneumatic hammer for breaking rocks, concrete and pavement. They produce high amplitude vibrations with low frequencies.	20 - 30
Jumping jack compactor 	Compacting machine for gravel powered by combustion engine that generate vibrations with mechanical transmission elements.	10 - 20
Miter saw 	Electrical disc saw for metal cutting that generate low amplitude vibrations associated to the rotational speed of the disc.	2.5 - 5

Chainsaw 	Portable, mechanical saw powered by a combustion engine.	5 - 12
Brush cutter 	Agricultural tool used to trim grass, weeds and small trees in areas not accessible by a lawn mower. Powered by electrical motor or combustion engine.	2 - 23
Grinder/disc saw 	Electrical hand tool for different usages such as cutting and grinding depending on the type of disc mounted.	1 - 15
Hammer drill 	Drill with hammering action that has two discs or gears that impact each other transmitting impacts to the drill bit.	6 – 35
Rotary hammer 	Powerful electric tool that pounds the drill bit in and out while rotating with a piston-crankshaft mechanism.	5 – 24

Table 1. Typical ranges of vibration for hand power tools (Ideara, 2014)

2.3 Impact tools and their working principles

Particular attention is put to impact tools in this work. These tools include the impact wrench, the rotary hammer, the hammer drill, the jackhammer, among others. The working principle of each of these tools is described in this section, because of the special interest of this research on impacts and vibrations production, and the effects they can produce on human health.

2.3.1 Impact wrench

The impact wrench is a tool that provides a high amount of torque and allows bolts installation and removal at very high speeds. The torque application is not constant, but intermittent. Its working principle could be understood as a common wrench used to loosen a screw or bolt, being hit by a hammer and making it turn gradually. When the impact wrench is energized, an internal hammer strikes an anvil that is connected to a chuck mandrel and the socket on the operating end of the tool. This commonly happens 2 times per rotation. The hammer goes back and forth with a spring. This torque is transmitted to the chuck and that rotation energy is used for loosen or tighten a nut, screw or bolt. This mechanism allows the hammer to spin freely before and after impacting the anvil (Dahl, 2016). Internal parts of an impact wrench and an example of its use can be seen in Figure 1 and Figure 2, respectively.

The hammering effect is the characteristic that distinguishes this tool from conventional drills, and allows the user to imprint a higher force than that generated with a common wrench or ratchet. Additionally, this effect also helps to remove rust on the nut or bolt that could make its extraction difficult. The power source of an impact gun can be electricity,

compressed air and even lithium batteries. These tools can provide torque from 100 to 700 lb·ft (from 120 N·m to 850 N·m) depending on the model with a breakaway point that represents a security measure for applications that require excessive amount of torque; in this case the hammering mechanism will be disengaged for preventing tool damage (Dahl, 2016).

Figure 1. Impact wrench (Dahl, 2016)

Figure 2. Impact wrench use (Dewalt, 2018)

2.3.2 Jack hammer

A Jackhammer is a powerful tool, pneumatically or electro-mechanically driven, used in construction sites for breaking rock or pavement. There also exists a larger version that is hydraulically powered. A jackhammer operates by moving an internal hammer up and down transmitting the impacts to the chisel, producing 25 to 30 impacts per second (Woodford, 2017).

As it is explained in Figure 3, the pneumatic jackhammer working principle is based on the movement of a reciprocating valve that allows the sequential pass of compressed air in two different directions, making a piston to go up and down, striking the drill bit repeatedly into the ground. The valve's main function is to regulate the air command and send it on either one side or the other of the plunger or piston. Another basic component is the cylinder in

which the piston moves. This last component hits the head of the tool located at the lower end of the hammer which transmits the impact to the ground, breaking it. The source of power is an independent compressor, able to supply a volume of compressed air suitable to the tool (Woodford, 2017)

The hydraulic version works with a (hydraulic) fluid instead of compressed air, at higher pressures. This device is usually larger and is mounted on an excavator for operation. Figure 4, shows an example of the use of a pneumatic jackhammer.

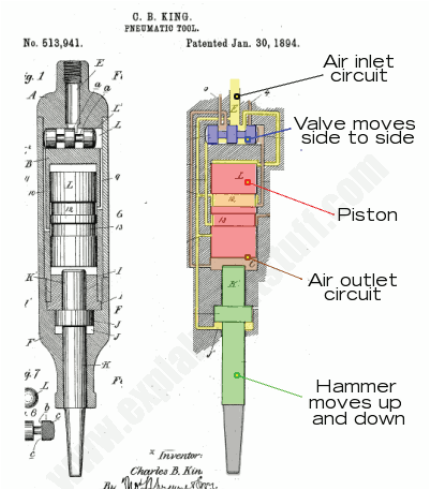

Figure 3. Jackhammer working principle (Woodford, 2017)

Figure 4. Jackhammer use (2017)

2.3.3 Hammer drill

A hammer drill is an electrical power tool used for hard surfaces drilling due to its hammering action. This action can be understood as hitting the back of the drill with a hammer. This mechanism allows it to break a surface more quickly and with less effort. Its hammering mechanism is based on 2 splined discs or gears that rotate while contacting each other. When this happens, the impacts and vibration waves are transmitted to the drill

bit and provide the hammering action (Yagid, 2009). This principle is illustrated in Figure 6 along with an example of this tool shown in Figure 5.

A hammer drill normally has two operation modes. The first mode is normal drilling and the second mode adds the hammering action to the former function. When enabling the hammer mode, a spring forces the two ratcheting disks together. When the hammer drill is working, one of the disks rotates against the other, which creates the impact waves that are sent to the drill bit. It is important to mention, that one disk stays steady during the work and the other one rotates attached to the main shaft (2009).

Figure 5. Hammer drill (Bosch, 2018)

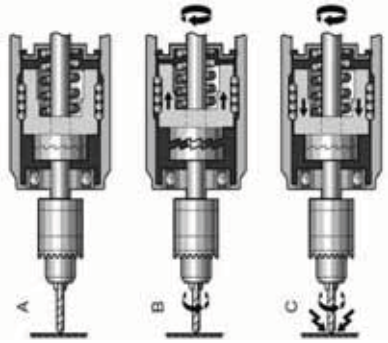

Figure 6. Hammer drill working principle (Family Handyman, 2018)

2.3.4 Rotary hammer

Finally, a rotary hammer is a power tool used for harder works than the hammer drill. In this case, the hammering action is achieved by the motion of a reciprocating piston that compresses the air that is in front of it, provoking powerful impacts that are transmitted directly to the drill bit. This tool has also two operation modes, hammer-drilling and hammer-only without rotation. This tool helps the user to do the same jobs as a hammer drill or a common drill, but in less time, especially for drilling masonry (Griffin, 2018)

The piston goes back and forth in the cylinder at frequencies around 33 Hz. The reciprocating piston sets the ram in motion and the ram hits the striker. The shockwaves of the impacts travel from the striker to the chisel tip and provide the hammering action to the drilling. As it is seen on Figure 7, the piston is not in direct contact with the ram nor with the striker, because the energy of the impacts would be transmitted back to the motor, causing undesirable damage. It is important to mention that the shockwaves travel through the chisel at around 18 km/h, enough to shatter concrete (N.A., Family Handyman, 2018).

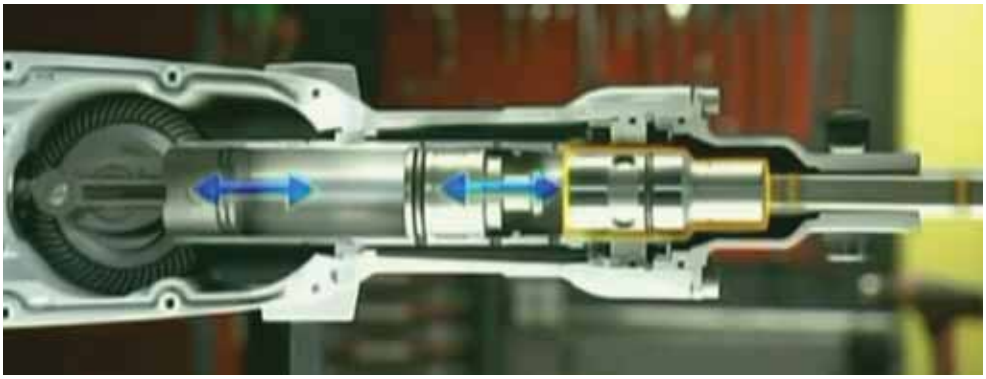

Figure 7. Rotary hammer working principle (Discovery, 2010)

As it would be described later in this manuscript, the experimental part of this section is based on a rotary hammer, for that reason explaining the working principle of this impact tool is important. The main characteristics of the specific model chosen for the experiments are described in section 4.2.1.

Figure 8. Rotary hammer components (Family Handyman, 2018)

Figure 9. Rotary hammer application (Family Handyman, 2018)

2.4 Vibrations effects on health

Vibration is understood as any oscillatory movement of a body with respect to an equilibrium position that is transmitted through a medium. When vibrations are intense, they could have harmful effects on human's health. The severity of the threat to health depends on the frequency of vibration, time of exposure, intensity of the phenomenon and its path into the human body (Hernández, 2012)

It is important to mention that vibrations are determined by their amplitude and frequency. The amplitude of vibrations is usually measured with its acceleration (m/s^2 or dB), whereas the frequency is measured in hertz (Hz). The acceleration decibel is defined by:

$$dB = 20\, log\, \frac{a}{a_0} \tag{2.1}$$

Where a_0 is a reference acceleration equal to 10^{-6} m/s^2 (ISO 1683).

Vibrations can affect the human organism in two ways, local (specific area of the body, i.e. the hands of a worker using a rotary hammer) and global (the whole body, i.e. a worker using a truck). For that reason, there are norms that define orthogonal axes for the measurement of vibrations as shown in Figure 10 and Figure 11. These norms are UNE-EN ISO 5349-1 (2002) and UNE-EN ISO 2631-1 (2008) (Hernández, 2012).

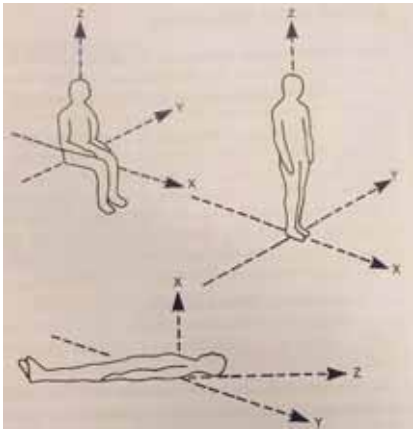

Figure 10. Coordinate system for measurement of complete-body vibrations (Majewski, 2017)

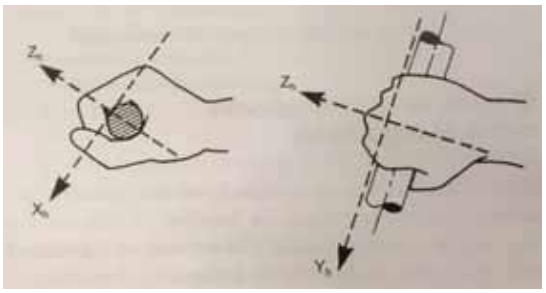

Figure 11. Coordinate system for measurement of hand-arm vibrations (Majewski, 2017)

Particularly, rotary and impact tools produce high levels of vibrations. Therefore, the constant use of this type of tools in sectors like industry, forestry and construction along with other activities where vibrations exposure is repetitively experienced, can cause medical issues like neck pain, headaches, dizziness, and other diseases (i.e. carpal tunnel syndrome and Raynaud phenomenon) (Castro, Palacios, García, & Moreno, 2014).

The grade of affection to the human body produced by vibrations is determined by external and internal factors. The external factors depend on the oscillatory movement itself, i.e. frequency and amplitude of vibrations, point of application, direction, and working method. Tool characteristics such as weight, equilibrium and supports are also considered an external factor. Internal factors are those related to the user itself, i.e. its physique, weight, working posture, health conditions, etc. (Hernández, 2012).

Vibrations produced by power tools and industrial equipment do not have a fixed frequency; they are a superposition of vibrations with different frequencies. As it was already mentioned the frequencies of interest for industrial safety vary from 1 to 1500 Hz. Within this range, there are different effects of vibrations produced at different frequencies. When the frequency is below 3 Hz, the human body moves as a rigid unit; at these frequencies the main adverse effect is dizziness. As the frequency of vibration increases the body parts tend to respond to the fluctuating forces in different ways. When the frequency

goes from 4 to 12 Hz, abdominal parts and shoulders start to vibrate amplifying the body's response to vibration. When the frequency reaches 20 Hz, the skull begins to vibrate affecting visibility. After going higher than 60 Hz, the eyeballs tend to resonate with the vibrating forces. The frequency of the power tools such as sanders, chainsaws and impact tools varies from 20 to 1000 Hz (Ideara, 2014). The mentioned effects can be understood as short term ones because they are an immediate response to the presence of vibrations and they disappear gradually when the source of vibrations is removed.

However, there are long term effects that are produced by the continuous usage of devices that transmit high levels of vibrations to the body, mainly through the hand-arm system; resulting in muscular, osteoarticular, neurological and vascular disorders (Hernández, 2012). The muscular disorders are those injuries that affect muscles, joints and tendons. These are associated with pain and discomfort, in addition to soreness and strength loss. Moreover, loss of mobility can also be a consequence. Also, tendinitis or Dupuytren contracture can occur. The Dupuytren contracture affects the palm connecting tissues that produce the retraction of one finger, commonly the fourth or fifth one (Hernández, 2012). Also, the long term exposure to complete body vibrations can affect the spinal column of the worker, causing a degenerative alteration of the vertebrae and intervertebral discs (Castro, Palacios, García, & Moreno, 2014).

Moreover, the osteoarticular disorders affect elbow articulation, shoulder, wrist and carpal bones. On the one hand, elbow arthrosis produced by the use of percussion tools is characterized by an intense pain suffered in the elbow area, that does not allow the worker to continue on duty for several weeks. On the other hand, Kienböck's disease is related to the carpal bones, associated with pain and loss of mobility and gripping strength. Disorders with osteoarticular origin are irreversible (Ideara, 2014).

The neurological disorders produced by vibratory tools include the loss of sensibility and numbness of hands and fingers. This could result in the worker's loss of ability to perform precision tasks. In the vascular category, particular attention is put to the Vibration-induced white finger syndrome (VWF), or Raynaud's phenomenon; caused by the continuous exposure of the hand-arm system to intense vibrations.

Raynaud's syndrome main characteristic is the intermittent whitening of one or more fingers produced by the affectation to the hand nerves and joints. Specifically, it affects the blood flow (vascular effect) and causes loss of touch sensation (neurological effect) in fingers (Ideara, 2014).

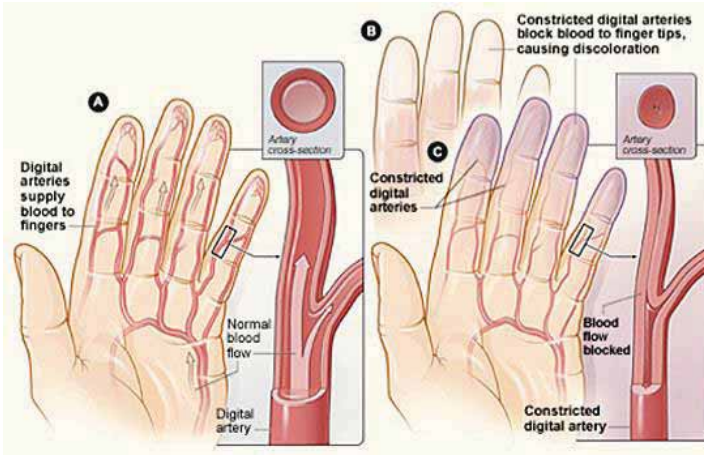

Figure 12. White finger syndrome (Ideara, 2014)

Figure 13. WFS effects (2014)

In addition to that, there are other general disorders that not only affect the hand-arm system. In these cases, vibrations are transmitted from hands to other parts of the body depending on the type of vibration, its frequency and mainly the posture of the person. The most common ailments of this kind are lumbar pain and hearing impairment. Lumbar pain can be caused by degenerative changes like displacement of lumbar discs. "With regarding to hearing, the human threshold can be displaced from 3 to 8 kHz if the weighted

acceleration exceeds an effective value of 1.2 m/s^2 with simultaneous exposure to noise, at a level equivalent to 80 dBA" (Ideara, 2014, p. 49).

2.5 Damping systems for impact tools

After the description of the health risks that the use of impact tools can produce, it is important to mention the different kinds of damping systems that have been developed by leading companies of this sector. Companies like Makita, Bosch and Dewalt have designed their own mechanisms that absorb, reduce or dissipate the vibrations produced by power tools in order to prevent user's health disorders. Some of these systems and their working principles will be described in this section.

2.5.1 Makita Antivibration Technology

Makita, the Japanese manufacturer of power tools, has developed an antivibrations system known as AVT. This technology is based on 3 different vibrations damping mechanisms which are the Active-Dynamic Vibration Absorber, a vibration absorbing housing and a damper spring; all of them illustrated in Figure 14.

Figure 14. Makita AVT (Makita UK, 2018)

Makita's Active-Dynamic Vibration absorber counteracts the shake produced by the piston and the striker. The movement of these components shifts air pressure between crank room and barrel room, which helps to push two counterweights towards the opposite side, cancelling out vibration (Makita UK, 2018). This mechanism is illustrated in Figure 15.

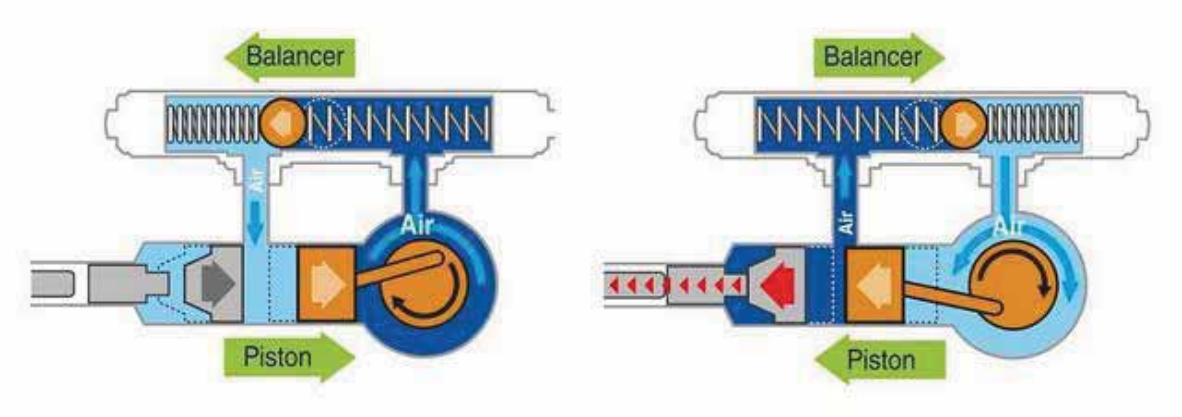

Figure 15. Active-Dynamic Vibration absorber (2018)

Vibration is also absorbed by the housing due to a complete separation of the main and side handles from the transmission section. Springs are added to the main handle for more effective vibration absorption. Besides that, the damper spring, which is represented in Figure 16, provides additional support for attenuating vibrations. Its working principle is based on providing a reaction force against the striking energy coming from the tip of the bit.

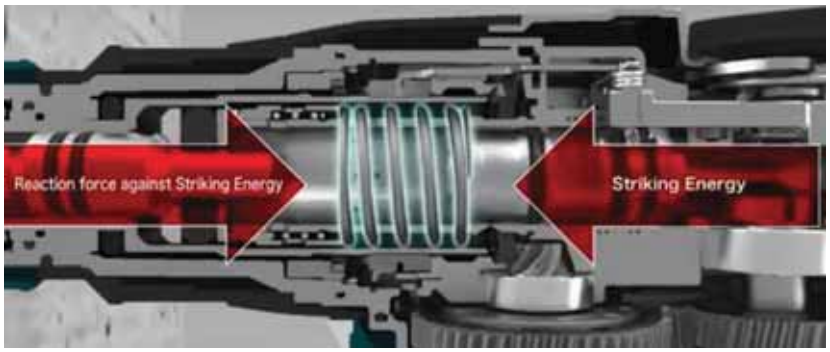

Figure 16. Damper spring mechanism (Makita, 2015)

2.5.2 Dewalt Antivibration Technology

Dewalt has two similar anti vibration systems in some of their tools. These include a floating grip and an active vibration control. The objective of the floating grip mechanism is to decouple the handle from the main unit. The handle is connected to a spring loaded on both ends, attached to a steel rod that is also connected to the unit. In this way, the complete handle is damped and horizontal longitudinal vibrations are reduced by 50% (Dewalt, 2018). The floating handle mechanism is illustrated in the following figures (17, 18).

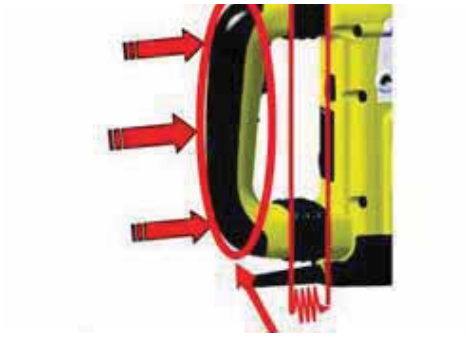

Figure 17. Floating handle (Dewalt, 2018)

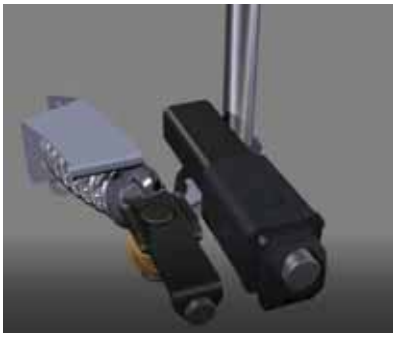

Figure 18. Floating handle components (2018)

The Active Vibration Control, seen in Figure 19 and Figure 20, is a system that is similar to the one of Makita. The spring loaded AVC mass balances the movement of the mechanism by translating in the opposite direction of vibrations, cancelling out the excitation force. This reduces vibration up to 30%.

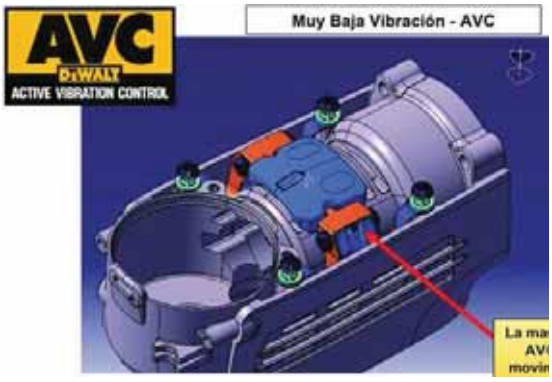

Figure 19. Dewalt Active Vibration Control (2018)

Figure 20. Dewalt AVC components (2018)

CHAPTER III – Dynamic Eliminator of Vibrations

3.1 Introduction

In this chapter, the theory behind a Dynamic Eliminator of Vibrations is explained. Also, a DEV model with two rotary drums with free elements inside is proposed and described. Governing equations of the system are established and they are solved with Matlab for certain input parameters.

3.2 Frahm's undamped dynamic vibration absorber

The DEV also called Dynamic Vibrations Absorber was first proposed by Hermann Frahm about a century ago. Frahm's undamped dynamic vibration absorber demonstrates that the magnitude of a system's response to an excitation can be reduced if an auxiliary mass, called vibration absorber, is attached to the main body and the natural frequency of this subsystem is equal or very similar to the frequency of excitation (Majewski, 2017)

In words of Jens T. Broch, a DEV is defined as that of "attaching to a vibrating structure a resonance system which counteracts the original vibrations. Ideally, such a system would completely eliminate the vibrations of a structure, in account of its own vibrations" (1972). Thus, the main mass and the absorber, seen in Figure 21, constitute a two-degree-of-freedom system with two natural frequencies. There are two main parameters that can be selected in the design of a DEV for tuning the performance of the absorber: mass and stiffness. M and k are selected with the purpose of making the natural frequency of the subsystem equal to the excitation frequency, that is to say: $\omega = \sqrt{\frac{k}{m}} = \Omega$ (Rao, 2011).

This principle is commonly used for machinery that operates at constant speed or for systems with a major frequency component because the DEV is tuned to a particular

frequency and it can only effectively work over a narrow range of frequencies. Examples of applications are reciprocating tools and constant-speed internal combustion engines. Also this type of vibration absorbers are found in high-voltage transmission lines in form of dumbbell-shaped devices that mitigate wind-induced vibrations (Rao, 2011).

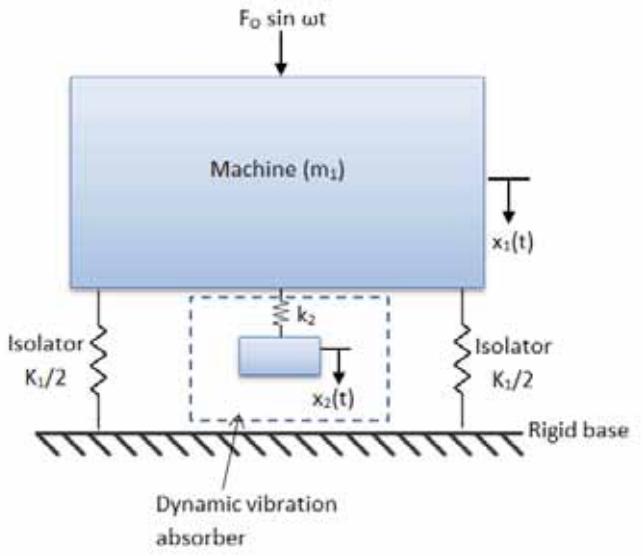

Figure 21. Undamped Dynamic Vibration Absorber (Rao, 2011)

3.3 Proposed Dynamic Eliminator of Vibrations

In this work, the proposed model for a DEV consists of two rotary drums with 2 free elements inside each of them. The free elements can either be rollers or spheres. The working principle of this model is based on the capability of the spheres to reorganize themselves inside the drums in such a way to generate a resultant centrifugal force that counterbalances the vibration forces transmitted through the main body (Majewski, 1987). Hence, the forces acting on this body are cancelled out and the vibrations dissipate. This is possible if the difference between the frequency of vibration of the main body and the angular velocity of the drums is not too big, making the free elements to rotate in unison with the vibrations of the base. This model is illustrated in Figure 22.

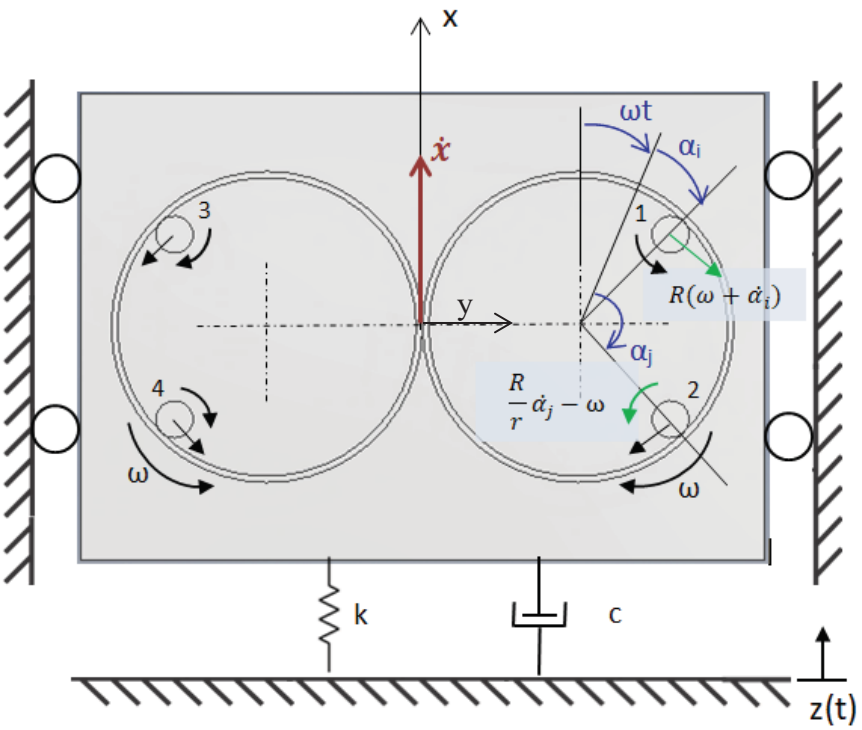

Figure 22. Proposed DEV

Where,
R, is the radius of the drum
r, is the radius of the sphere
k, is the stiffness of the spring
c, is the damping coefficient of the system
ω, is the frequency of excitation equal to the rotary speed of the drums
α_i, is the phase angle of i-th free element with respect to the vertical axis
$\dot{\alpha}_i$, is the relative angular velocity of the i-th free element with respect to the drum
$\dot{x}$, is the velocity of the main body in vertical direction
$z(t) = z_o cos\omega t$, is the external excitation of the system

As it can be seen in this initial model, the displacement of the main body is only allowed in the vertical direction, named as "x".

The model is solved using Lagrange equations; for this purpose, the resultant velocity of the free bodies is needed and it is found using its x and y components.

$$V_{xi} = \dot{x} - R(\omega + \dot{\alpha}_i)\sin(\omega t + \alpha_i)$$

$$V_{yi} = R(\omega + \dot{\alpha}_i)\cos(\omega t + \alpha_i)$$

$$V_i^2 = V_{xi}^2 + V_{yi}^2$$

Kinetic and potential energy are used as defined by Lagrange:

$$\frac{d}{dt}\left(\frac{\partial T}{\partial \dot{q}_i}\right) - \frac{\partial T}{\partial q_i} + \frac{\partial V}{\partial q_i} = Q_i \tag{3.1}$$

Where,
q_i, represents the generalized coordinates
$\dot{q}_i$, represents the generalized velocities
T, is the kinetic energy of the system
V, is the potential energy of the system
Q_i, represents generalized non-conservative forces

Kinetic energy:

$$T = \frac{1}{2}\left[M\ddot{x}^2 + m\sum_{i=1}^{n} V_i^2 + B\left(\frac{R}{r}\dot{\alpha}_1 - \omega\right)^2 + B\left(\omega - \frac{R}{r}\dot{\alpha}_2\right)^2\right] \tag{3.2}$$

Where,
M, is the mass of the main body.
m, is the mass of the spheres.
$B = \frac{2}{5}mr^2$, is the mass moment of inertia of the spheres.

Potential energy due to the spring:

$$V = \frac{1}{2}[k(x-z)^2] \tag{3.3}$$

Non-conservative forces due to damping are obtained from virtual work equation ($\delta W = F\delta x + T\delta\alpha = Q_X\delta x + Q_\alpha\delta\alpha$):

$$\delta W = -c(\dot{x} - \dot{z})\delta x - c_r m R^2 \dot{\alpha}\delta\alpha$$

Where c_r, is the coefficient of viscous resistance for the free elements.

Therefore,

$$Qx = -c(\dot{x} - \dot{z}) \tag{3.4}$$

$$Q\alpha_i = -c_r m R^2 \dot{\alpha}_i \tag{3.5}$$

The derivatives of the kinetic and potential energy are obtained and the results are substituted in the Lagrange equation:

$$(M+nm)\ddot{x} - mR\left[\sum_{i=1}^{n}(\omega+\dot{\alpha}_i)^2\cos(\omega t+\alpha_i) + \sum_{i=1}^{n}\ddot{\alpha}_i\sin(\omega t+\alpha_i)\right] + k(x-z)$$

$$= -c\left(\dot{x} - z(\dot{t})\right)$$

$\rightarrow (M+nm)\ddot{x} + c\dot{x} + kx$

$$= mR\left[\sum_{i=1}^{n}(\omega+\dot{\alpha}_i)^2\cos(\omega t+\alpha_i) + \sum_{i=1}^{n}\ddot{\alpha}_i\sin(\omega t+\alpha_i)\right] + cz(\dot{t}) + kz \tag{3.6}$$

Where n, is the number of free elements.

$$\left(mR^2 + \frac{BR^2}{r^2}\right)\ddot{\alpha}_i - mRsin(\omega t+\alpha_i)\ddot{x} = -c_r m R^2\dot{\alpha}_i \tag{3.7}$$

The system is then solved for $\ddot{x}$ and $\ddot{\alpha}$. $z(\dot{t})$ is substituted with $z(\dot{t}) = -cz_0\omega\sin(\omega t)$

$$\ddot{x} = \frac{1}{M+nm}\left\{mR\left[\sum_{i=1}^{n}(\omega+\dot{\alpha}_i)^2\cos(\omega t+\alpha_i) + \sum_{i=1}^{n}\ddot{\alpha}_i\sin(\omega t+\alpha_i)\right] - c\dot{x} - kx\right.$$
$$\left. + kz_0\cos(\omega t) - cz_0\omega\sin(\omega t)\right\} \tag{3.8}$$

$$\ddot{\alpha}_i = \frac{mR}{meq}[sin(\omega t+\alpha_i)\ddot{x} - c_r R\dot{\alpha}_i] \tag{3.9}$$

Where $meq = mR^2 + \frac{BR^2}{r^2} = mR^2 + \frac{2mr^2R^2}{5r^2} = \frac{7}{5}mR^2$, is the equivalent mass of the system.

A change of variable is done, where the term $\boldsymbol{\omega t}$ is substituted by the dimensionless time variable $\boldsymbol{\tau}$ for simplicity of the equations. The expressions obtained are:

$$x'' = \omega^2 \ddot{x} = \frac{1}{M+nm}\left\{mR\left[\sum_{i=1}^{n}(1+\alpha_i{}')^2\cos(\tau+\alpha_i) + \sum_{i=1}^{n}\alpha_i{}''\sin(\tau+\alpha_i)\right]\right.$$
$$\left. -\frac{cx'}{\omega} - \frac{kx}{\omega^2} + \frac{kz_0}{\omega^2}\cos(\tau) - \frac{cz_0\sin(\tau)}{\omega}\right\} \quad (3.10)$$

$$\alpha_i{}'' = \omega^2\ddot{\alpha} = \frac{mR}{meq}\left[sin(\tau+\alpha_i)x'' - \frac{c_r R\alpha_i{}'}{\omega}\right] \quad (3.11)$$

The expression for centrifugal force can be used to determine the optimal mass of the free elements because with this reaction the excitation force is cancelled out.

$$F_0 = \sqrt{(kz_0)^2 + (c\omega z_0)^2} = nmR\omega^2$$

$$m \cong \frac{\sqrt{(kz_0)^2 + (c\omega z_0)^2}}{nR\omega^2} \quad (3.12)$$

Additionally, the natural frequency of the system is determined by:

$$\omega_0 = \sqrt{\frac{k}{M+nm}} \quad (3.13)$$

3.3.1 Matlab application

The obtained system of equations for the model is solved using Matlab due to its complexity. Matlab function ode45 is used for this purpose. In order to utilize this function, the system needs to be transformed into a system of 1st order differential equations.

First, the independent degrees of freedom are listed as follows for a DEV model of 4 free elements, two inside each drum:

$x(1) = x$ $\quad$ $x(5) = \alpha_2$ $\quad$ $x(9) = \alpha_4$
$x(2) = x'$ $\quad$ $x(6) = \alpha_2{}'$ $\quad$ $x(10) = \alpha_4{}'$
$x(3) = \alpha_1$ $\quad$ $x(7) = \alpha_3$
$x(4) = \alpha_1{}'$ $\quad$ $x(8) = \alpha_3{}'$

Furthermore, the system of equations is defined as:

$$D(1) = \frac{dx}{d\tau} = x' = x(2)$$

$$D(2) = \frac{d^2x}{d\tau^2} = x'' = \frac{1}{M+nm}\left\{\begin{array}{c} mR\sum_{i=1}^{n}(1+\alpha_i{}')^2\cos(\tau+\alpha_i) - \frac{cx'}{\omega} - \frac{kx}{\omega^2} + \frac{kz_0}{\omega^2}\sin(\tau) \\ -\frac{cz_0\cos(\tau)}{\omega} \end{array}\right\}$$

$$D(3) = \frac{d\alpha_1}{d\tau} = \alpha_1{}' = x(4)$$

$$D(4) = \frac{d^2\alpha_1}{d\tau^2} = \alpha_1{}'' = \frac{mR}{meq}\left[sin(\tau+\alpha_1)x'' - \frac{c_rR\alpha_1{}'}{\omega}\right]$$

$$D(5) = \frac{d\alpha_2}{d\tau} = \alpha_2{}' = x(6)$$

$$D(6) = \frac{d^2\alpha_2}{d\tau^2} = \alpha_2{}'' = \frac{mR}{meq}\left[sin(\tau+\alpha_2)x'' - \frac{c_rR\alpha_2{}'}{\omega}\right]$$

$$D(7) = \frac{d\alpha_3}{d\tau} = \alpha_3{}' = x(8)$$

$$D(8) = \frac{d^2\alpha_3}{d\tau^2} = \alpha_3{}'' = \frac{mR}{meq}\left[sin(\tau+\alpha_3)x'' - \frac{c_rR\alpha_3{}'}{\omega}\right]$$

$$D(9) = \frac{d\alpha_4}{d\tau} = \alpha_4{}' = x(8)$$

$$D(10) = \frac{d^2\alpha_4}{d\tau^2} = \alpha_4{}'' = \frac{mR}{meq}\left[sin(\tau+\alpha_4)x'' - \frac{c_rR\alpha_4{}'}{\omega}\right]$$

As it can be seen, the terms referring to $\sum_{i=1}^{n}\alpha_i{}''\sin(\tau+\alpha_i)$ are neglected in the solution of the system due to their small impact in the equations. The full Matlab code can be found in the Appendix A.

Parameters are assigned to the constants of the system and the results are presented graphically with the help of Matlab.

- Experiment 3.1: 1 sphere per drum, same initial position for both spheres

Parameters:

n = 3 Degrees of Freedom, ω = 100 rad/s, M = 4 kg, m = 0.054 kg, R = 0.05 m, r = 0.01 mm, c = 20 kg/s, c_r=4 rad/s, k = 5000 N/m, z_0 = 0.01 m

With 2 spheres and external excitation defined as $z(t) = z_o cos\omega t$

$$m \cong \frac{\sqrt{(kz_0)^2 + (c\omega z_0)^2}}{nR\omega^2} = \frac{\sqrt{((5000)(0.01))^2 + ((20)(100)(0.01))^2}}{2(0.05)(100^2)} = 0.054\ kg$$

$$\omega = \sqrt{\frac{k}{M + nm}} = \sqrt{\frac{5000}{4 + 2(0.054)}} = 34.9\ \frac{rad}{s}$$

Initial conditions: $x = 0;\ x' = 0;\ \alpha_1 = 1\ rad;\ \dot{\alpha}_1 = 0;\ \alpha_2 = 1\ rad;\ \dot{\alpha}_2 = 0$

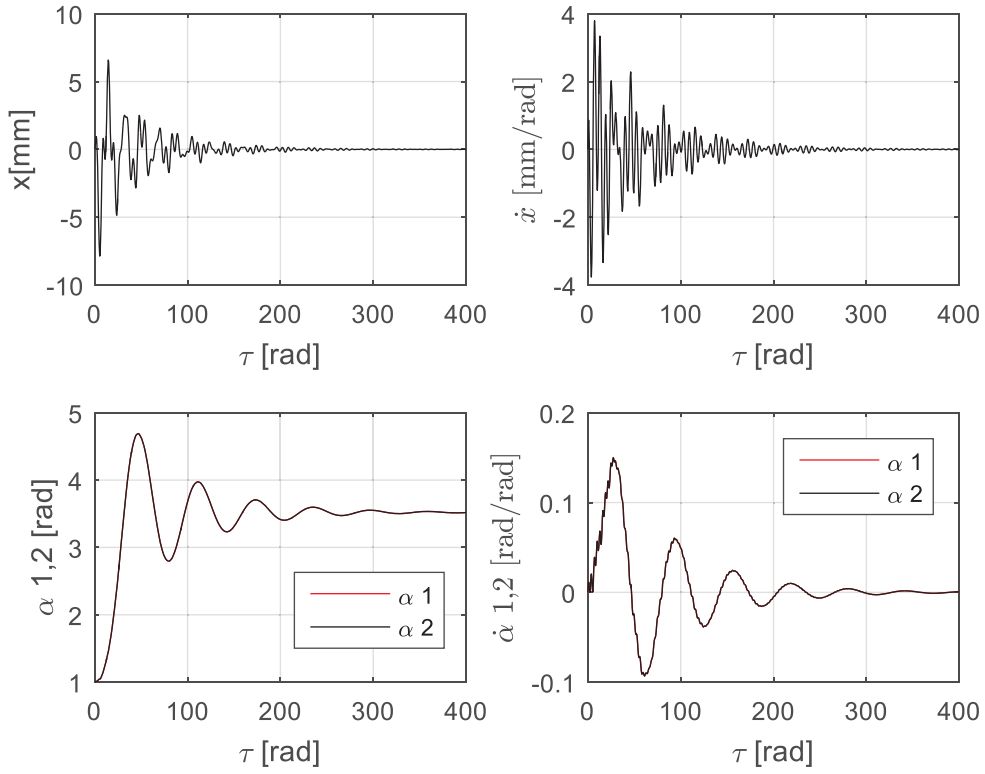

Figure 23. Experiment 1 results (same initial position)

The plots show that vibrations are damped from 7.2 mm of amplitude to 0.01 mm in 4 seconds. Reduction is around 720 times compared to the initial amplitude. Actually, in this

case, two curves are plotted for α and $\dot{\alpha}$ but, as they start from the same position, they follow the same path towards the equilibrium position.

The equilibrium positions found by the free elements are:

Final position of free elements			
Left drum		Right drum	
α_2	3.5179 rad 201.6°	α_1	3.5179 rad 201.6°

Table 2. Final position of free elements experiment 1

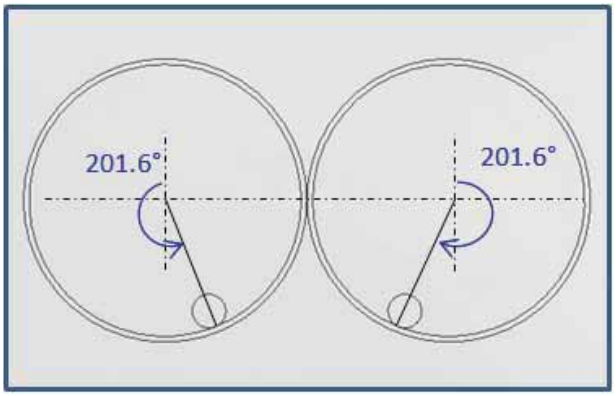

Figure 24. Experiment 1 equilibrium position

- Experiment 3.2: 1 sphere per drum, different initial position for both spheres

If the initial position of the balls is not the same ($\alpha_1 = 1\,rad;\ \alpha_2 = -1\,rad$), the system is still balanced; however, it is more difficult for the free elements to achieve the same final position which could make their location to be slightly asymmetric.

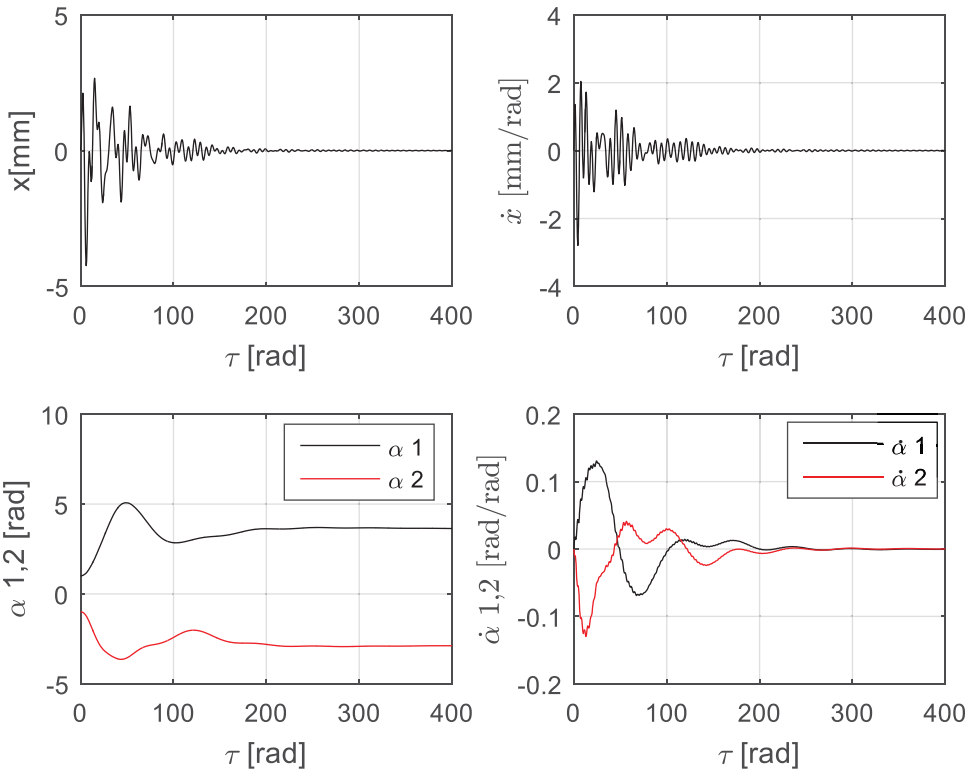

Figure 25. Experiment 2 results (different initial position)

The plots show that vibrations are damped from 3.1 mm of amplitude to 0.01 mm in 4 seconds. Reduction is around 300 times of initial amplitude of vibration.

The final positions of the free elements are:

Final position of free elements			
Left drum		Right drum	
α_2	-2.881 rad -165.07°	α_1	3.6404 rad 208.6°

Table 3. Final positions of free elements experiment 2

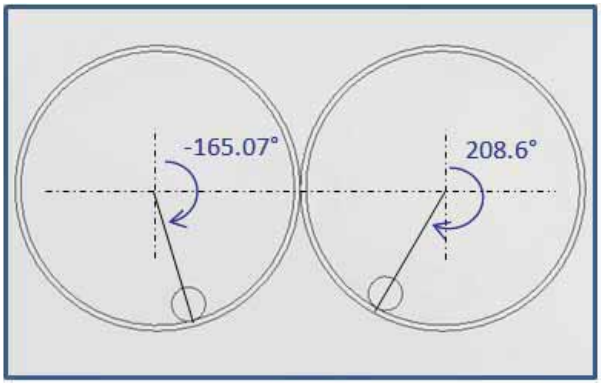

Figure 26. Experiment 2 equilibrium position

- Experiment 3.3: 1 sphere per drum, same initial position, $\omega < \omega_0$

It is important to mention that the Dynamic Eliminator of Vibrations only works effectively for frequencies that are over the natural frequency of the system. If the excitation frequency is smaller than the natural frequency of the system, the free elements of the DEV enlarge the vibrations amplitude instead of attenuating them.

An example of this phenomenon is showed in Figure 27, where the excitation frequency and angular velocity of the drums (same value) are below the natural frequency of the system and very close to resonance.

$$m = \frac{\sqrt{(kz_0)^2 + (c\omega z_0)^2}}{nR\omega^2} = \frac{\sqrt{((5000)(0.01))^2 + ((20)(30)(0.01))^2}}{2(0.05)(30^2)} = 0.56\ kg$$

$$\omega = \sqrt{\frac{k}{M + nm}} = \sqrt{\frac{5000}{4 + 2(0.56)}} = 31.25\ \frac{rad}{s}$$

Frequency of excitation $\omega = 30\frac{rad}{s}$

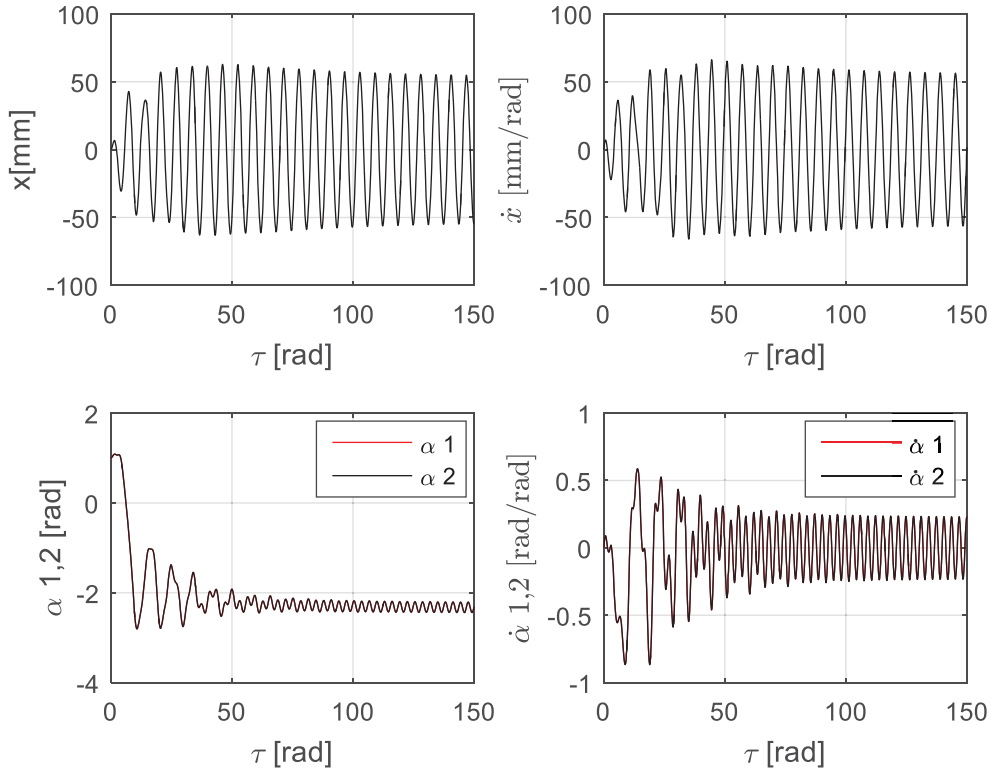

Figure 27. Experiment 3 results ($\omega < \omega_0$)

- Experiment 3.4: 2 spheres per drum, same initial position

With 4 spheres and external excitation defined as $z(t) = z_o cos\omega t$, vibrations are damped as it is seen on Figure 28.

Parameters:

n = 5 DOF, ω = 100 rad/s, M = 4 kg, m = 0.03 kg, R = 0.05 m, r = 0.006 mm, c = 20 kg/s, c_r=4 rad/s, k = 5000 N/m, z_0 = 0.01 m

$z(t) = z_o cos\omega t$

With 2 spheres and external excitation defined as $z(t) = z_o cos\omega t$

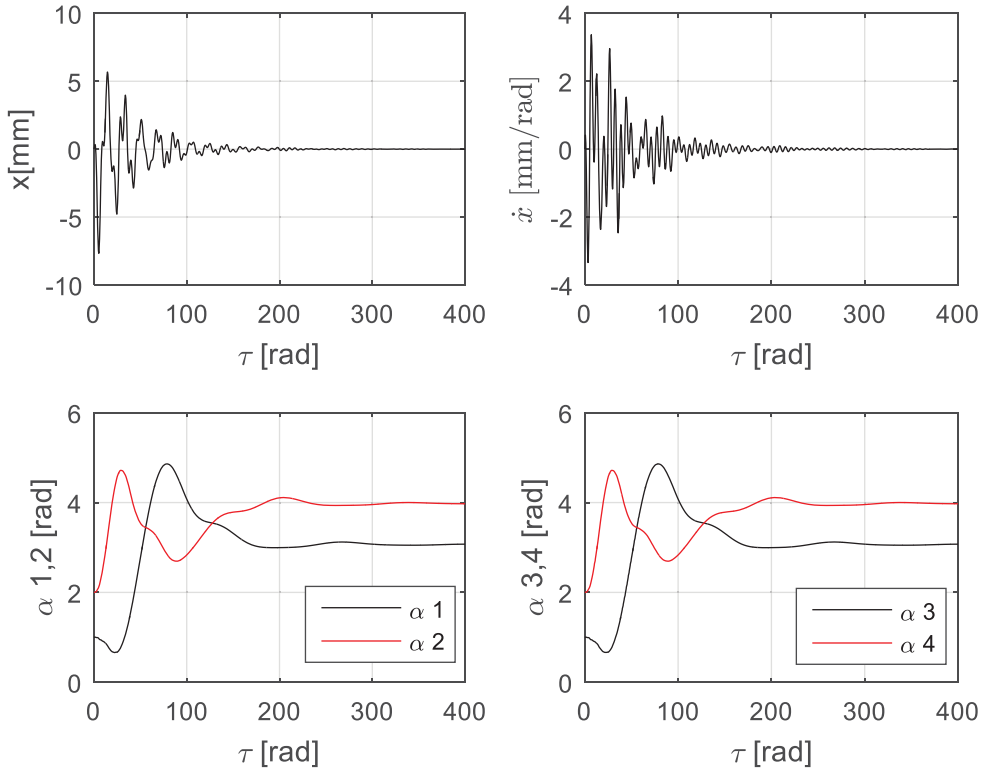

Figure 28. 4 spheres - DEV results

α_1 and α_3 are plotted in black and α_2 and α_4 in red. Final position of free elements is registered to confirm that an equilibrium position for damping vibrations in vertical direction is found.

Final position of free elements			
Left drum		Right drum	
α_3	3.0736 rad 176.104°	α_1	3.0736 rad 176.104°
α_4	3.9727 rad 227.619°	α_2	3.9727 rad 227.619°

Table 4. Final positions of free elements experiment 4

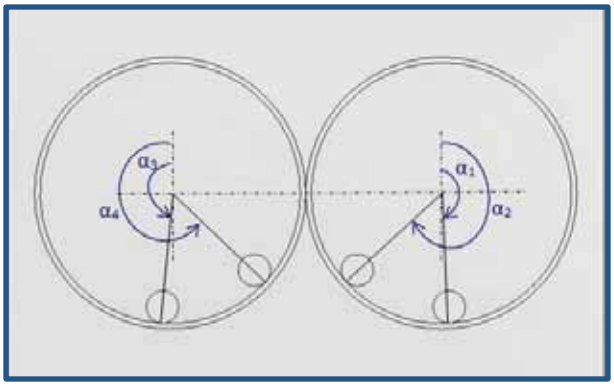

Figure 29. Experiment 4 equilibrium position

Amplitude of vibration is reduced from 6.6 mm to 0.001 mm. Reduction is more than 3000 times compared to the initial condition. This can be observed in Figure 30, where a zoom of the final part of Figure 28 (x vs τ) is presented.

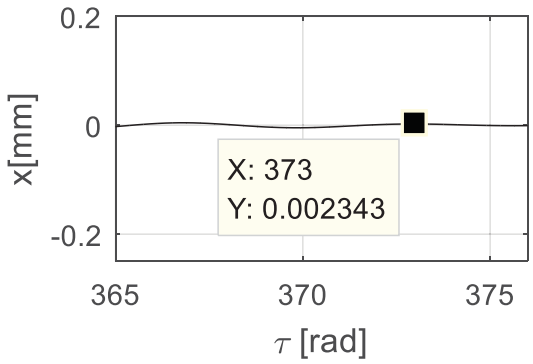

Figure 30. Vibrations amplitude reduction for 4-element DEV

If mass used is exactly 0.027 kg. The free elements position overlays because they try to balance the system in the same way it was done with just 2 elements.

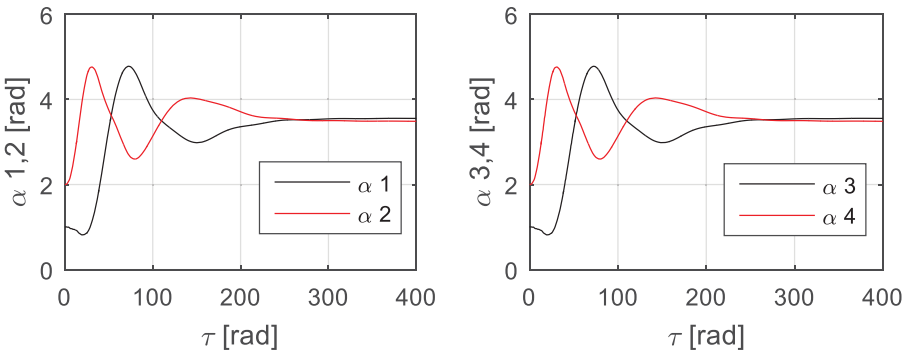

Figure 31. Ideal results - 4 elements

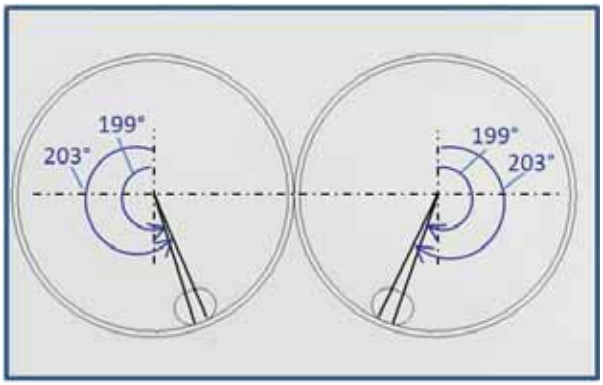

Figure 32. Ideal equilibrium position - 4 elements

3.4 How this DEV works? - Inertial Force

The diagrams and plots presented show how the free elements inside the drums eliminate the object vibrations. Their final positions are opposite to the excitation of the system and this allows them to counteract the produced vibrations.

This phenomenon happens as a result of the inertial force. Due to the action of this force, the free elements move synchronically with the excitation and at some point they found the equilibrium positions where the system stabilizes and the object stops vibrating. Therefore, the working principle of this model of Dynamic Eliminator of Vibrations is based on the existence and action of this inertial force.

The action of the inertial force and its impact in the equilibrium position of the free elements can be better explained with the following equations. This model is only developed in the vertical direction, just as illustrative principle of the DEV.

The governing equation for the main body in the system presented in Figure 22 has a general shape of:

$$M\ddot{x} + c\dot{x} + kx = F_0 cos\omega t + \sum_{j=1}^{n} mR(\omega + \alpha_j)^2 \cos(\omega t + \alpha_j) \quad (3.14)$$

Where F_0, is the excitation force.

As F_0 and the centrifugal force are harmonic, the system's response will also be harmonic. Therefore, vibrations can be defined as:

$$x \cong A_0 \cos(\omega t - \varphi) + \sum_{j=1}^{n} A_j \cos(\omega t + \alpha_j - \varphi) \quad (3.15)$$

$$\dot{x} \cong -A_0 \omega \sin(\omega t - \varphi) - \sum_{j=1}^{n} A_j \omega \sin(\omega t + \alpha_j - \varphi) \quad (3.16)$$

$$\ddot{x} \cong -A_0 \omega^2 \cos(\omega t - \varphi) - \sum_{j=1}^{n} A_j \omega^2 \cos(\omega t + \alpha_j - \varphi) \quad (3.17)$$

Besides that, as the inertial force is given by the free elements. The equation that describes the force produced by the free elements is:

$$m_b R\ddot{\alpha}_i = m_b \ddot{x} \sin(\omega t + \alpha_i) \quad (3.18)$$

Where, the viscous damping force is not considered in this case.

Then, knowing the expression for vibrations and the previous equation, inertial force can be determined as the average value of the elements force:

$$F_i = \frac{1}{T} \int_0^T m_b \ddot{x} \sin(\omega t + \alpha_i)\, dt \quad (3.19)$$

Where, T is the period of vibration.

Substituting the expression for $\ddot{x}$:

$$F_i = \frac{m_b}{T} \int_0^T \sin(\omega t + \alpha_i) \left[-A_0 \omega^2 \cos(\omega t - \varphi) - \sum_{j=1}^{n} A_j \omega^2 \cos(\omega t + \alpha_j - \varphi) \right] dt$$

With the identity $sinxcosy = \frac{1}{2}[\sin(x-y) + \sin(x+y)]$, the system is simplified for its solution.

$$F_i = \frac{m_b}{T}\int_0^T \left\{ \frac{-A_0\omega^2}{2}[\sin(\omega t + \alpha_i - \omega t + \varphi) + \sin(\omega t + \alpha_i + \omega t - \varphi)] \right.$$

$$\left. - \sum_{j=1}^{n} \frac{A_j\omega^2}{2}\left[sin\left(\omega t + \alpha_i - \omega t - \alpha_j + \varphi\right) + sin\left(\omega t + \alpha_i + \omega t + \alpha_j - \varphi\right)\right] \right\} dt$$

$$\rightarrow F_i = \frac{m_b}{T}\int_0^T \left\{ \frac{-A_0\omega^2}{2}[\sin(\alpha_i + \varphi) + \sin(2\omega t + \alpha_i - \varphi)] \right.$$

$$\left. - \sum_{j=1}^{n} \frac{A_j\omega^2}{2}\left[sin\left(\alpha_i - \alpha_j + \varphi\right) + sin\left(2\omega t + \alpha_i + \alpha_j - \varphi\right)\right] \right\} dt$$

Both terms that have $[\sin(2\omega t + \ldots)]$ integrated over a period (0→T) will give 0 as a result of the integral. Then, the previous expression is reduced to:

$$\rightarrow F_i = \frac{m_b}{T}\int_0^T \left\{ \frac{-A_0\omega^2}{2}\sin(\alpha_i + \varphi) - \sum_{j=1}^{n} \frac{A_j\omega^2}{2} sin\left(\alpha_i - \alpha_j + \varphi\right) \right\} dt$$

As the change of α_i over time is too small, this term can be assumed as constant. Therefore, the equation is re-arranged as:

$$\rightarrow F_i = \frac{m_b}{T}\left[\frac{-A_0\omega^2}{2}\sin(\alpha_i + \varphi) - \sum_{j=1}^{n} \frac{A_j\omega^2}{2} sin\left(\alpha_i - \alpha_j + \varphi\right) \right] \int_0^T dt$$

Final expression of the inertial force evaluated in the vertical direction is:

$$\rightarrow F_i = \frac{-m_b\omega^2}{2}\left[A_0 \sin(\alpha_i + \varphi) + \sum_{j=1}^{n} A_j sin\left(\alpha_i - \alpha_j + \varphi\right) \right] \qquad (3.20)$$

If there is a system with just one free element and one rotary drum:

1 sphere $i = 1$, and j only goes from 1 to 1. Therefore, $\alpha_i = \alpha_j$. The previous equation can be expressed as:

$$\rightarrow F_1 = \frac{-m_b\omega^2}{2}[A_0 \sin(\alpha_1 + \varphi) + A_1 sin(\varphi)] \tag{3.21}$$

Also, as there is only one sphere, the amplitude of its response A_1 must be equal to the amplitude of excitation A_0 in order to damp vibrations ($A_0 = A_1$).

$$\rightarrow F_1 = \frac{-A_0 m_b\omega^2}{2}[\sin(\alpha_1 + \varphi) + sin(\varphi)] \tag{3.22}$$

With the phase angle φ being defined as:

$$tan\varphi = \frac{(c_1 + c_2)\omega}{(k_1 + k_2) - M\omega^2}$$

$$\varphi = \pi + arctan\left(\frac{(c_1 + c_2)\omega}{(k_1 + k_2) - M\omega^2}\right), \quad for\ \omega > \omega_0 \tag{3.23}$$

Where, c_1, c_2, k_1, k_2 depend on the system configuration and refer to the damping coefficients and the stiffness of the springs respectively. M represents the mass of the main body and ω the frequency of excitation.

These equations are input to Matlab and graphic solution is obtained.

3.4.1 Inertial force solution with Matlab

For easier computation of inertial force, the expression (3.22) is defined as:

$$\frac{F_1}{A_0 m_b\omega^2} = -\frac{1}{2}[\sin(\alpha + \varphi) + sin(\varphi)] \tag{3.24}$$

Equations are coded in Matlab and the following parameters are assigned to the system: M=4.175 kg, c_1=10 kg/s, c_2=10 kg/s, k_1=10000 N/m, k_2=10000 N/m and ω=100 rad/s.

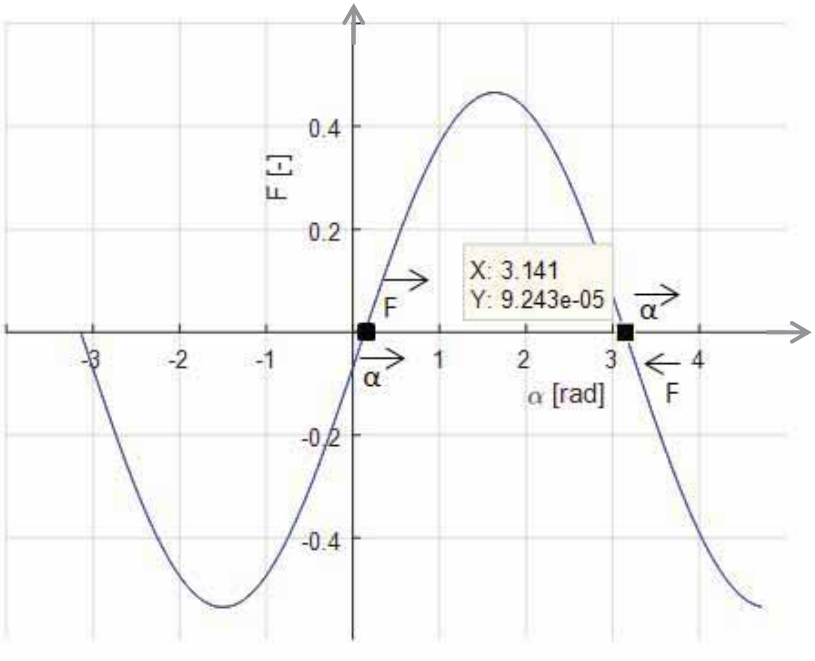

Figure 33. Inertial Force as function of α

The curve crosses the horizontal axes in two positions between 0 and 2π, in these two points the inertial force is 0, meaning the body is in equilibrium and vibrations are absorbed. However, one of these positions represents true equilibrium, whereas the other one is not a stable position for the free element.

On the one hand, for one free element in the system, the true equilibrium position is the one found at π. This is determined because whenever the free element tries to move towards an increase in the angle α, the inertial force becomes negative and pushes the element back. Moreover, when the sphere tries to move towards a decrease in angle α from this position, the inertial force becomes positive, returning the free element to the equilibrium position. The free element oscillates in this way around this point, until inertial force is zero and vibrations of the main body do not exist.

On the other hand, if the free element is located at the position close to $\alpha=0$, when it moves towards an increase in alpha, the inertial force becomes positive and helps the sphere to escape from this position. Same applies when the sphere moves towards negative alpha and the inertial force helps it to move away.

Hence, this section explains how the free elements inside the drums are able to find and stay in an equilibrium position, in which they are able to counteract the excitation forces and eliminate vibrations.

Moreover, this kind of Dynamic Eliminator of Vibrations is modelled as part of a rotary hammer system in order to determine the feasibility of implementation to this impact tool. First, the rotary hammer working principle is modelled in sections 4.3 and 4.4 of this document and then in chapter 5 models are brought up together

CHAPTER IV – Rotary Hammer experiments and modelling

4.1 Introduction

An impact tool was chosen with the intention to develop a mathematical model of the Dynamic Eliminator of Vibrations based on real data of the vibrations produced by this device. Hence, with the use of a real device and the experimental measurement of vibrations amplitude and frequency, the results and damping capability of the EDV could be determined accurately.

4.2 Experimental Set-up

The experiments and models developed in this work were based on the Makita Rotary Hammer HR2511. This tool's characteristics are provided in the following section along with a more detailed description of its design and its working principle. For developing the mathematical model of the EDV, it is also important to determine how impacts are produced by this tool.

4.2.1 Makita Rotary Hammer HR2511

The Makita HR2511 is a rotary hammer featuring a 2 mode function to fulfill different drilling applications. As any other rotary hammer it has a drilling function with pounding action and a "hammering-only" one. This device, shown in Figure 34, has a net weight of 4.25 kg and an overall length of 370 mm. It has the capacity of drilling wood, steel and concrete; being this last one its main application.

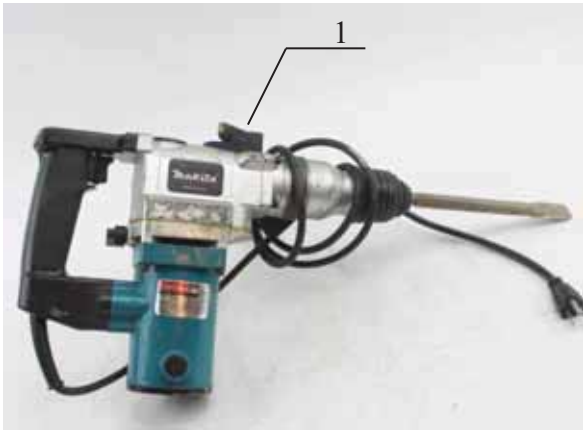

Figure 34. Makita HR2511

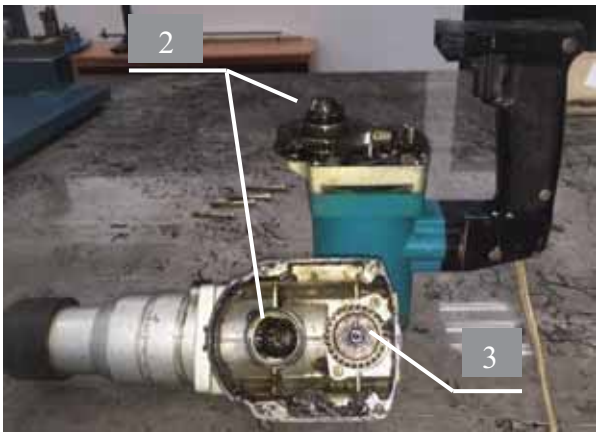

Figure 35. HR2511 inside view

The tool was disassembled with the purpose of a better understanding of the mechanisms that allow it to function in two ways. In Figure 34, there is a switch (1) on the top of the device that enables these two functions by coupling a set of bevel gears (2 - Figure 35) that provokes the rotation of the drill bit. Otherwise, if the link between them is broken, the bevel gear starts to rotate freely, enabling the hammering-only function.

The top part of the rotary hammer is shown on Figure 36. The device has a helical gear (3) that is connected to the piston-crankshaft mechanism making it work. This mechanism is the one that produces the tool's pounding action. Also, a hole is seen with the crown gear (2.1) that allows the rotation of the drill bit when engaged. On the bottom part of the gear box, seen in Figure 37 and Figure 38, there are several other components. First, there is a shaft (4) that is directly driven by the motor. This shaft is also in contact with the helical gear (3) connected to the piston, which has the support of a bearing (5). The piston gear is also connected to another helical gear (6), the biggest one in Figure 38, which rotates along with the pinion (2.2) that enables the drill bit rotating action.

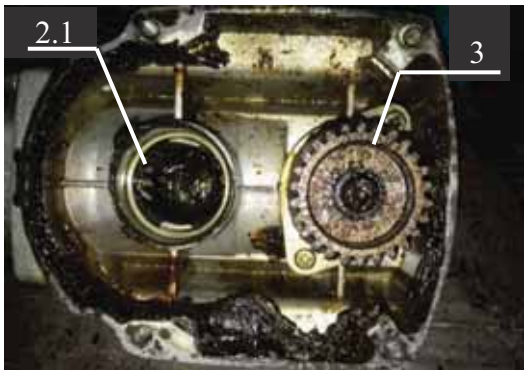

Figure 36. Top section of gearbox

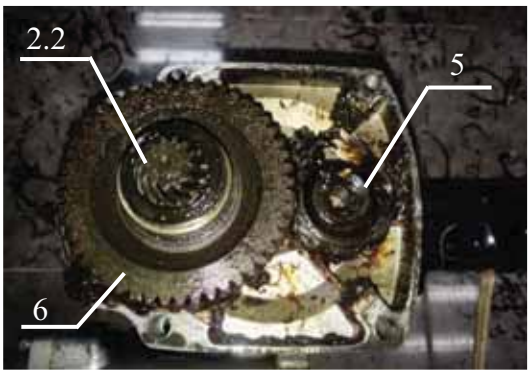

Figure 37. Bottom section of gearbox

Figure 38. Components description

Inside the hammer cylinder, there is an air chamber with a striker inside. For the hammering-only mode, this striker is not directly hit by the piston but moved by the air compression in the chamber. After air is compressed the striker hits the chisel. The shockwaves of each impact travel from the striker to the tip of the chisel. Piston and striker can be observed in Figure 39 and Figure 41, respectively.


Figure 39. Piston (front view)


Figure 40. Piston (top view)


Figure 41. Striker

In figures 42-44, components can be better appreciated with more detailed pictures and a cross section of a similar device (in this case the bevel gear (6) is in direct contact with the motor shaft (4), contrary to what it was described before).

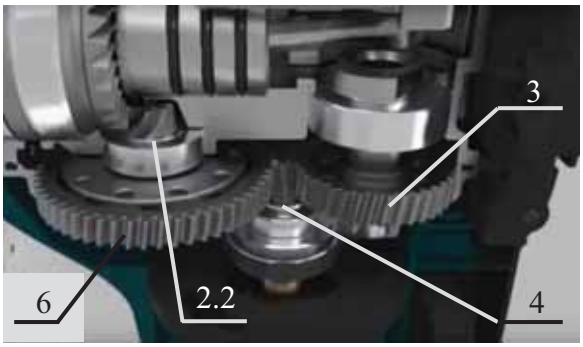

Figure 42. Transmission gear box

Figure 43. Tranmission gear box

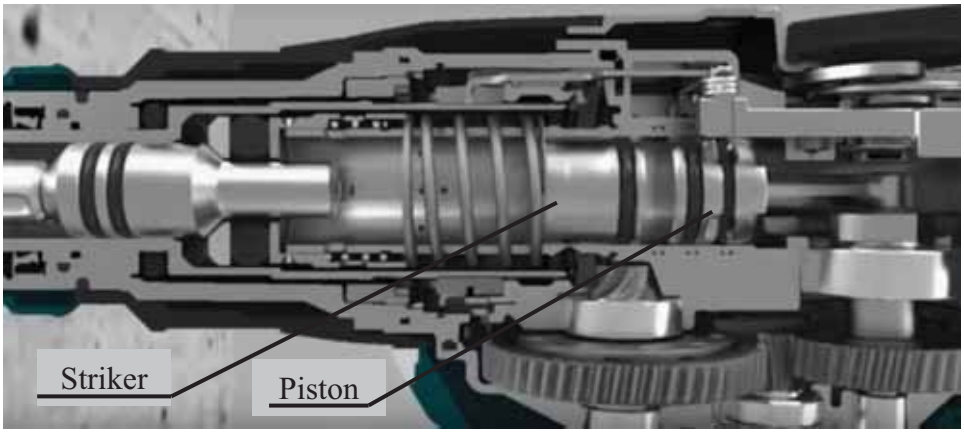

Figure 44. Makita's rotary hammer cross section

In the Table 5, the main parameters of the rotary hammer are presented. A detailed parts diagram of this rotary hammer is shown in the Appendix section of this document.

Makita Rotary hammer	
Voltage	120 v
Frequency	60 Hz
Power	1.3 HP or 850 W
Engine RPM	800-900 rpm
Blows per minute	3000-3200

Table 5. Rotary hammer main parameters

The main dimensions needed for describing and modelling the rotary hammer were measured and the obtained values are summarized in Table 6.

Rotary hammer external dimensions/parameters			
Length with chisel [mm]	575	Mass with chisel [kg]	4.50
Length without chisel [mm]	370	Mass without chisel [kg]	4.25
Hammer height [mm]	235	Chisel length (uninstalled) [mm]	250
Hammer case width [mm]	91.5	Base diameter [mm]	80
Rotary hammer internal dimensions/parameters			
Piston diameter [mm]	22	Striker mass [kg]	0.075
Piston height [mm]	27.5	Max piston displacement [mm]	20
Striker diameter [mm]	22	Max striker displacement [mm]	85
Striker height [mm]	30	Max chisel displacement [mm]	17.5

Table 6. Makita rotary hammer dimensions

4.2.2 Equipment for measuring vibrations

Some experiments were carried out with the objective of analyzing the vibrations produced by the rotary hammer while impacting different materials such as concrete and asphalt. Also, vibrations were measured in free state, that is to say, rotary hammer was actioned without hitting any surface. With these experiments, a better understanding of the hammer vibration modes was acquired.

Vibrations were only measured in one direction. For all the tests, the chisel was pointing down and the vibrations were analyzed in the vertical direction. This was done because this is the main axis in which the rotary hammer and its internal components translate.

Special equipment was used for performing the experiments. The main devices needed for these tests were an accelerometer, a signal amplifier, and a dynamic signal analyzer. First, the Brüel & Kjaer “4507B” accelerometer is attached to the rotary hammer case in the proper position to sense vibrations in the desired direction. This accelerometer was then connected to Brüel and Kjaer “Nexus” conditioning amplifier that enlarges the signals detected by the accelerometer. Then, the output of the amplifier works as input of the Data

Physics “Quatro” dynamic signal analyzer that processes the analogue signals emitted by the amplifier and converts them into digital signals that the computer can read. Finally, vibrations can be analyzed in the “SignalCalc 240” software easily, where parameters like acceleration and frequency can be represented graphically. This process is illustrated in Figure 45 and the input parameters used for measuring vibrations in the SignalCalc 240 software are shown in Figure 46.

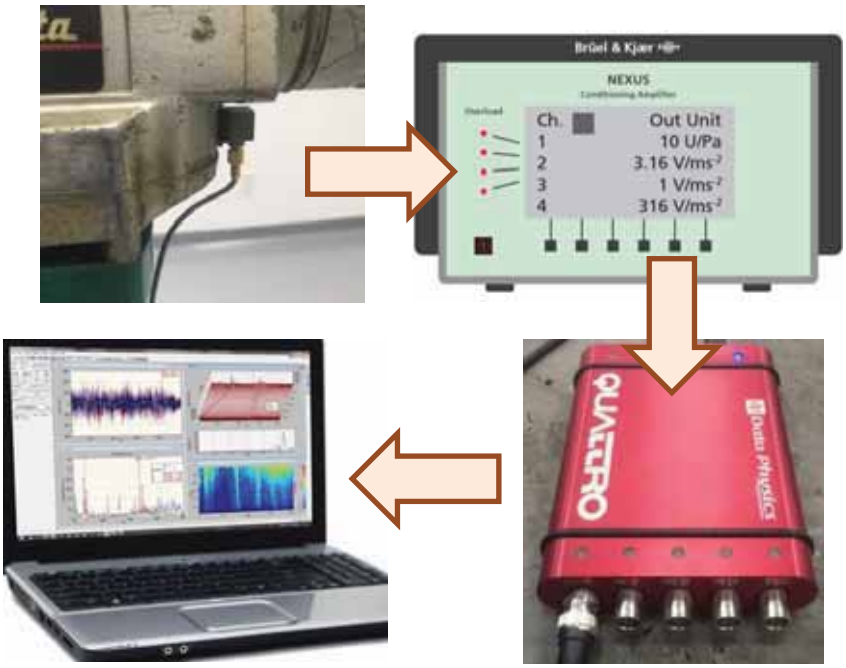

Figure 45. Vibrations measuring equipment layout

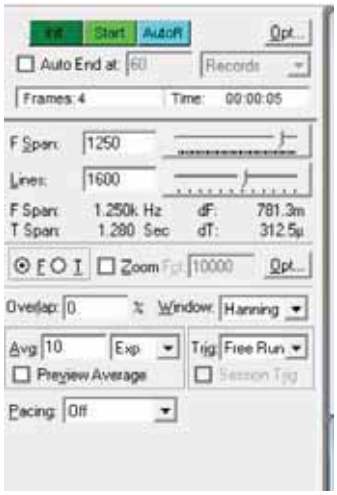

Figure 46. Software parameters for sensing vibrations

Three experiments were carried out in order to be able to understand and analyze the vibrations produced by the impact tool chosen.

4.2.3 Makita rotary hammer experiments

- Experiment 1. Without impact

The first experiment was performed without contact with other surfaces. The rotary hammer was actioned for a few seconds and the vibrations produced by the movement of its internal components were registered. The obtained results are shown in Figure 47 and Figure 48.

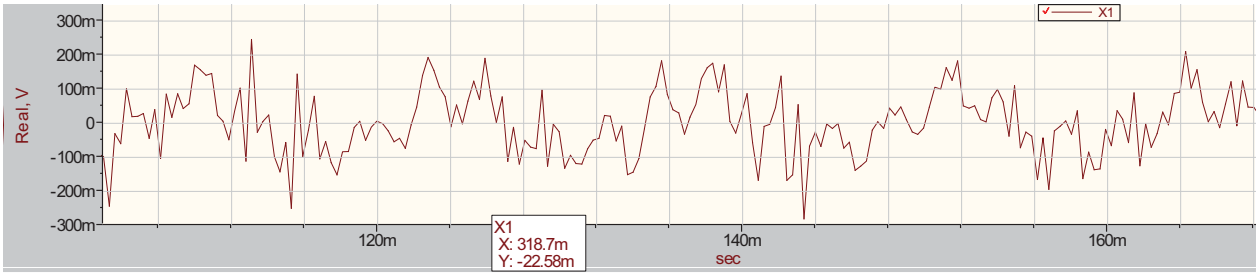

Figure 47. Rotary hammer vibrations without impacts

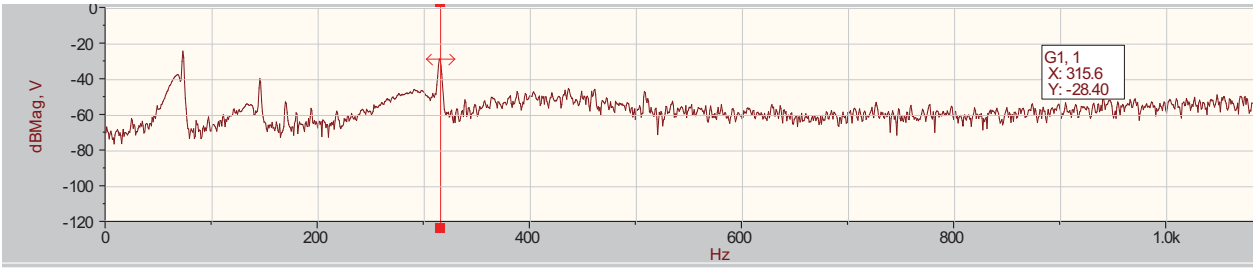

Figure 48. Frequencies of vibration (without impacts)

In the previous experiments, three main frequencies are identified.

- F_1 = 72.66 Hz
- F_2 = 145.3 Hz
- F_3 = 315.6 Hz

It is evident that the first two frequencies are harmonic ones, as F_2 is two times F_1. However, F_3 represents a peak for another mode of vibration.

Next, two impact tests were done as it is shown in Figure 50. The first test was done against an asphalt cylinder and the second one with a concrete sample (R_c=250 kg/cm^2). Both test samples were created in the universities pavements laboratory and are presented in Figure 49.

Figure 49. Test samples

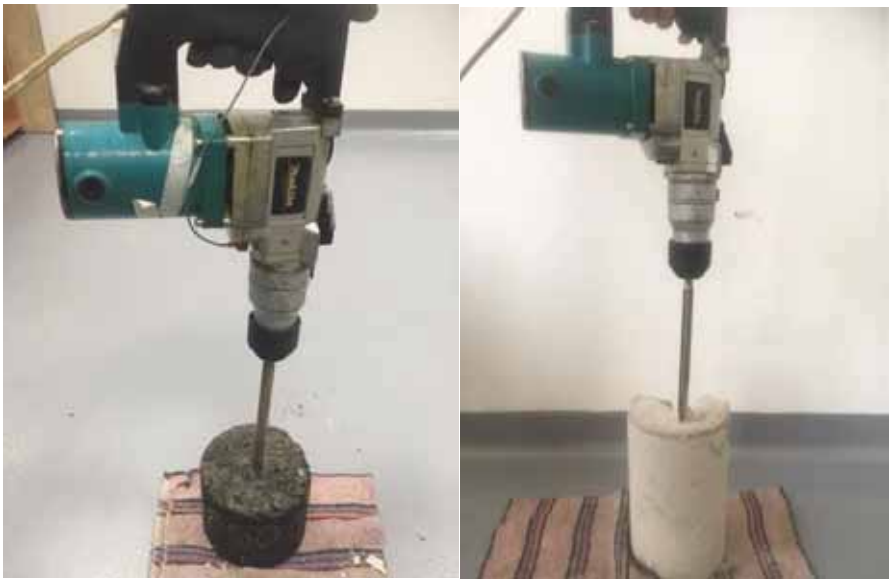

Figure 50. Tests on asphalt (left) and concrete (right)

- Experiment 2: Impacts on asphalt

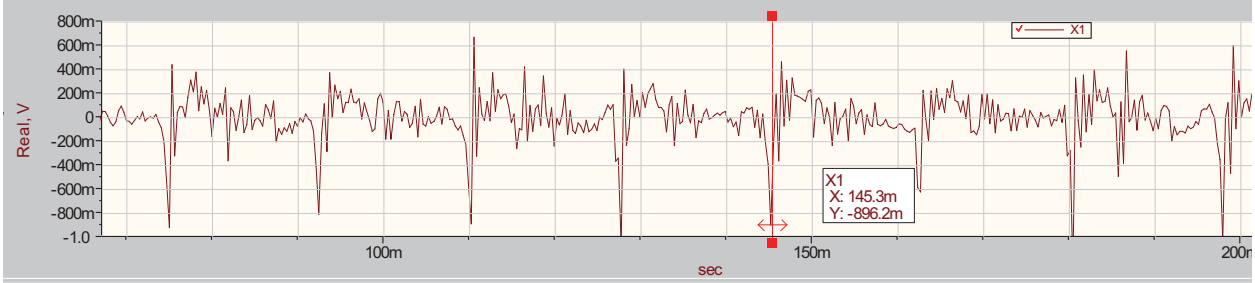

Figure 51. Hammer vibrations during impact with asphalt

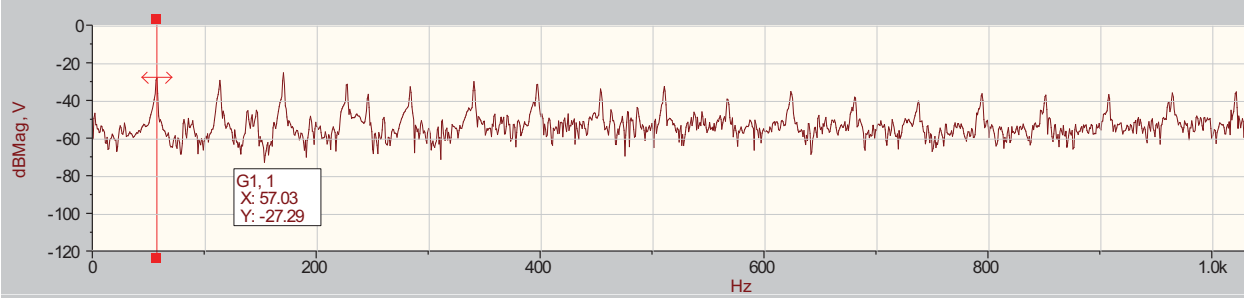

Figure 52. Frequencies of vibration for test on asphalt

Vibrations are found to be harmonic. The times at which the peaks of amplitude (volts) appear on Figure 51 are used for calculating the period and frequency of vibration as it is shown in Table 7. This results on a frequency of vibration of 57.15 Hz. Which is almost the same value found for the first peak in the frequencies plot (Figure 52). The following peaks just represent the second harmonic, the third one and so on.

Time [ms]	Period T [ms]
75.31	17.19
92.5	17.80
110.3	17.50
127.8	17.50
145.3	-
Avg Period T [ms]	17.497
Frequency 1/T [Hz]	57.15

Table 7. Period of vibration for impacts on asphalt

- Experiment 3: Impacts on concrete

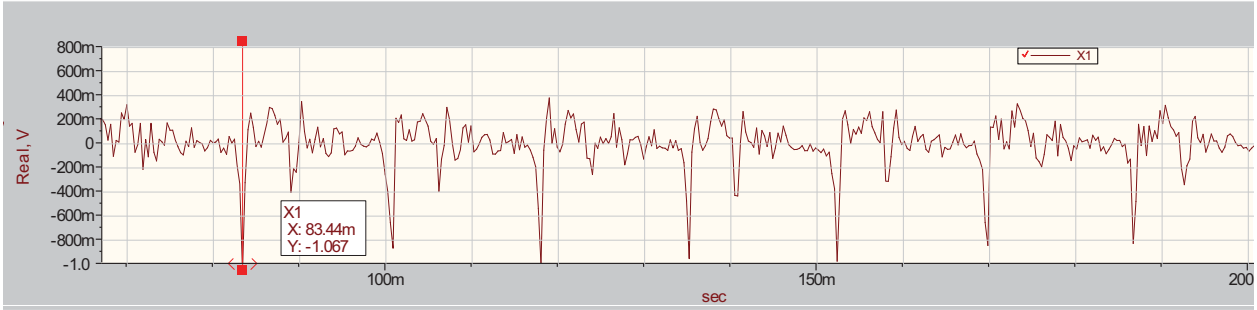

Figure 53. Hammer vibrations during impact with concrete

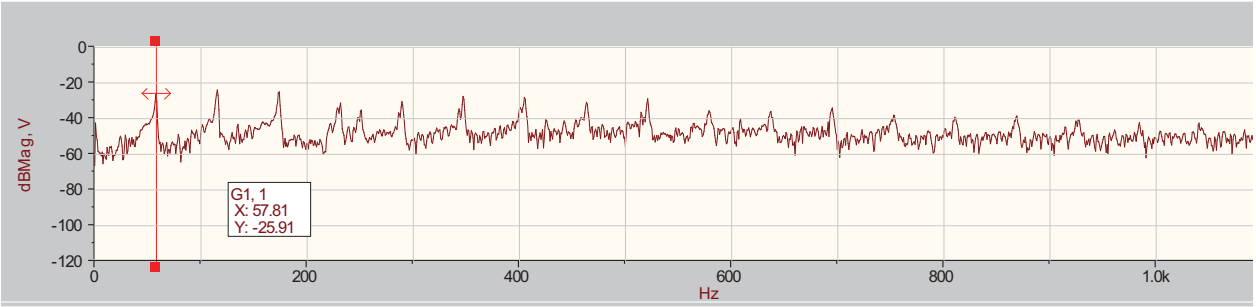

Figure 54. Frequencies of vibration for test on concrete

The results obtained in the experiments performed on concrete are very similar to the ones obtained with asphalt. In both cases, vibrations reach amplitudes of more than one volt. The frequency of the first harmonic is 57.8 Hz (Figure 54), almost the same one as in the previous test.

However, acceleration of vibration cannot be obtained straight forward from the software, further interpretation is required. For this purpose, a calibration exciter is needed to convert the volts obtained as vibrations to acceleration in m/s^2. The calibration exciter used is the Type 4294 also from Brüel & Kjaer. This device is an electromagnetic exciter with an internal built in piezoelectric accelerometer for servo regulation of amplitude. The exciter can be seen in Figure 55.

Figure 55. Brüel & Kjaer calibration exciter

The calibrator vibrates at a known frequency (f=159.15 Hz ± 0.02%) and an acceleration of 10 m/s^2. With these values, the calibrator is turned on and vibrations are measured with the same equipment used for the tests. Voltage and frequencies of vibration are obtained and from this a constant is calculated to determine the acceleration and amplitude of vibration of the values registered in the tests.

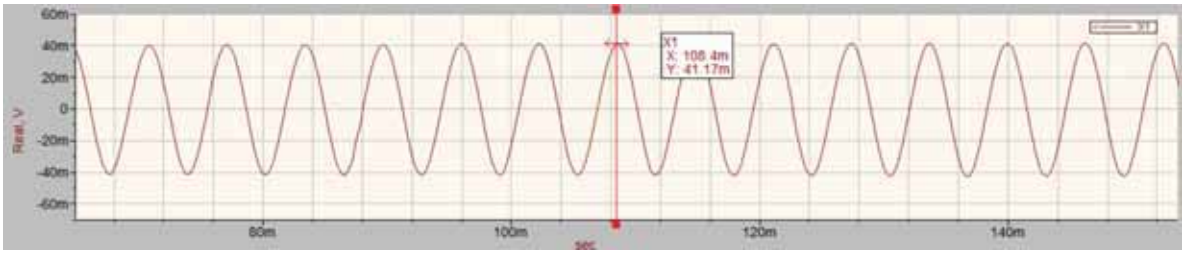

Figure 56. Vibrations produced by calibration exciter

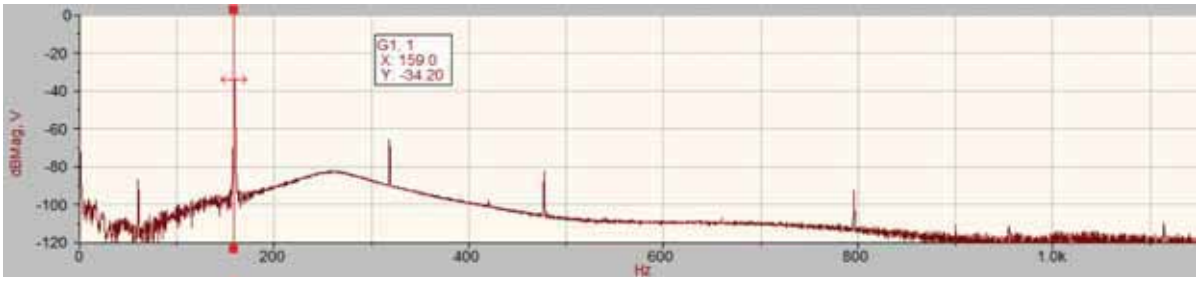

Figure 57. Frequencies of vibration of calibration exciter

The results obtained in the calibration are: $f = 159.0\,Hz$, $dB = -34.2$, and $V = 41.705\,mV$

With these values a conversion constant is calculated:

$$C = \frac{a_c}{u_c} = \frac{10\ m/s^2}{41.705\ mV} = 0.24\ \frac{m/s^2}{mV}$$

Then, with this constant, the maximum acceleration of vibrations for tests in asphalt and concrete can be determined. Voltage obtained for both concrete and asphalt is very similar so a common value is used.

$$a = (685\ mV)\left(0.24\frac{m/s^2}{mV}\right) = 164.4\ m/s^2$$

The frequency of the first harmonic can be used to compute the amplitude of these peaks of vibration in millimetres.

$$a_{accel} = a_{disp}\omega^2$$

$$\rightarrow a_{disp} = \frac{164.4\ m/s^2}{[2\pi(57.8\ Hz)]^2} = 0.00125\ m = 1.25\ mm$$

This value represents the magnitude in millimeters of the maximum peak of vibration as a result of the superposition of all the frequencies involved in the production of the hammer impacts.

Though, the amplitude of just the first mode of vibration can be determined with the decibels and the frequency of the first harmonic.

	Calibration Exciter	Rotary hammer (Impacts on concrete
f_1	159 Hz	57.8 Hz
dB	-34.2	-25.91

Table 8. Frequency of the 1st harmonic for exciter and hammer

Using equation (2.1) acceleration of the first harmonic can be found in the following way:

$$20\log\frac{a_{hammer}}{a_{ref}} = -25.91 \quad (4.1)$$

$$20\log\frac{a_{exciter}}{a_{ref}} = -34.2 \quad (4.2)$$

Expression (4.2) is subtracted from expression (4.1) and the next equation is obtained

$$20\log\frac{a_{hammer}}{a_{ref}} - 20\log\frac{a_{exciter}}{a_{ref}} = -25.91 - (-34.2)$$

$$\rightarrow 20log\frac{a_{hammer}}{a_{ref}}\frac{a_{ref}}{a_{exciter}} = 8.29$$

$$\rightarrow \frac{a_{hammer}}{a_{exciter}} = 10^{\frac{8.29}{20}}$$

$$\rightarrow a_{hammer} = 10(10^{\frac{8.29}{20}}) = 25.97\frac{m}{s^2} \rightarrow amplitude\ of\ the\ 1st\ harmonic$$

It is important to mention that, for the development of these expressions, the vibrations of the exciter are assumed to be harmonic, neglecting the secondary peaks found in the frequency spectre shown in Figure 57.

The result of the calculation can be verified with the values for continuous vibration levels for a rotary hammer presented in Table 1, were typical range varies from 5 to 24 m/s^2.

The obtained frequencies can be applied in the mathematical models developed and the possibility of damping the first modes of vibration can be determined. Also, a comparison can be made between the amplitudes of vibration measured and the values obtained in the models.

4.3 Modelling of rotary hammer – Kinetic model with algebraic equations

The rotary hammer working principle was modeled in two ways. A first model was proposed based on rigid body kinetics theory. There are two main elements that constitute this model, the piston and the striker. This model tries to imitate the motion of this tool. The piston goes back and forth as part of a crank-rod mechanism with a sinusoidal motion. While doing it, the piston hits the striker which translates towards the chisel. In this case, the chisel is assumed to be static due to the minimum displacement it experiences and the way the shockwaves travel through it. Figure 58 helps to visualize the proposed model.

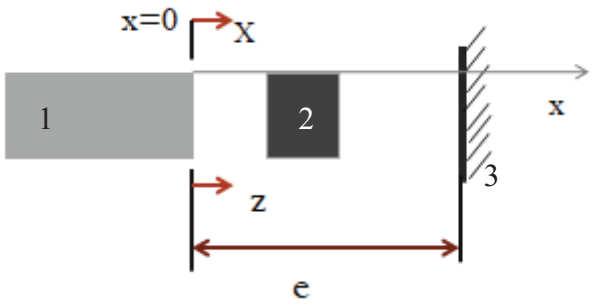

Figure 58. Rotary hammer modelling

Where,

1, corresponds to the piston

2, corresponds to the striker

3, corresponds to the chisel (assumed as static)

x, is the position of the striker along horizontal axis

z, is the position of the piston

e, is the maximum displacement of the striker

The governing equations developed for describing the behavior of these elements are presented as follows.

The motion of the piston is:

$$z = asin(\omega t) \tag{4.3}$$

Where ω, is the angular velocity of the piston and a is the amplitude of its movement.

The time for first impact (t_1) - Piston vs Striker reads:

$$z(t_1) = \text{asin}(\omega t_1) = x_o$$

$$\rightarrow t_1 = \left(\frac{1}{\omega}\right) arcsin\left(\frac{x_0}{a}\right) \tag{4.4}$$

Where x_0, is the position of the striker.

The velocity of piston after first impact (v_{z1}) is:

$$v_{z1} = \dot{z} = a\omega cos(\omega t_1) \tag{4.5}$$

The velocity of striker after first impact (v_1) is:

$$k_1 = \frac{v_{z2} - v_1}{v_0 - v_{z1}}, \qquad v_{z1} = v_{z2}$$

$$v_1 = v_{z1}(1 + k_1) - v_0 k_1 \tag{4.6}$$

Where k_1, is the restitution coefficient for the impact between piston and striker and v_0 is the initial velocity of the striker.

The position and time for second impact (t_2), striker vs chisel (using equation for position between 1st and 2nd impact) are given by:

$$x(t_2) = x_0 + v_1(t_2 - t_1) = e$$

$$\rightarrow t_2 = t_1 + \frac{e - x_0}{v_1} \tag{4.7}$$

$$x_2 = x_0 + v_1(t - t_1) \tag{4.8}$$

The velocity of striker after impact with chisel (v_2) is obtained as:

$$k_2 = \frac{v_2 - 0}{0 - v_1}, \qquad chisel\ is\ assumed\ static$$

$$\rightarrow v_2 = -k_2 v_1 \tag{4.9}$$

Where k_2, is the restitution coefficient for the impact between striker and chisel.

The position of striker after impact with chisel and before new impact with piston (x_3) is:

$$x_3 = e + v_2(t - t_2) \tag{4.10}$$

The position and time for third impact (t_3) - Piston vs striker (again), are given by:

$$As\ x_3 = z(t_3)\ \ and\ \ z(t_3) = asin(\omega t_3)$$

$$asin(\omega t_3) - (v_2(t_3 - t_2)) - e = 0 \tag{4.11}$$

$$Solve\ for\ t_3\ with\ Matlab$$

Finally, the velocity of striker after impact with piston is:

$$v_3 = v_{z(t3)}(1 + k_1) - v_2 k_1 \tag{4.12}$$

In addition to these equations, a special case was found that needed further attention. This case is illustrated in Figure 59 and it happens when the piston (z) is coming back and the striker (x) is moving at higher velocity so they collide on their way back. Therefore, the striker bounces back but with less energy. Hence, if the striker is moving too slow, the piston could make a complete cycle and be able to hit the striker again.

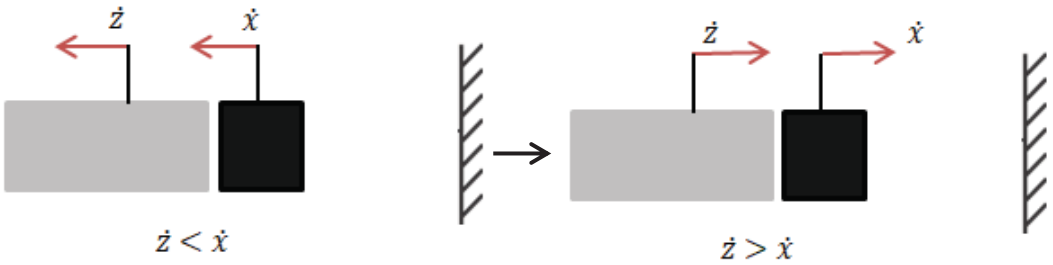

Figure 59. Striker (x) colliding with returning piston (z)

This extra collision with the piston is the one considered in these equations.

As time for impact in this special case (t_{sp}) is unknown, it has to be determined before computing the velocity of the striker after this second impact, as follows:

$$As\ x_{sp} = z(t_{sp})\ \ and\ \ z(t_{sp}) = asin(\omega t_{sp})$$

$$asin(\omega t_{sp}) - (v_3(t_{sp} - t_3)) - x_3 = 0 \tag{4.13}$$

$$Solve\ for\ t_{sp}\ with\ Matlab$$

The velocity of striker after being hit by piston twice is:

$$v_{sp} = v_{z(tsp)}(1 + k_1) - v_3 k_1 \tag{4.14}$$

The average forces exerted on each impact are computed by using the equation of Conservation of Linear Momentum.

$$G_2 - G_1 = \int_0^{t_1} F_1 dt = F_1 \Delta t_1$$

$$\rightarrow F_{avg} = F_1 = \frac{G_1 - G_0}{\Delta t_1} = \frac{m(V_1 - V_0)}{\Delta t_1} \quad (4.15)$$

Where, G_1 and G_2 are the linear momentum at time t_1 and t_2, respectively. Also, V_1 and V_0 stand for the velocity of the body before and after impact, m is the mass of the body and Δt represents the duration of the impact as a really short amount of time.

It is important to mention that the maximum force is two times bigger than the average force.

Matlab program was developed with these equations with the objective of obtaining a graphical representation of the behavior of the rotary hammer inner components.

4.3.1 Matlab application

Again, the equations shown in last section are programmed in Matlab with the purpose of being able to play with the different parameters that define the system and observe, in a graphic way, the obtained results. Matlab code is programmed in different sections. Functions that describe the displacement and the velocity of the piston and the striker are defined first. Subsequently, they are called inside a cyclic structure for computing the parameters according to the number of impacts given by the simulation time defined.

Input parameters for this program are:

x_0, striker initial position [mm]
v_0, initial velocity of striker [mm/s]
e, striker maximum displacement [mm]
a, amplitude of piston's movement [mm]
k_1, restitution coefficient for impact between piston-striker [-]

k_2, restitution coefficient for impact between striker and chisel [-]
ω, angular velocity of the piston [rad/s]
t_f, simulation time [s]
m, mass of the striker [kg]
dt_1, time delta of impact duration between piston and striker [s]
dt_2, time delta of impact duration between striker and chisel [s]

The following parameters apply for the 3 cases that are going to be presented in this section: x_0 = 5 mm, v_0 = 0 m/s, e = 85 mm, a=10 mm, t_f = 3 s, m = 0.075 kg, dt_1 = 0.003 s, dt_2 =0.002 s.

- Experiment 1: ω = 70 rad/s, k_1 = 0.7, k_2 = 0.8

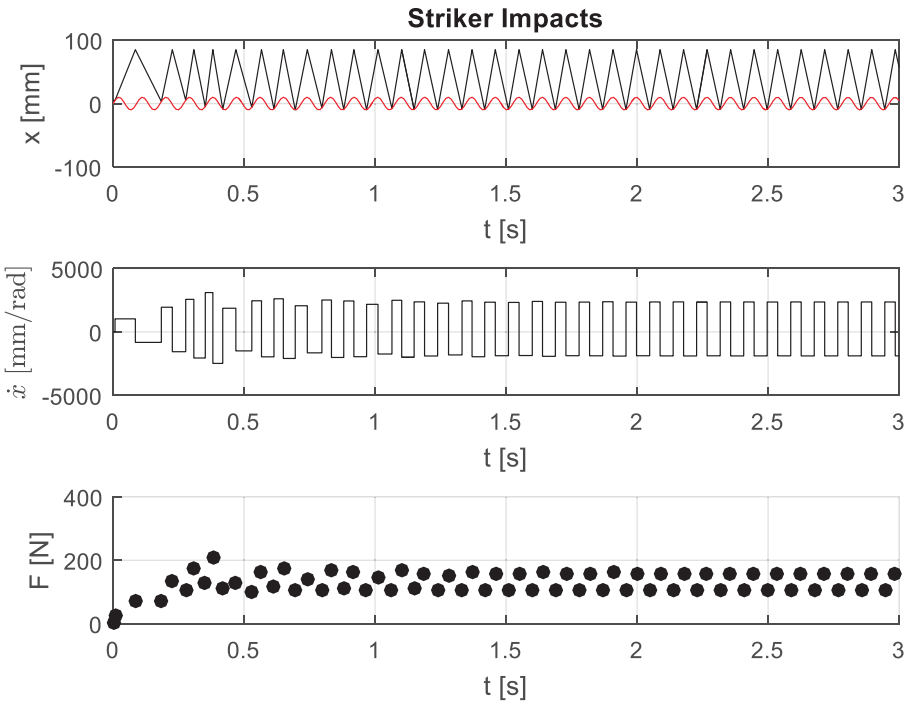

Figure 60. Experiment 1 (kinetic model)

In the first chart of Figure 60, the black line represents the motion of the striker; whereas the red sinusoidal curve represents the motion of the piston. Then, every time these lines touch each other, it means the piston has just hit the striker.

The velocity of the striker shown in chart 2 has a step-shape because its travelling direction changes suddenly after each impact. That is why the velocity is constant during fractions of a second and at a certain point, the striker hits either the chisel or the piston, bouncing away in the opposite direction to the one it had before the impact.

In the case of the third chart of Figure 60, the average force is plotted with dots instead of a continuous curve. This happens because the force is only present at the instant at which the striker impacts another component, and it becomes zero whenever the striker is travelling towards the other body.

- Experiment 2: $\omega = 100$ rad/s, $k_1 = 0.7$, $k_2 = 0.8$

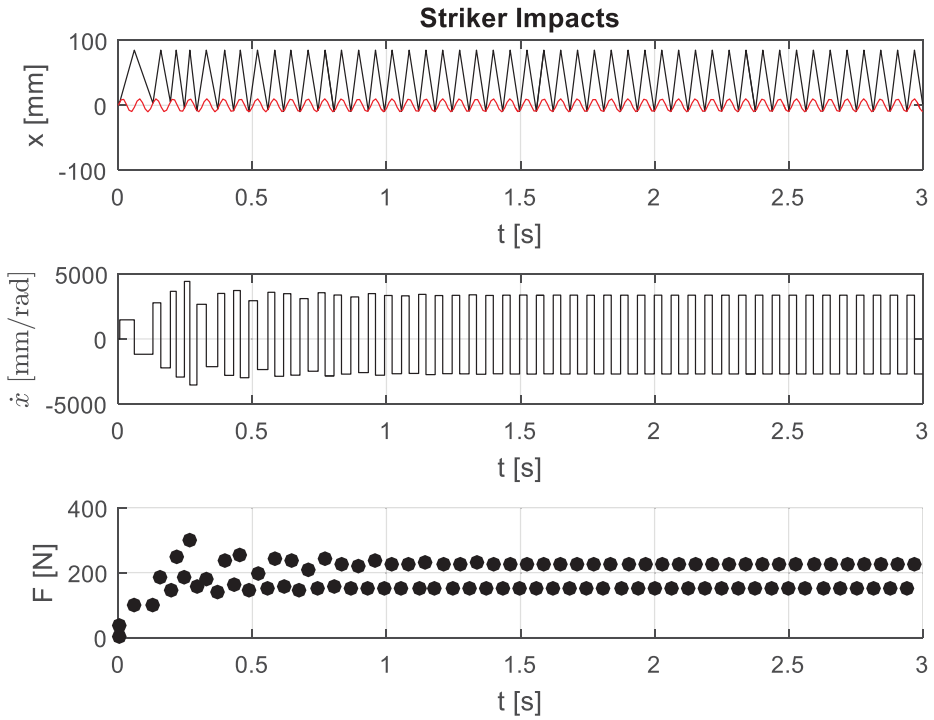

Figure 61. Experiment 2 (kinetic model)

- Experiment 3: ω = 100 rad/s, k_1 = 0.5, k_2 = 0.6

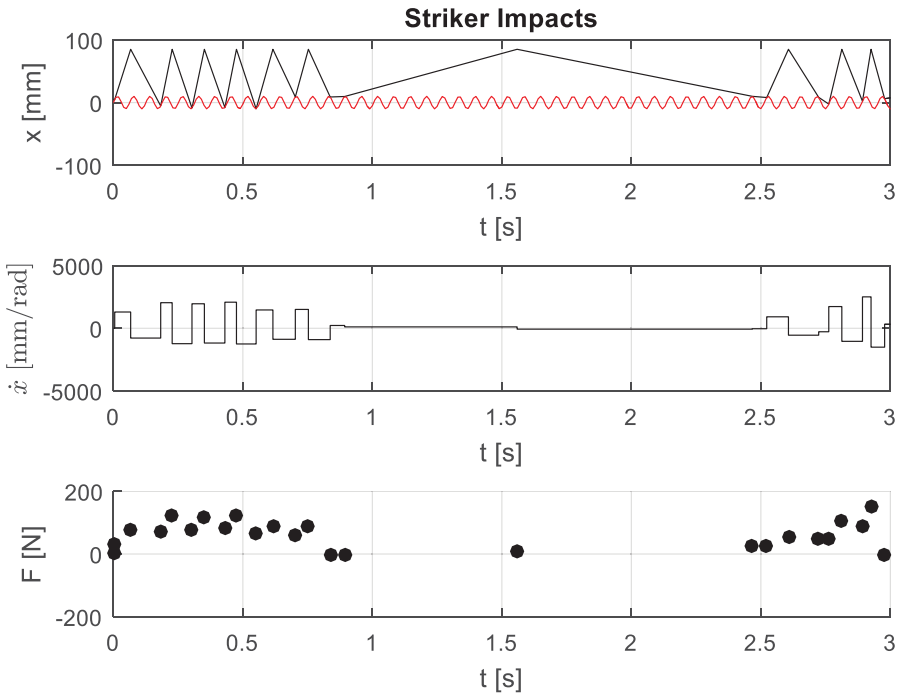

Figure 62. Experiment 3 (kinetic model)

In these experiments the impact of the angular velocity of the piston and the restitution coefficient on the model is reviewed. From first to second experiment, the rotational speed of the piston increases from 70 rad/s to 100 rad/s. This increases the travel speed of the striker, as well as the average force produced at each impact. That is to say, the striker hits the chisel 8 times in 0.5 seconds with ω=100 rad/s, whereas for the speed of ω=70 rad/s the striker only hits the chisel in 6 occasions. Therefore, an increase in the angular velocity of the piston would mean an increase on the velocity at which the striker travels resulting in higher impact forces.

In the third case, the coefficients of restitution k_1 and k_2 are both reduced in 0.2 [-]. This action means that the striker loses more energy on each impact than in the previous experiments. Under these parameters, the striker only hits the chisel 4 times during the first 0.5 seconds. Additionally, there is a point (t=0.84 s) where the striker collides with the

piston on its way back. Therefore, the striker loses more energy than the usual and travels back to the chisel at a very low speed causing the phenomenon observed in
Figure 62 (no striker-chisel collision for a long time) between the 0.84 s and the 2.53 s.

4.4 Modelling of rotary hammer – Dynamic model with differential equations

As it was already seen, the mathematical model from section 4.3 is based on algebraic equations and served as a preliminary model for the system. Nevertheless, in order to combine the model of a rotary hammer with the one of the Dynamic Eliminator of Vibrations, both systems need to be based on the same type of equations, in this case, differential equations.

For that reason, Newton's Second Law is applied for the analysis of the rotary hammer system. The first challenge encountered was to model the contacts piston-striker and striker-chisel. In the real rotary hammer system, the piston and the striker are never in contact. That is to say, the striker moves as a reaction of the air compression that piston exerts on it. On the other hand, the striker actually hits the chisel, but they are in contact for fractions of a second. Therefore, modelling of the link between these bodies was not straight forward.

In order to be able to develop differential equations using Newton's Second Law, both interactions between the bodies were modelled as springs with two special characteristics. The first characteristic is a really high stiffness for the springs. This idea is based on the principle that a very stiff spring could represent an impact with a solid surface. The second characteristic refers to the action of making the spring forces zero whenever two bodies are not in contact. Additionally, damping is added between each body to take into consideration the energy loss after each impact. This approach is illustrated in Figure 63.

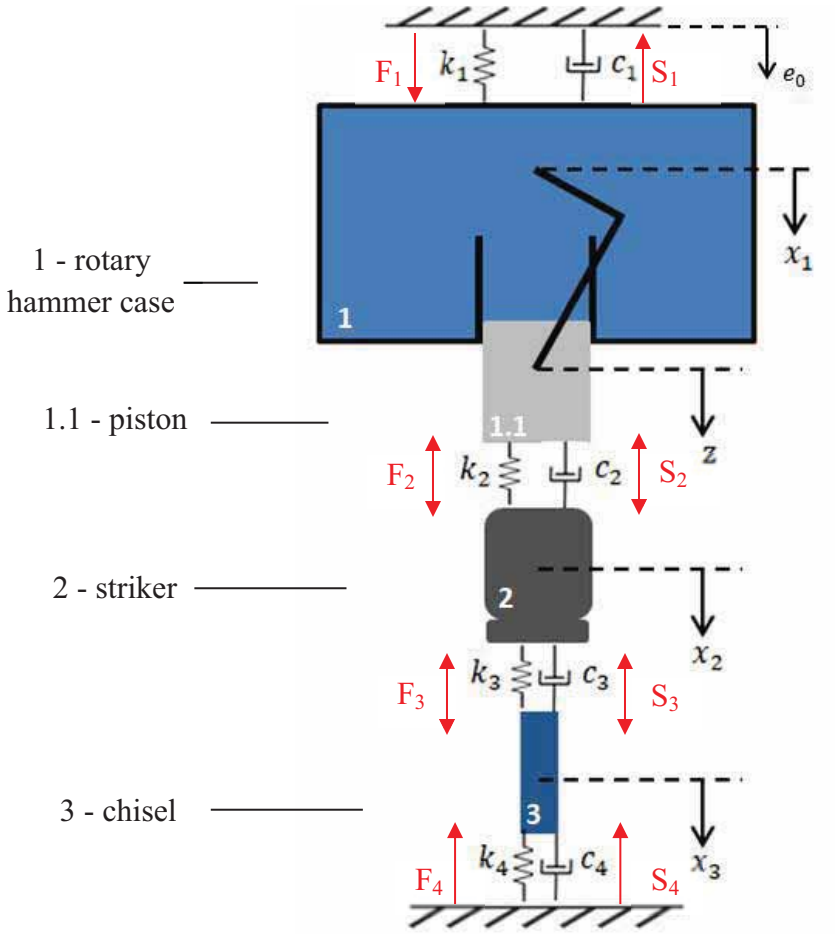

Figure 63. Rotary hammer model

Where,

e_0, hammer initial displacement

k_1, stiffness of the hand-arm system

k_2, stiffness of spring that represents air contact between piston and striker

k_3, stiffness of spring that represents direct contact between striker and chisel

k_4, stiffness of spring that represents direct contact between chisel and the floor

c_1, damping coefficient for hand-arm system

c_2, damping coefficient between piston and striker

c_3, damping coefficient between striker and chisel

c_4, damping coefficient between chisel and floor

x_1, displacement of the main body or hammer case in vertical direction

z, equation for movement of the piston

x_2, displacement of the striker in vertical direction

x_3, displacement of the chisel in vertical direction

ω, angular velocity of the piston crankshaft mechanism

The forces interacting in the system are defined in this way:

Springs	Dampers
$F_1 = k_1(e_0 - x_1)$	$S_1 = c_1\dot{x}_1$
$F_2 = k_2\,(x_1 + z - x_2)$	$S_2 = c_2\,(\dot{x}_1 + \dot{z} - \dot{x}_2)$
$F_3 = k_3(x_2 - x_3)$	$S_3 = c_3(\dot{x}_2 - \dot{x}_3)$
$F_4 = k_4x_3$	$S_4 = c_4\dot{x}_3$

The governing equations for this system are obtained following Newton's Second Law:

$$\sum F = ma$$

$$m_1\frac{d^2x_1}{dt^2} = F_1 - S_1 - F_2 - S_2 \tag{4.16}$$

$$m_2\frac{d^2x_2}{dt^2} = F_2 + S_2 - F_3 - S_3 \tag{4.17}$$

$$m_3\frac{d^2x_3}{dt^2} = F_3 + S_3 - F_4 - S_4 \tag{4.18}$$

Just using springs to represent the impact between components would mean that they are always in contact. For that reason, an extra condition is added to the formulation of F_2, F_3, F_4, the forces that represent the impacts between piston-striker, striker-chisel and chisel-surface, respectively. This formulation specifies that if the resultant force of these springs is negative, the force will be automatically equal to 0. This only happens when Δx is smaller than 0.

$$F_i = \begin{Bmatrix} F_i, & if\ \Delta x \geq 0 \\ 0, & if\ \Delta x < 0 \end{Bmatrix}, \qquad for\ i = 2,3,4$$

It is important to mention that Δx is considered as the displacement of the upper body minus the one of the lower body (see Figure 63), i.e. for the contact striker-chisel, $\Delta x = x_2 - x_3$. Hence, if $\Delta x < 0$, means that $x_3 > x_2$ and that the striker and chisel are being displaced away from each other, avoiding any interaction.

4.4.1 Matlab application

This system is also modelled in Matlab to observe the behaviour of all the internal elements of the hammer, as well as the produced forces.

The independent degrees of freedom identified in Figure 63 are listed below for constituting the differential equations system for Matlab solution with function ode45.

$x(1) = x_1$ $\quad$ $x(3) = x_2$ $\quad$ $x(5) = x_3$
$x(2) = \dot{x}_1$ $\quad$ $x(4) = \dot{x}_2$ $\quad$ $x(6) = \dot{x}_3$

Furthermore, the system of equations is defined as:

$$D(1) = \frac{dx_1}{dt} = \dot{x}_1 = x(2)$$

$$D(2) = \frac{d^2x_1}{dt^2} = \ddot{x}_1 = \frac{F_1 - S_1 - F_2 - S_2}{m_1}$$

$$D(3) = \frac{dx_2}{dt} = \dot{x}_2 = x(4)$$

$$D(4) = \frac{d^2x_2}{dt^2} = \ddot{x}_2 = \frac{F_2 + S_2 - F_3 - S_3}{m_2}$$

$$D(5) = \frac{dx_2}{dt} = \dot{x}_3 = x(6)$$

$$D(6) = \frac{d^2x_3}{dt^2} = \ddot{x}_3 = \frac{F_3 + S_3 - F_4 - S_4}{m_3}$$

Input parameters are given to the system and the results are plotted as in previous applications.

For the first experiment, masses of the bodies are assigned as: $m_1 = 4.175$, $m_2 = 0.075$ $m_3 = 0.025$ [kg]. Stiffness of each of the springs is: $k_1 = 10000$, $k_2 = 10000$, $k_3 = 100000$, $k_4 = 200000$ [N/m]. Damping coefficients are: $c_1 = 20$, $c_2 = 5$, $c_3 = 5$, $c_4 = 2$, [kg/s]. Other parameters are defined as: $z_0 = 0.01$ [m], $\omega = 100$ [rad/s], $e_0 = 0.02$ [m].

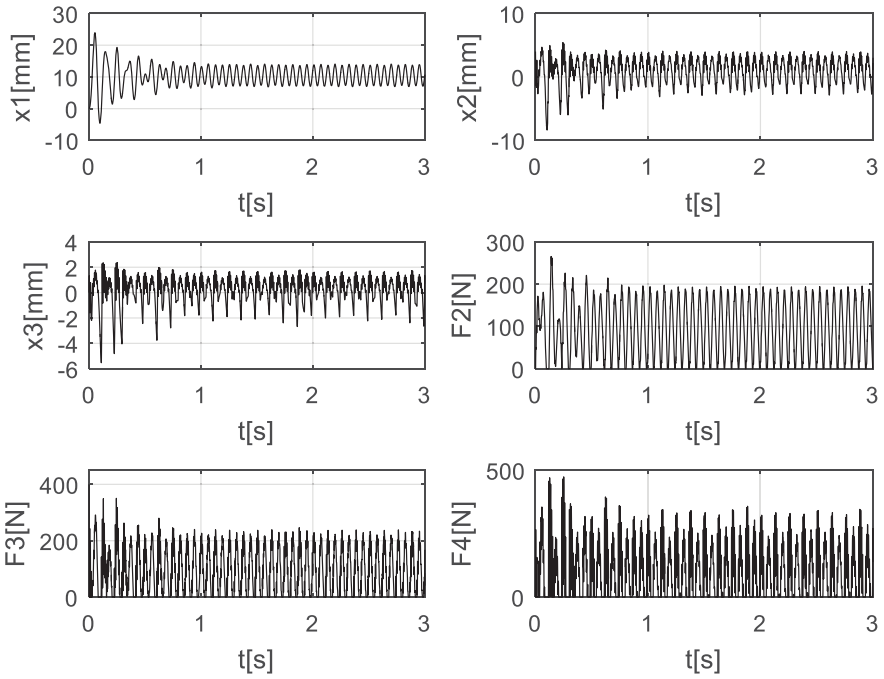

Figure 64. Experiment 1 results (dynamic model)

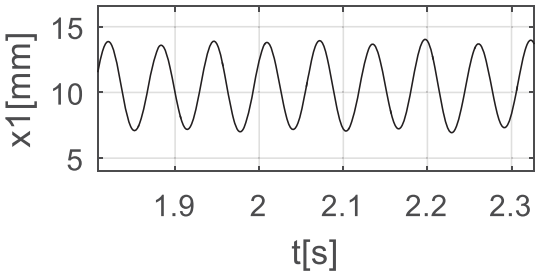

Figure 65. Amplitude of vibration of hammer case

Amplitude of vibration registered for 100 rad/s with the selected stiffness and damping coefficients, is around 3.4 mm once the movement of the components is periodic. It is seen in Figure 64, that vibrations and forces become periodic after 0.75 seconds.

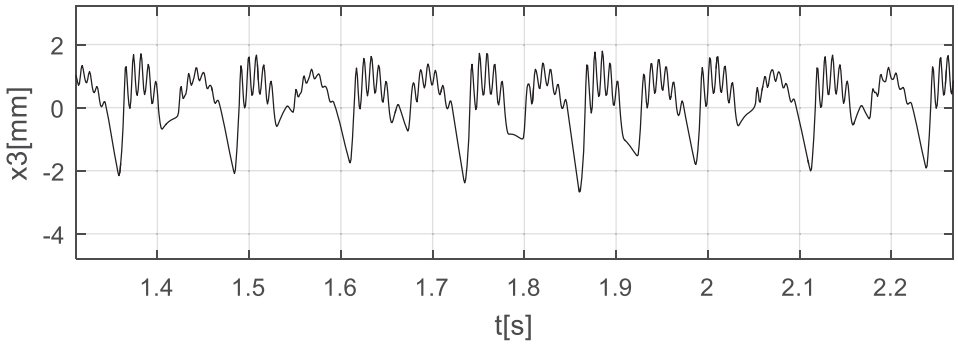

Figure 66. Impacts between chisel and floor

Additionally, from the vibrations graph plotted for the chisel (x_3), the impacts production phenomenon can be observed, presenting a periodic behavior every 0.125 seconds. Also, when the plotted line crosses the x=0 axis, it can be understood as the chisel penetration into the material.

- Experiment 2: ω = 80 rad/s

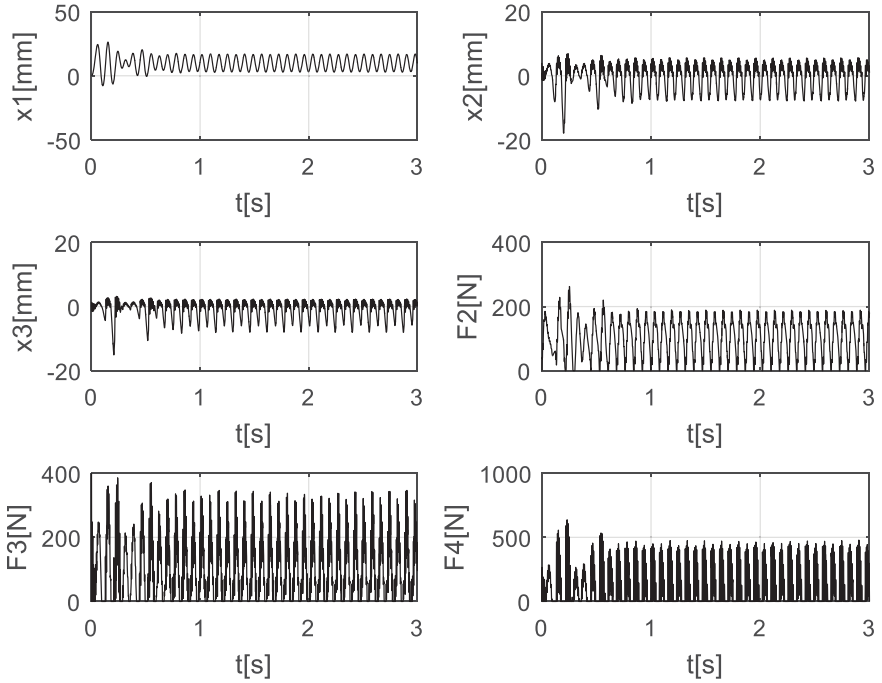

Figure 67. Experiment 2 results (dynamic model)

When the angular velocity of the piston is reduced from 100 to 80 rad/s, the amplitude of vibration of the main body increases to 7 mm. With this, the impact force between chisel

and floor also increases almost reaching 500 N. This phenomenon is opposite to what it was observed in the kinetics model. This happens because in the first model, the increase in angular velocity also increases the linear velocity of the piston, resulting in a bigger impact force transmitted to the striker. In this case, springs are added to the system, therefore conditions change. The natural frequency of thes system is estimated as $\omega = \sqrt{\frac{20000\ N/m}{4.175\ kg}} = 69.21 \frac{rad}{s}$. Therefore, when the frequency of excitation of the piston decreases from 100 to 80 rad/s it gets closer to the natural frequency, resulting in an increase of the amplitude of vibration and impact forces.

In general, this model appears to be a good option to represent the behavior of the internal components of the rotary hammer and the way impacts and vibrations are transmitted between each of the bodies. In the next chapter, the feasibility of eliminating the produced vibrations by this impact tool is explored.

CHAPTER V - Implementation of the Dynamic Eliminator of Vibrations to the Rotary Hammer

5.1 Introduction

As result of this work, the Dynamic Eliminator of Vibrations model proposed is implemented on the mathematical model that describes the motion of the internal components of a rotary hammer. For this purpose, the DEV model used has 2 drums with 2 free elements (spheres or rollers) inside of each one; along with the model for the device based on differential equations developed on the previous chapter. In this section, the possibility of damping vibrations for the chosen device is explored and the parameters under which this can be achieved are determined. Also, the complete system behavior is described.

5.2 Mathematical modelling of rotary hammer with DEV analyzed in one direction (model with 2 drums and 4 spheres)

The complete model for the rotary hammer with the implementation of Dynamic Eliminator of Vibrations can be observed in Figure 68. This system is first analyzed with vibrations in vertical direction, called x. In this direction there are 3 independent degrees of freedom corresponding to the motion of the main body or rotary hammer case (x_1), the striker (x_2), and the chisel (x_3). Z defines the motion of the piston that is powered by a motor. This is the main excitation of the system. Two drums are attached to the main body with 2 free elements on each one, 4 in total. These drums are also connected to the motor and rotate with the same angular velocity of the piston. Additionally, they rotate in opposite directions; the left drum in the front view rotates in counterclockwise direction whereas the right drum in clockwise direction.

As it was described in chapter 4, air compression phenomenon between piston and striker, and impacts for striker-chisel and chisel-floor contacts; are modelled with very high-stiffness springs. Variable e_0 represents the initial displacement of the system and refers to the force exerted on the rotary hammer handle towards the ground or contact surface, by the user. All the other variables are described on models presented in chapters 3 and 4.

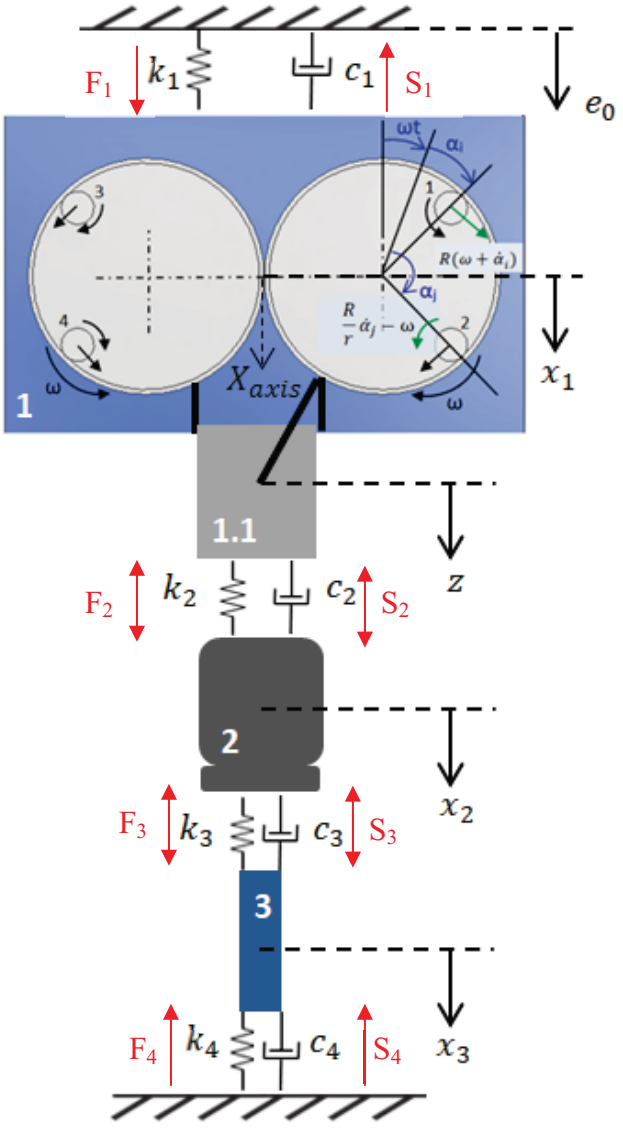

Figure 68. Rotary Hammer with DEV

Spring forces

$$F_1 = k_1(e_0 - x_1)$$

$$F_2 = k_2\,(x_1 + z - x_2)$$

$$F_3 = k_3(x_2 - x_3)$$

$$F_4 = k_4 x_3$$

Special condition

$$F_{2,3,4} = \begin{Bmatrix} F_{2,3,4}, & if\ \Delta x \geq 0 \\ 0, & if\ \Delta x < 0 \end{Bmatrix}$$

Damping forces

$$S_1 = c_1\dot{x}_1$$

$$S_2 = c_2\,(\dot{x}_1 + \dot{z} - \dot{x}_2)$$

$$S_3 = c_3(\dot{x}_2 - \dot{x}_3)$$

$$S_4 = c_4\dot{x}_3$$

Governing equations for this system obtained with Lagrange equations for the DEV section, equations (3.8), (3.9) and Newton's 2nd law equations (4.16)-(4.18) for the rotary hammer components are brought up together and presented here:

$$\ddot{x}_1 = \frac{-m_b R[\sum_{i=1}^{n}(\omega + \dot{\alpha}_i)^2 \cos(\omega t + \alpha_i) + \sum_{i=1}^{n} \ddot{\alpha}_i \sin(\omega t + \alpha_i)] + F_1 - S_1 - F_2 - S_2}{m_1 + n m_b} \quad (5.1)$$

$$\ddot{x}_2 = \frac{F_2 + S_2 - F_3 - S_3}{m_2} \quad (5.2)$$

$$\ddot{x}_3 = \frac{F_3 + S_3 - F_4 - S_4}{m_3} \quad (5.3)$$

$$\ddot{\alpha}_i = \frac{m_b R}{meq}\,[-sin(\omega t + \alpha_i)\ddot{x}_i - c_r R \dot{\alpha}_i], \qquad for\ i = 1,2,3,4 \quad (5.4)$$

Where, $meq = m_b R^2 + \frac{BR^2}{r^2} = m_b R^2 + \frac{2}{5} m_b R^2 = \frac{7}{5} m_b R^2$

And, m_b is the mass of the free elements

The sign in the equations of $\ddot{x}_1$ and $\ddot{\alpha}_i$ related to the vertical displacement of the free elements changes because the positive values are considered downwards for the independent coordinates x_1, x_2, x_3.

Again, ωt is substituted by variable τ and term $\alpha_i{}'' \sin(\tau + \alpha_i)$ is neglected due to its small magnitude and unimportant affection to the final result.

$$x_1{}'' = \frac{1}{m_1 + n m_b}\left\{ m_b R\left[-\sum_{i=1}^{n} (1 + \alpha_i{}')^2 \cos(\tau + \alpha_i) \right] + \frac{F_1 - S_1\omega - F_2 - S_2\omega}{\omega^2} \right\} \quad (5.5)$$

$$x_2{}'' = \frac{F_2 + S_2\omega - F_3 - S_3\omega}{m_2\omega^2} \quad (5.6)$$

$$x_3{}'' = \frac{F_3 + S_3\omega - F_4 - S_4\omega}{m_3\omega^2} \quad (5.7)$$

$$\alpha_i'' = \frac{m_b R}{meq}\left[-sin(\tau + \alpha_i)x_1'' - \frac{c_r R \alpha_i'}{\omega}\right] \; fr\; i = 1,2,3,4 \qquad (5.8)$$

This system of equations is again solved with the help of Matlab. Thus, results and basis of Matlab code can be seen in the next section.

5.2.1 Matlab application

First, the independent degrees of freedom are listed as follows for a DEV model of 4 free elements, two inside each drum:

$x(1) = x_1$	$x(5) = \alpha_2$	$x(9) = \alpha_4$	$x(13) = x_3$
$x(2) = x_1'$	$x(6) = \alpha_2'$	$x(10) = \alpha_4'$	$x(14) = x_3'$
$x(3) = \alpha_1$	$x(7) = \alpha_3$	$x(11) = x_2$	
$x(4) = \alpha_1'$	$x(8) = \alpha_3'$	$x(12) = x_2'$	

Therefore, the system of equations is defined as:

$$D(1) = \frac{dx_1}{d\tau} = x_1' = x(2)$$

$$D(2) = \frac{d^2x_1}{d\tau^2} = x_1'' = \frac{1}{m_1 + nm_b}\left\{-m_b R\left[\sum_{i=1}^{n}(1+\alpha_i')^2\cos(\tau+\alpha_i)\right] + \frac{F_1 - S_1\omega - F_2 - S_2\omega}{\omega^2}\right\}$$

$$D(3) = \frac{d\alpha_1}{d\tau} = \alpha_1' = x(4)$$

$$D(4) = \frac{d^2\alpha_1}{d\tau^2} = \alpha_1'' = \frac{m_b R}{meq}\left[-sin(\tau+\alpha_1)x_1'' - \frac{c_r R \alpha_1'}{\omega}\right]$$

$$D(5) = \frac{d\alpha_2}{d\tau} = \alpha_2' = x(6)$$

$$D(6) = \frac{d^2\alpha_2}{d\tau^2} = \alpha_2'' = \frac{m_b R}{meq}\left[-sin(\tau+\alpha_2)x_1'' - \frac{c_r R \alpha_2'}{\omega}\right]$$

$$D(7) = \frac{d\alpha_3}{d\tau} = \alpha_3' = x(8)$$

$$D(8) = \frac{d^2\alpha_3}{d\tau^2} = \alpha_3'' = \frac{m_b R}{meq}\left[-sin(\tau + \alpha_3)x_1'' - \frac{c_r R \alpha_3'}{\omega}\right]$$

$$D(9) = \frac{d\alpha_4}{d\tau} = \alpha_4' = x(8)$$

$$D(10) = \frac{d^2\alpha_4}{d\tau^2} = \alpha_4'' = \frac{m_b R}{meq}\left[-sin(\tau + \alpha_4)x_1'' - \frac{c_r R \alpha_4'}{\omega}\right]$$

$$D(11) = \frac{dx_2}{d\tau} = x_2' = x(12)$$

$$D(12) = \frac{d^2x_2}{d\tau^2} = x_2'' = \frac{F_2 + S_2\omega - F_3 - S_3\omega}{m_2\omega^2}$$

$$D(13) = \frac{dx_3}{d\tau} = x_3' = x(14)$$

$$D(14) = \frac{d^2x_3}{d\tau^2} = x_3'' = \frac{F_3 + S_3\omega - F_4 - S_4\omega}{m_3\omega^2}$$

Finally, the term x_1'' in the expressions of $D(4), D(6), D(8), D(10)$ is substituted by $D(2)$ for its solution. Full Matlab code can be reviewed in appendix section of this document.

The masses assigned to the model are the ones obtained from the Makita rotary hammer presented in chapter 3. The stiffness of the springs and the damping coefficients elected in previous section are suitable for this model.

The mass of hammer case including piston (m_1) is 4.175 kg. The mass of the striker (m_2) is 0.075 kg, whereas the mass of the chisel (m_3) is 0.25 kg. The angular velocity of the piston (excitation frequency) is 100 rad/s ≈ 950 rpm. The damping coefficients between each impact are c_1 = 20 kg/s; c_2 = 5 kg/s; c_3 = 5 kg/s; c_4 = 2 kg/s; c_R = 2 rad/s. The stiffness of the hand-arm system is k_1=10000 N/m. The stiffness of the springs that represent impacts are k_2=10000 N/m; k_3=100000 N/m; k_4=200000 N/m. The radius of the drums is R=0.05 m. The amplitude of the piston translation is z_0 = 0.01 [m], and the handle initial displacement is e_0 = 0.02 [m].

Due to the complexity of this new system, the mass of the spheres is determined from trial and error, by running the code several times until a proper value is found. A mass of 0.05 kg allows the system to absorb the produced vibrations of x_1.

Then, with the density of the steel $\rho = 7850\ kg/m^3$ the radius of the spheres is computed.

$$r = \sqrt[3]{\frac{3\ (0.05\ kg)}{4\pi(7850\frac{kg}{m^3})}} = 0.0115\ m = 11.5\ mm$$

Consequently, the system is solved with these parameters and the results are shown in Figure 69. For this case, initial positions of the spheres were α_1, α_3 = 2.8 rad; α_2, α_4 = 3.2 rad.

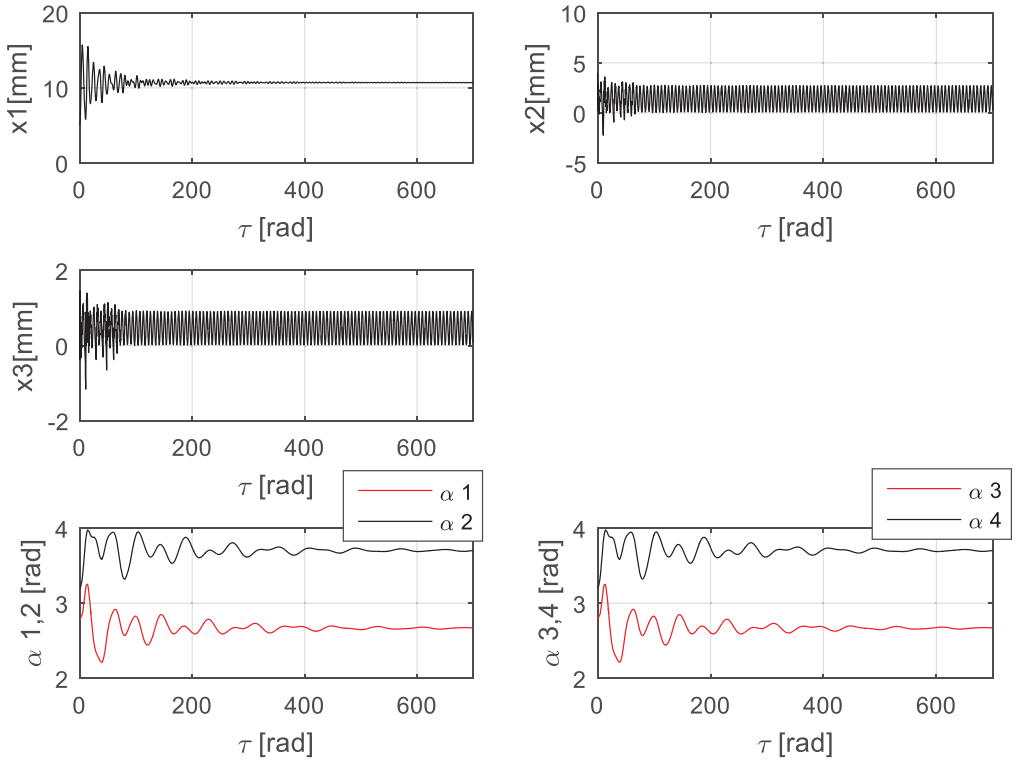

Figure 69. Vibrations of the rotary hammer with 4-ball DEV

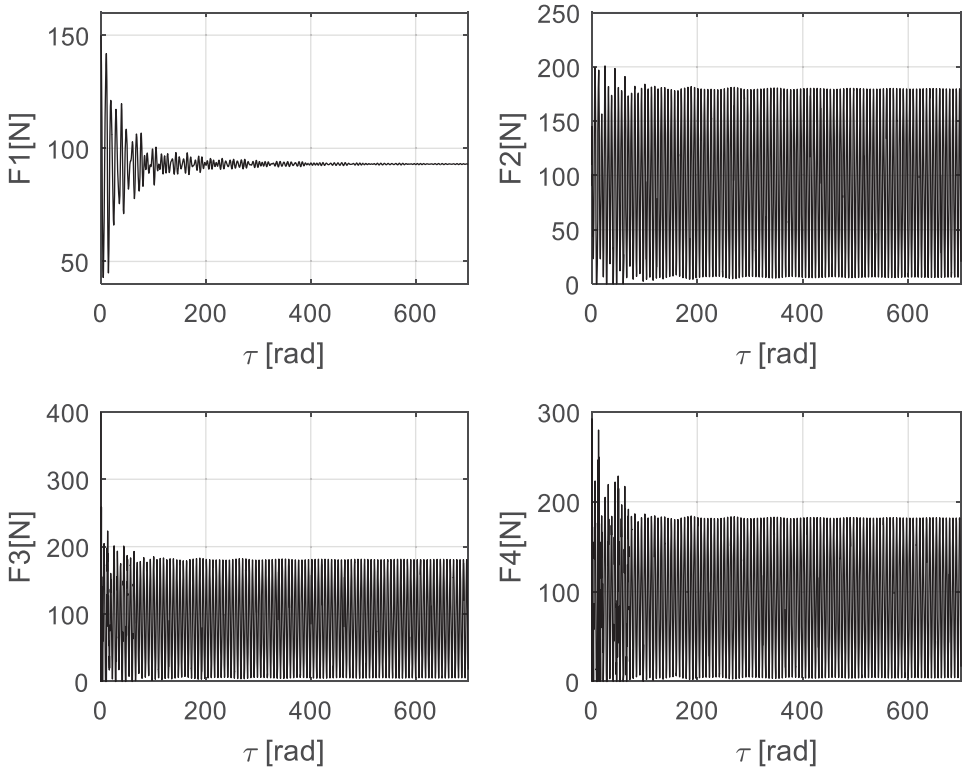

Figure 70. Forces in rotary hammer with 4-ball DEV

Final position of free elements			
Left drum		Right drum	
α_3	2.6703 rad 153°	α_1	2.6703 rad 153°
α_4	3.7026 rad 212.14°	α_2	3.7026 rad 212.14°

Table 9. Equilibrium position of free elements in DEV application to rotary hammer

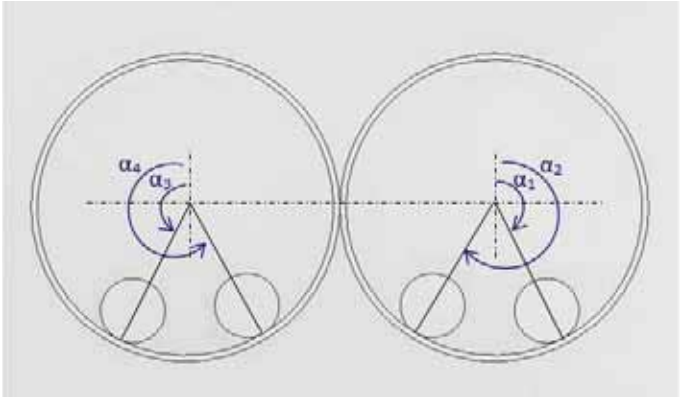

Figure 71. Equilibrium position diagram for DEV

Vibrations are reduced from 5 mm of initial amplitude to 0.07 mm in just 4 seconds. After 6 seconds vibrations practically disappear.

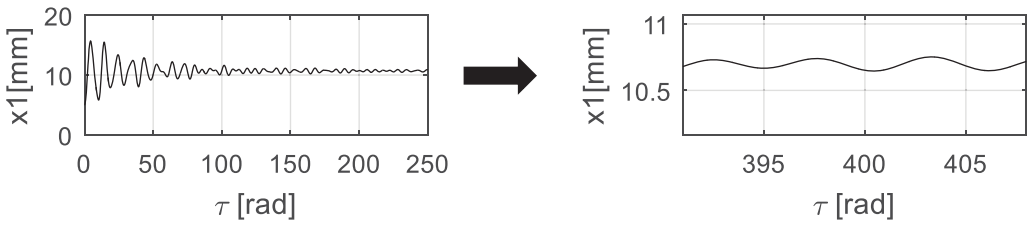

Figure 72. Vibrations absorption

Vibrations of the chisel as well as the exerted forces on the ground behave in the following way. Amplification is done to Figure 69 and Figure 70 for better appreciation of vibrations.

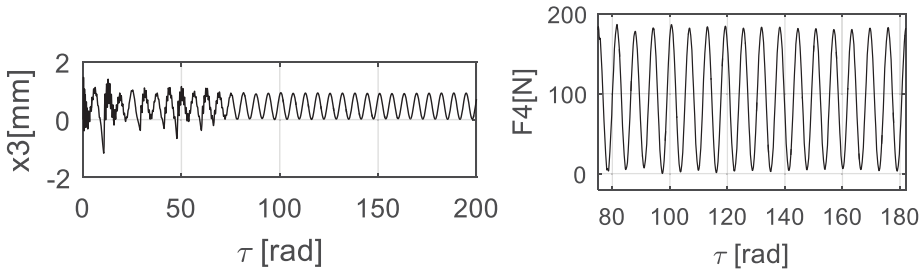

Figure 73. Vibrations of the chisel

A second experiment is run to explore the effect of the viscous damping (produced by the fluid inside the drums) on the movement of the main body or hammer case.

If the viscous damping for the spheres is increased by 4 times (c_R = 8 rad/s) vibrations are fully damped in approximately 3.5 seconds. Also, it is easier for the free elements to find and stay in the equilibrium position because the residual forces that try to push them away from this position are not enough to overcome the viscous damping force. This can be seen in Figure 74.

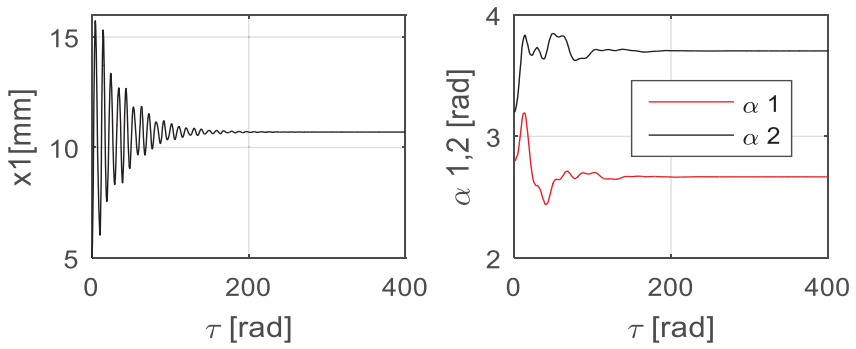

Figure 74. Influence of increase in viscous damping coefficient.

However, if the viscous damping coefficient is now reduced 4 times (c_R = 0.5 rad/s) is not possible of the DEV to eliminate the vibrations of the main body.

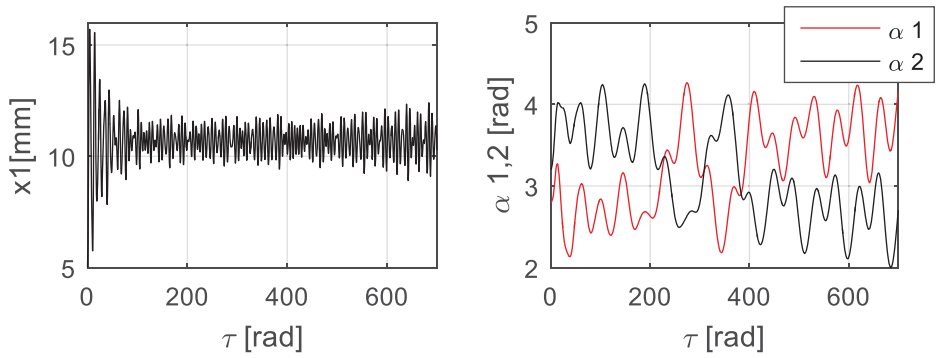

Figure 75. Influence of reduction in viscous damping coefficient.

As it can be observed in Figure 75, where x_1 is plotted against τ, the free elements inside the drum are not able to find a stable position that can counteract the forces exerted on the main body due to the excitation of the system. In this case other parameters such as the mass of the spheres would need to be adjusted to explore the possibility of damping vibrations.

It is also important to mention that Forces F_2, F_3 and F_4 are not really affected by the increase or reduction of the viscous damping coefficient, their magnitude remains almost

the same. Full results of these experiments can be seen in the appendix section of this document.

5.3 Mathematical modelling of rotary hammer with DEV analyzed in two directions (model with 2 drums and 4 spheres)

The next stage of this work is to analyze the system developed in the previous section but in two directions of the coordinate system. Now, translation is not only considered in the vertical direction (x axis) but also in the horizontal one (y axis) for the main body. Bodies 3, 4 that represent the striker and chisel in the system are only analyzed in the x axis.

Moreover, a spring is added to the rotary hammer that actuates in y-direction and represents the stiffness of the user's hand-arm system and the force exerted by actuating the tool. Besides, a damper is also added representing natural conditions of the vibration attenuating process.

It is important to mention that this damping coefficient added to the system of equations is needed to show the vibrations amplitude reduction in both directions. This happens because a DEV is only capable of damping excited vibrations but it cannot absorb the vibrations produced by the natural frequencies of a system. In this case, the excitation is only provided in the vertical direction, therefore DEV does not really work for the horizontal direction.

The system's equations are very similar to those presented in section 5.2.

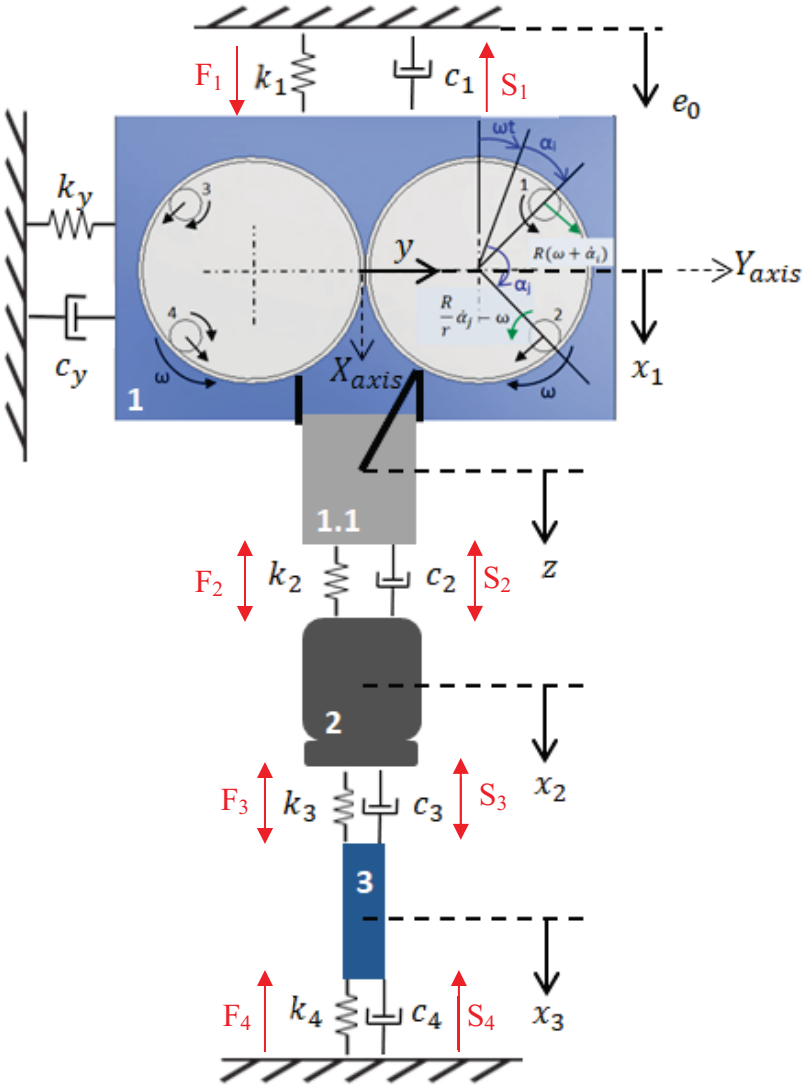

Spring forces

$$F_1 = k_1(e_0 - x_1)$$

$$F_2 = k_2\,(x_1 + z - x_2)$$

$$F_3 = k_3(x_2 - x_3)$$

$$F_4 = k_4 x_3$$

$$F_y = k_y y$$

Damper forces

$$S_1 = c_1 \dot{x}_1$$

$$S_2 = c_2\,(\dot{x}_1 + \dot{z} - \dot{x}_2)$$

$$S_3 = c_3(\dot{x}_2 - \dot{x}_3)$$

$$S_4 = c_4 \dot{x}_3$$

$$S_y = c_y \dot{y}$$

Figure 76. Rotary Hammer with DEV (XY analysis)

The special condition for the springs that represent an impact is also added as:

$$F_i = \begin{Bmatrix} F_i, & if\ \Delta x \geq 0 \\ 0, & if\ \Delta x < 0 \end{Bmatrix}, \qquad for\ i = 2,3,4$$

Lagrange equations method is applied for each of the independent coordinates. The development of the equations for x_1'', x_2'', x_3'' is already presented in section 5.2 for equations (5.5)-(5.7). For the new independent degree of freedom, associated with vibrations along the horizontal axis, named as Y, the equation is obtained as follows.

$$V_{xi} = \dot{x} + R(\omega + \dot{\alpha}_i)\sin(\omega t + \alpha_i) \quad \text{for } i = 1,2,3,4$$

$$V_{yi} = \dot{y} + R(\omega + \dot{\alpha}_i)\cos(\omega t + \alpha_i) \quad \text{for } i = 1,2$$

$$V_{yi} = \dot{y} - R(\omega + \dot{\alpha}_i)\cos(\omega t + \alpha_i) \quad \text{for } i = 3,4$$

$$V_i^2 = V_{xi}^2 + V_{yi}^2$$

Kinetic and potential energy are expressed as defined by the Lagrange equation as:

$$\frac{d}{dt}\left(\frac{\partial T}{\partial \dot{q}_i}\right) - \frac{\partial T}{\partial q_i} + \frac{\partial V}{\partial q_i} = Q_i$$

Kinetic energy:

$$T = \frac{1}{2}\left[M\ddot{x}^2 + M\ddot{y}^2 + m_b V_1^2 + m_b V_2^2 + m_b V_3^2 + m_b V_4^2 + B\left(\frac{R}{r}\dot{\alpha}_1 - \omega\right)^2 + B\left(\frac{R}{r}\dot{\alpha}_2 - \omega\right)^2 + B\left(\omega - \frac{R}{r}\dot{\alpha}_3\right)^2 + B\left(\omega - \frac{R}{r}\dot{\alpha}_4\right)^2\right]$$

$$\rightarrow T = \frac{1}{2}\left[M(\ddot{x}^2 + \ddot{y}^2) + m_b\sum_{i=1}^{n} V_i^2 + B\sum_{i=1}^{2}\left(\frac{R}{r}\dot{\alpha}_i - \omega\right)^2 + B\sum_{i=3}^{4}\left(\omega - \frac{R}{r}\dot{\alpha}_i\right)^2\right] \quad (5.9)$$

Potential energy due to springs:

$$V = \frac{1}{2}\left[k_1(e_0 - x_1)^2 + k_2(x_1 + z - x_2)^2 + k_3(x_2 - x_3)^2 + k_4 x_3^2 + k_y y^2\right] \quad (5.10)$$

Non-conservative forces are obtained from virtual work equation ($\delta W = F\delta x + T\delta\alpha = Q_X\delta x + Q_\alpha\delta\alpha$). These forces are caused by damper action:

$$\delta W = (-S_1 - S_2)\delta x_1 + (S_2 - S_3)\delta x_2 + (S_3 - S_4)\delta x_3 + S_y\delta y + c_r mR^2[\dot{\alpha}_1\delta\alpha_1 + \dot{\alpha}_2\delta\alpha_2 + \dot{\alpha}_3\delta\alpha_3 + \dot{\alpha}_4\delta\alpha_4]$$

$$Qx_1 = (-S_1 - S_2) = -c_1\dot{x}_1 - c_2(\dot{x}_1 + \dot{z} - \dot{x}_2) \quad (5.11)$$

$$Qx_2 = (S_2 - S_3) = c_2(\dot{x}_1 + \dot{z} - \dot{x}_2) - c_3(\dot{x}_2 - \dot{x}_3) \quad (5.12)$$

$$Qx_3 = (S_3 - S_4) = c_3(\dot{x}_2 - \dot{x}_3) - c_4\dot{x}_3 \tag{5.13}$$

$$Qy = S_y = c_y\dot{y} \tag{5.14}$$

$$Q\alpha_i = c_r m R^2 \dot{\alpha}_i \; with \; i = 1,2,3,4 \tag{5.15}$$

Therefore,

The Lagrange's equations derivatives are obtained as mentioned in equation (3.1) for each one of the independent degrees of freedom. From there a differential equation is built for each variable in the system. Equations are solved for the main variable on each case in the same manner as it was done on section 3.3 and the results are shown below:

$$\ddot{x}_1 = \frac{1}{m_1 + nm_b}\left\{-m_b R\left[\sum_{i=1}^{n}(\omega + \dot{\alpha}_i)^2\cos(\omega t + \alpha_i) + \sum_{i=1}^{n}\ddot{\alpha}_i \sin(\omega t + \alpha_i)\right] + F_1 - S_1\omega - F_2 - S_2\omega\right\} \tag{5.16}$$

$$\ddot{y} = \frac{1}{m_1 + nm_b}\left\{m_b R\left[\sum_{i=1}^{2}(\omega + \dot{\alpha}_i)^2\sin(\omega t + \alpha_i) - \sum_{i=3}^{4}(\omega + \dot{\alpha}_i)^2\sin(\omega t + \alpha_i) - \sum_{i=1}^{2}\ddot{\alpha}_i\cos(\omega t + \alpha_i) + \sum_{i=3}^{4}\ddot{\alpha}_i\cos(\omega t + \alpha_i)\right] - F_y - S_y\right\} \tag{5.17}$$

$$\ddot{x}_2 = \frac{F_2 + S_2 - F_3 - S_3}{m_2} \tag{5.18}$$

$$\ddot{x}_3 = \frac{F_3 + S_3 - F_4 - S_4}{m_3} \tag{5.19}$$

$$\ddot{\alpha}_i = \frac{m_b R}{meq}\left[-sin(\omega t + \alpha_i)\ddot{x}_1 - cos(\omega t + \alpha_i)\ddot{y} - c_r R\dot{\alpha}_i\right], \qquad for \; i = 1,2 \tag{5.20}$$

$$\ddot{\alpha}_i = \frac{m_b R}{meq}\left[-sin(\omega t + \alpha_i)\ddot{x}_1 + cos(\omega t + \alpha_i)\ddot{y} - c_r R\dot{\alpha}_i\right], \qquad for \; i = 3,4 \tag{5.21}$$

In $\ddot{x}_1$ the $\sum_{i=1}^{n} \ddot{\alpha}_i \sin(\omega t + \alpha_i)$ is neglected due to the small impact it has on the equation, as well as the terms $[-\sum_{i=1}^{2} \ddot{\alpha}_i \cos(\omega t + \alpha_i) + \sum_{i=3}^{4} \ddot{\alpha}_i \cos(\omega t + \alpha_i)]$ for the $\ddot{y}$ equation, where the value of this part of the equation is very small compared to the other terms.

Then, these equations are solved for the main independent variable on each case and ωt is again substituted by time τ.

$$\tau = \omega t \rightarrow \frac{d\tau}{dt} = \omega \; and \; \frac{dx}{dt} = \frac{dx}{d\tau}\frac{d\tau}{dt} = \omega \frac{dx}{d\tau}$$

$$x_1'' = \frac{1}{m_1 + n m_b}\left\{-m_b R\left[\sum_{i=1}^{n}(1+\alpha_i')^2 \cos(\tau + \alpha_i)\right] + \frac{F_1 - S_1\omega - F_2 - S_2\omega}{\omega^2}\right\} \quad (5.22)$$

$$y'' = \frac{1}{m_1 + n m_b}\left\{m_b R\left[\sum_{i=1}^{2}(1+\alpha_i')^2 \sin(\tau + \alpha_i) - \sum_{i=3}^{4}(1+\alpha_i')^2 \sin(\tau + \alpha_i)\right] - \frac{F_y}{\omega^2} - \frac{S_y}{\omega}\right\} \quad (5.23)$$

$$x_2'' = \frac{F_2 + S_2\omega - F_3 - S_3\omega}{m_2\omega^2} \quad (5.24)$$

$$x_3'' = \frac{F_3 + S_3\omega - F_4 - S_4\omega}{m_3\omega^2} \quad (5.25)$$

$$\alpha_i'' = \frac{mR}{meq}\left[-sin(\tau + \alpha_i)x_1'' - cos(\omega t + \alpha_i)y'' - \frac{c_r R \alpha_i'}{\omega}\right] \qquad for\ i = 1{,}2 \quad (5.26)$$

$$\alpha_i'' = \frac{mR}{meq}\left[-sin(\tau + \alpha_i)x_1'' + cos(\omega t + \alpha_i)y'' - \frac{c_r R \alpha_i'}{\omega}\right] \qquad for\ i = 3{,}4 \quad (5.27)$$

5.3.2 Matlab application

Due to the complexity of the system, the second degree differential equations are converted into first degree equations for its solution in Matlab. Similar to what was done for the other models, the system is solved with function ode45. The complete code is showed in

Appendix A. The 1st degree equations are presented here as well as the results of the simulation.

The degrees of freedom and their first derivatives are listed in this way for Matlab solution:

$x(1) = x_1$	$x(5) = \alpha_1$	$x(9) = \alpha_3$	$x(13) = x_2$
$x(2) = x_1'$	$x(6) = \alpha_1'$	$x(10) = \alpha_3'$	$x(14) = x_2'$
$x(3) = y$	$x(7) = \alpha_2$	$x(11) = \alpha_4$	$x(15) = x_3$
$x(4) = y'$	$x(8) = \alpha_2'$	$x(12) = \alpha_4'$	$x(16) = x_3'$

Then, the system of equations is now defined as:

$$D(1) = \frac{dx_1}{d\tau} = x_1' = x(2)$$

$$D(2) = \frac{d^2x_1}{d\tau^2} = x_1'' = \frac{1}{m_1 + nm_b}\left\{-m_bR\left[\sum_{i=1}^{n}(1+\alpha_i')^2\cos(\tau+\alpha_i)\right] + \frac{F_1 - S_1\omega - F_2 - S_2\omega}{\omega^2}\right\}$$

$$D(3) = \frac{dy}{d\tau} = y' = x(4)$$

$$D(4) = \frac{d^2y}{d\tau^2} = y'' = \frac{1}{m_1 + nm_b}\left\{\begin{array}{c} m_bR\left[\sum_{i=1}^{2}(1+\alpha_i')^2\sin(\tau+\alpha_i) - \sum_{i=3}^{4}(1+\alpha_i')^2\sin(\tau+\alpha_i)\right] \\ -\frac{F_y}{\omega^2} - \frac{S_y}{\omega} \end{array}\right\}$$

$$D(5) = \frac{d\alpha_1}{d\tau} = \alpha_1' = x(6)$$

$$D(6) = \frac{d^2\alpha_1}{d\tau^2} = \alpha_1'' = \frac{m_bR}{meq}\left[-sin(\tau+\alpha_1)x_1'' - cos(\omega t+\alpha_1)y'' - \frac{c_rR\alpha_1'}{\omega}\right]$$

$$D(7) = \frac{d\alpha_2}{d\tau} = \alpha_2' = x(8)$$

$$D(8) = \frac{d^2\alpha_2}{d\tau^2} = \alpha_2'' = \frac{m_bR}{meq}\left[-sin(\tau+\alpha_2)x_1'' - cos(\omega t+\alpha_2)y'' - \frac{c_rR\alpha_2'}{\omega}\right]$$

$$D(9) = \frac{d\alpha_3}{d\tau} = \alpha_3' = x(10)$$

$$D(10) = \frac{d^2\alpha_3}{d\tau^2} = \alpha_3'' = \frac{m_bR}{meq}\left[-sin(\tau+\alpha_3)x_1'' + cos(\omega t+\alpha_3)y'' - \frac{c_rR\alpha_3'}{\omega}\right]$$

$$D(11) = \frac{\alpha_4}{d\tau} = \alpha_4' = x(12)$$

$$D(12) = \frac{d^2\alpha_4}{d\tau^2} = \alpha_4'' = \frac{m_b R}{meq}\left[-sin(\tau + \alpha_4)x_1'' + cos(\omega t + \alpha_4)y'' - \frac{c_r R \alpha_4'}{\omega}\right]$$

$$D(13) = \frac{dx_2}{d\tau} = x_2' = x(14)$$

$$D(14) = \frac{d^2x_2}{d\tau^2} = x_2'' = \frac{F_2 + S_2\omega - F_3 - S_3\omega}{m_2\omega^2}$$

$$D(15) = \frac{dx_3}{d\tau} = x_3' = x(16)$$

$$D(16) = \frac{d^2x_3}{d\tau^2} = x_3'' = \frac{F_3 + S_3\omega - F_4 - S_4\omega}{m_3\omega^2}$$

For the Matlab code, the x_1'' and y'' terms that appear in equation of $D(6), D(8), D(10),$ $D(12)$ are substituted by their respective expression $D(2)$ and $D(4)$.

Almost the same parameters used for the unidirectional analysis are input to the system and the results are plotted with Matlab.

m_1=4.175 kg, m_2 = 0.075 kg, m_3 = 0.25 kg; mb=0.07 kg; ω = 100 rad/s; c_1 = 20 kg/s, c_2 = 5 kg/s, c_3 = 5 kg/s, c_4 = 5 kg/s, c_y = 20 kg/s cR = 2 rad/s; k_1=10000 N/m, k_2=10000 N/m, k_3=100000 N/m, k_4=200000 N/m; z_0 = 0.01 m; e_0 = 0.02 m. Radius of the drums R=0.05 m. Radius of the spheres r=0.0115 m

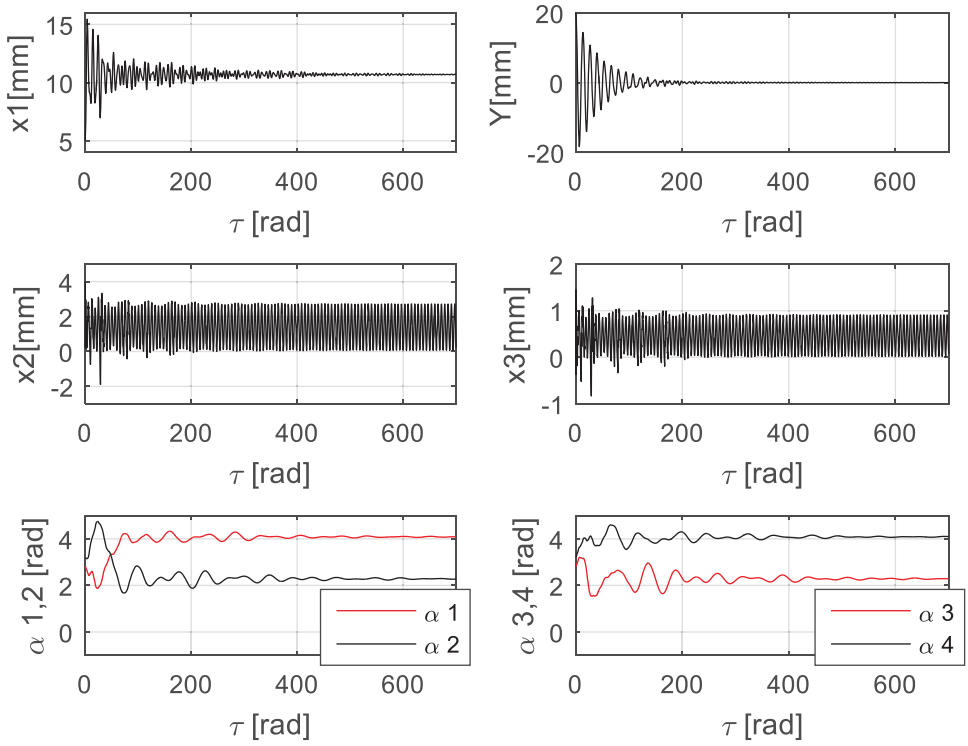

Figure 77. Vibrations in rotary hammer with 4-ball DEV

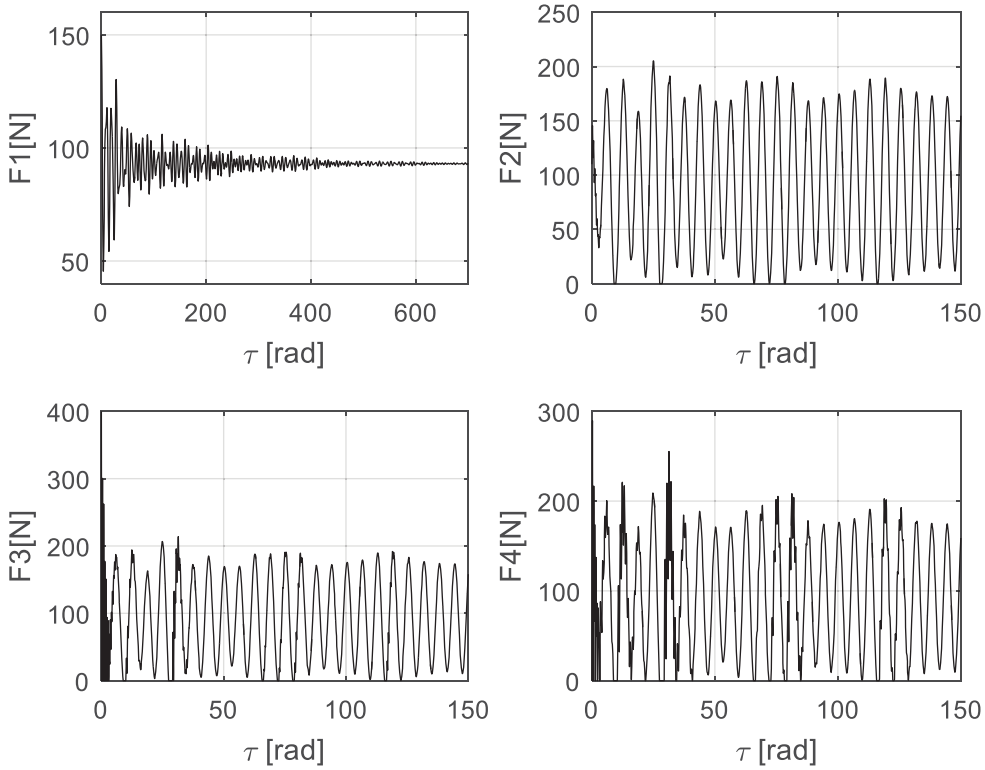

Figure 78. Forces in rotary hammer with 4-ball DEV

Adding the horizontal degree of freedom to the main body, does not really change the behaviour of the vibrations in x direction (vertical) and the forces produced by the impacts. Vibrations are again damped from 5.23 mm of amplitude to 0.05 mm after 6 seconds. However, equilibrium positions found by the free elements differ a little from what it was obtained in the model analyzed in just one direction.

Final position of free elements			
Left drum		Right drum	
α_3	2.2915 rad 131.29°	α_1	4.0857 rad 234.09°
α_4	4.0873 rad 234.18°	α_2	2.2949 rad 131.49°

Table 10. Equilibrium position of free elements in DEV application to rotary hammer

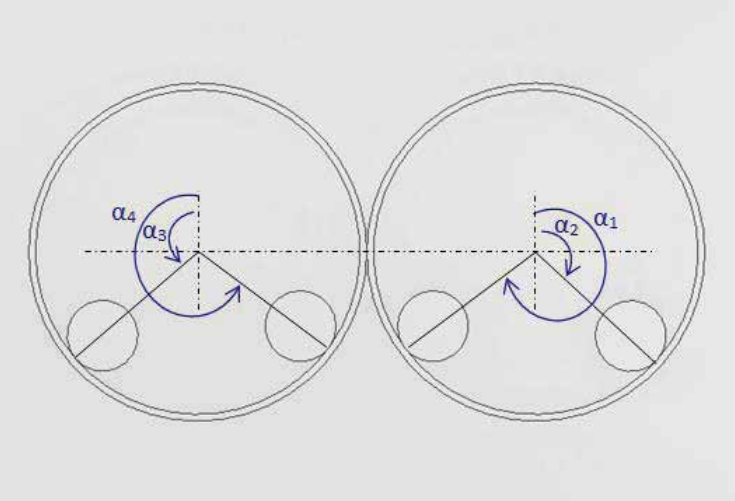

Figure 79. Equilibrium position diagram for DEV

With these results, it is clear that the Dynamic Eliminator of Vibrations is capable of absorbing the excitation produced by the piston movement in the dynamic model presented in section 4.4, where the amplitude of vibration of the system is 3.4 mm, once it is stable. Also, from the experiments performed on asphalt and concrete the frequency of the first harmonic is around 57.8 Hz for both tests. Therefore, this frequency is input as parameter for this system and the following results are obtained.

As the excitation frequency changes from 100 rad/s to 365 rad/s, a new mass needs to be determined in order to counteract the excitation force. As a starting point for the iterations the initial mass computed is:

$$m = \frac{\sqrt{[(20000N/m)(0.01m)]^2 + [(25kg/s)(365rad/s)(0.01m)]^2}}{4(0.05m)\left(\frac{365rad}{s}\right)^2} = 0.008\ kg$$

After some simulations optimal mass determined is: 0.007 kg. If free elements are to be steel balls, they would have a radius of 6 mm.

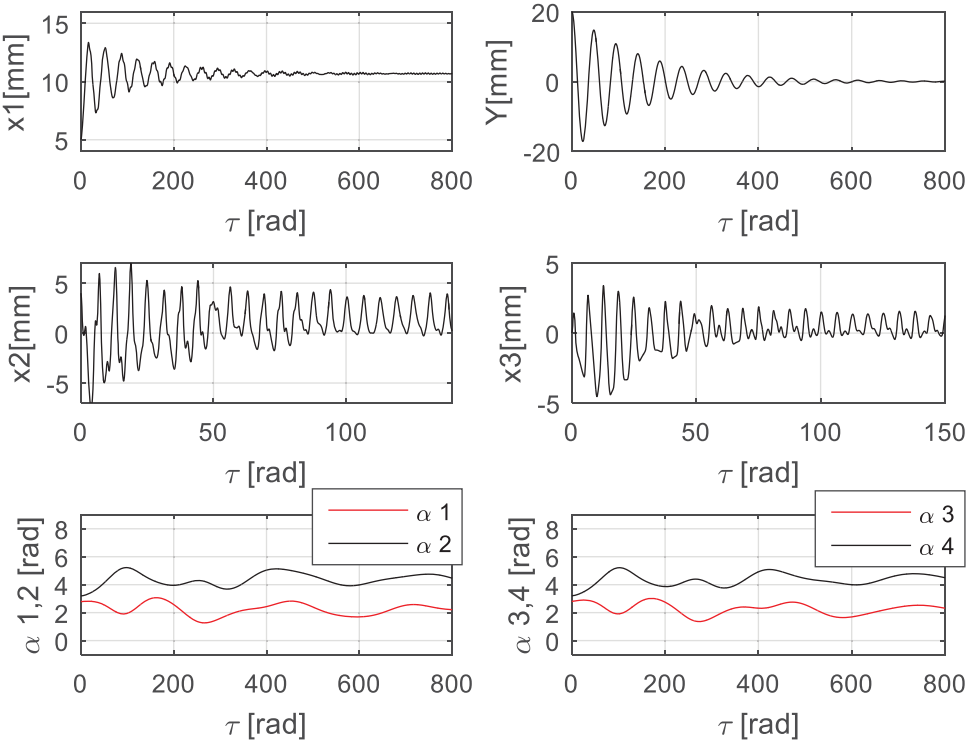

Figure 80. Vibrations results with f=57.8 Hz

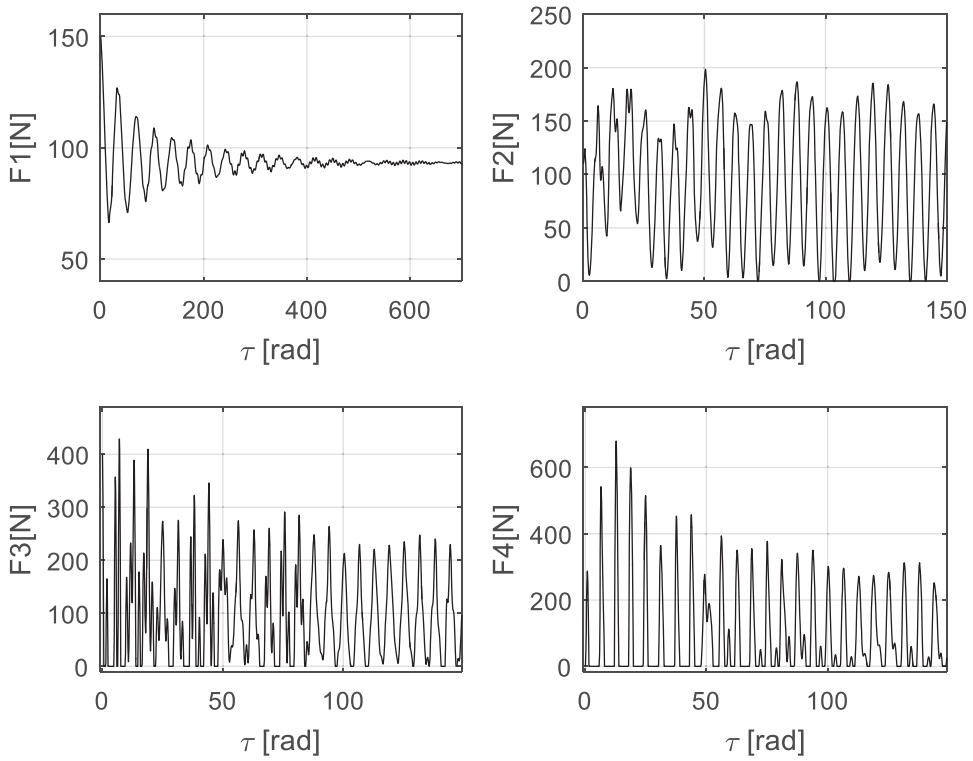

Figure 81. Forces of the system with f=57.8 Hz

Final position of free elements			
Left drum		Right drum	
α_3	2.3774 rad 136.2°	α_1	2.4136 rad 138.3°
α_4	4.5328 rad 259.7°	α_2	4.4816 rad 256.8°

Figure 82. Equilibrium positions when f=57.8 Hz

As the frequency of rotation of the drums is higher, the centrifugal force of the elements also increases. Therefore, less mass is needed to counteract the excitation force. Then, this space in this model can be optimized through several iterations of mass and radius of the spheres, resulting in smaller drums. The next iteration results in a mass of 20 grams (0.02 kg) and a sphere radius of 4 mm (for steel). This allows having a drum radius of 20 mm instead of 50 mm. This system results are presented in the next figure. It is important to mention that as ω=365 rad/s. Time of simulation ωt=1000 rad is equal to 2.74 seconds.

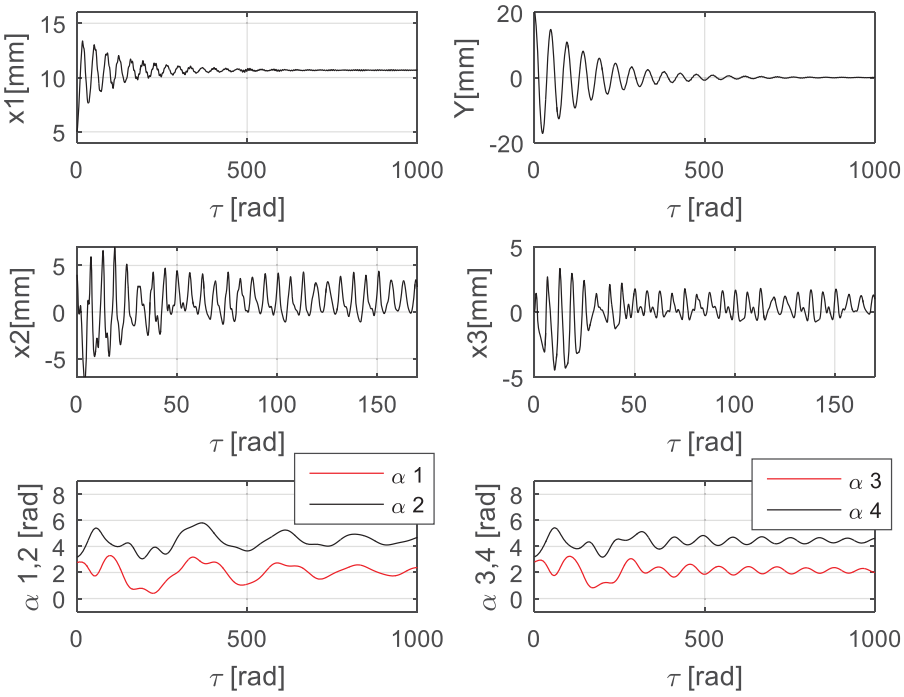

Figure 83. System's optimization results

In these two cases, vibrations seem to be damped faster; however, it is harder for the free elements to remain in the equilibrium position due to the high rotation velocities.

CHAPTER VI - Implementation of the DEV to the rotary hammer with the addition of the chisel chuck spring

6.1 Introduction

The working principle of the rotary hammer was examined more thoroughly and a new model was developed considering a condition that was not taken into account in the previous sections. This new model considers a spring connection between the hammer case and the chisel that transmits the vibrations directly to the main body without passing through the other components.

6.2 Modelling of rotary hammer - Dynamic model with chisel chuck spring

This model was developed due to the translation allowed to the chuck (1 in Figure 84) of the hammer relative to the tool itself. If force is applied to the tip of the chuck or the chisel, they can be contracted (towards the device) up to 17.5 mm. Once the force is removed, both components come back to their initial positions. This connection is done by a spring (2 in Figure 85) that is attached to the chuck (1) on one end and to a physical stop that is part of the rotary hammer on the other end. In this manner, the vibrations that travel along the chisel are not only transmitted to the striker on each impact, but they also enter directly to the rotary hammer case through this connection.

Figure 84. Rotary hammer chuck.

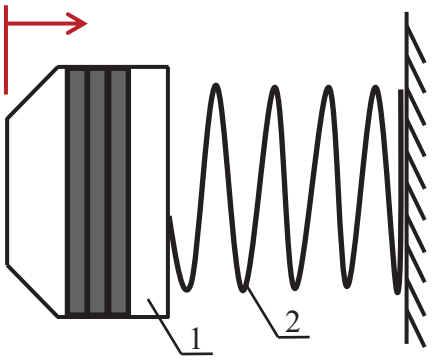

Figure 85. Chuck spring.

Thus, this connection is added to the model presented in Figure 63 (section 4.4) and the result is shown in Figure 86, where k_5 represents the chuck spring. All the variables used for the model presented in section 5.3 are applied in the same manner. The expression for the force of the chuck spring F_5 is defined in two parts. The first part considers the normal operating condition of the spring; whereas the second part considers a substantial increase in the stiffness of the spring referring to the moment when the spring goes to "solid state" (coils are in contact).

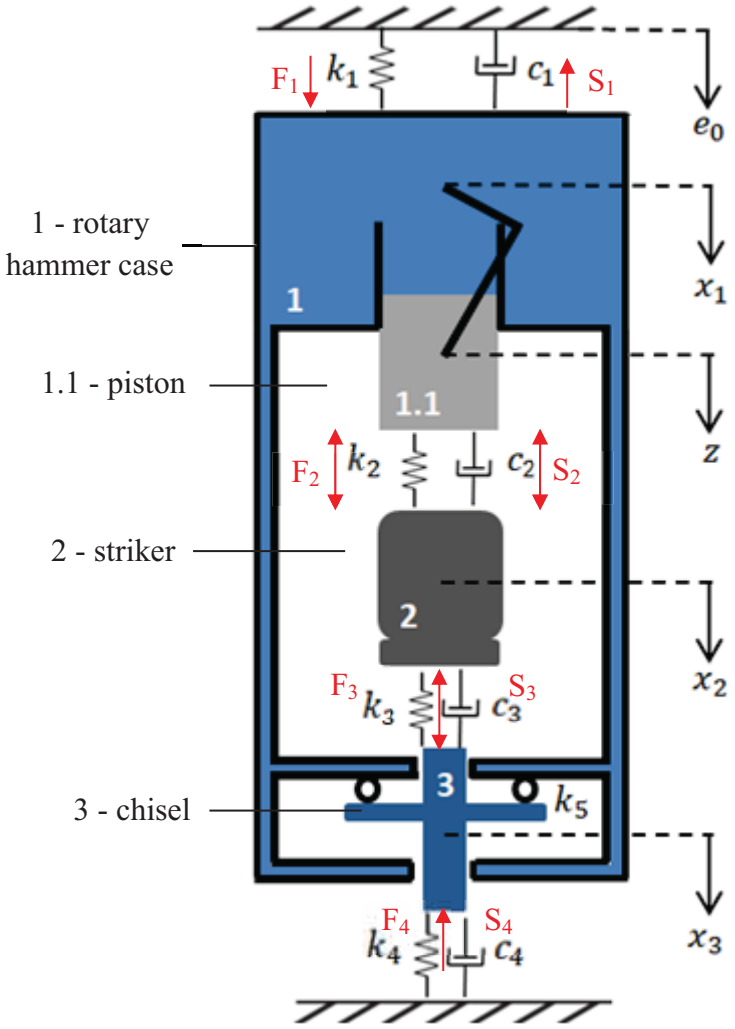

Figure 86. Rotary hammer with chuck spring

The forces that are acting over the rotary hammer are produced by the springs and dampers present in the system. These forces are defined as:

Springs	Dampers
$F_1 = k_1(e_0 - x_1)$	$S_1 = c_1\dot{x}_1$
$F_2 = k_2\,(x_1 + z - x_2)$	$S_2 = c_2\,(\dot{x}_1 + \dot{z} - \dot{x}_2)$
$F_3 = k_3(x_2 - x_3)$	$S_3 = c_3(\dot{x}_2 - \dot{x}_3)$
$F_4 = k_4 x_3$	$S_4 = c_4\dot{x}_3$

Special conditions:

$$F_i = \begin{Bmatrix} F_i, & if\ \Delta x \geq 0 \\ 0, & if\ \Delta x < 0 \end{Bmatrix}, \qquad for\ i = 2,3,4$$

$$F_5 = k_{51}(x_1 - x_3), \qquad for\ x_1 - x_3 < 14$$

$$F_5 = k_{51}(x_1 - x_3) + k_{52}e^{(x_1 - x_3)}, \qquad for\ 14 < x_1 - x_3 < 17.5$$

The governing equations of the system are:

$$m_1\frac{d^2x_1}{dt^2} = F_1 - S_1 - F_2 - S_2 - F_5 \tag{6.1}$$

$$m_2\frac{d^2x_2}{dt^2} = F_2 + S_2 - F_3 - S_3 \tag{6.2}$$

$$m_3\frac{d^2x_3}{dt^2} = F_3 + S_3 - F_4 - S_4 + F_5 \tag{6.3}$$

The system of equations is solved using Matlab and the results can be seen in section 6.2.1 of this document.

6.2.1 Matlab application

$x(1) = x_1$	$x(3) = x_2$	$x(5) = x_3$
$x(2) = \dot{x}_1$	$x(4) = \dot{x}_2$	$x(6) = \dot{x}_3$

Furthermore, the system of equations is defined as:

$$D(1) = \frac{dx_1}{dt} = \dot{x}_1 = x(2)$$

$$D(2) = \frac{d^2x_1}{dt^2} = \ddot{x}_1 = \frac{F_1 - S_1 - F_2 - S_2 - F_5}{m_1}$$

$$D(3) = \frac{dx_2}{dt} = \dot{x}_2 = x(4)$$

$$D(4) = \frac{d^2x_2}{dt^2} = \ddot{x}_2 = \frac{F_2 + S_2 - F_3 - S_3}{m_2}$$

$$D(5) = \frac{dx_2}{dt} = \dot{x}_3 = x(6)$$

$$D(6) = \frac{d^2x_3}{dt^2} = \ddot{x}_3 = \frac{F_3 + S_3 - F_4 - S_4 + F_5}{m_3}$$

The system is solved with Matlab and the obtained results are shown as follows.

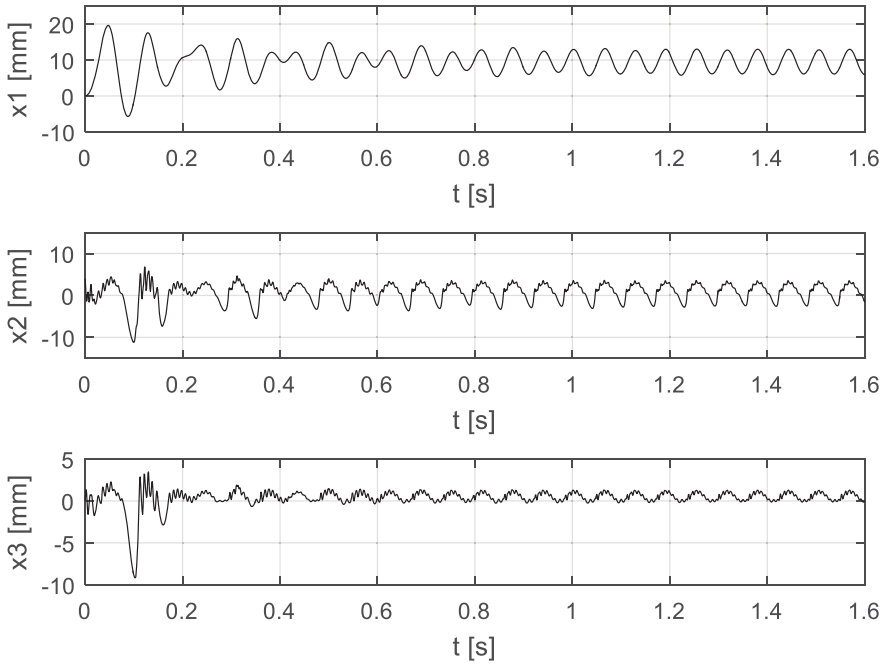

Figure 87. Rotary hammer vibrations (model with chuck spring)

The first peaks of vibration of the rotary hammer in Figure 87 vary around 12.5 mm of amplitude, however, once free vibrations are damped, vibrations of the system reach a steady state were the amplitude of vibrations produced by the external excitation is of 3.7

mm. The plot of x_3 shows several impacts with small amplitudes during one second, which represents the penetration of the chisel into the impacted surface.

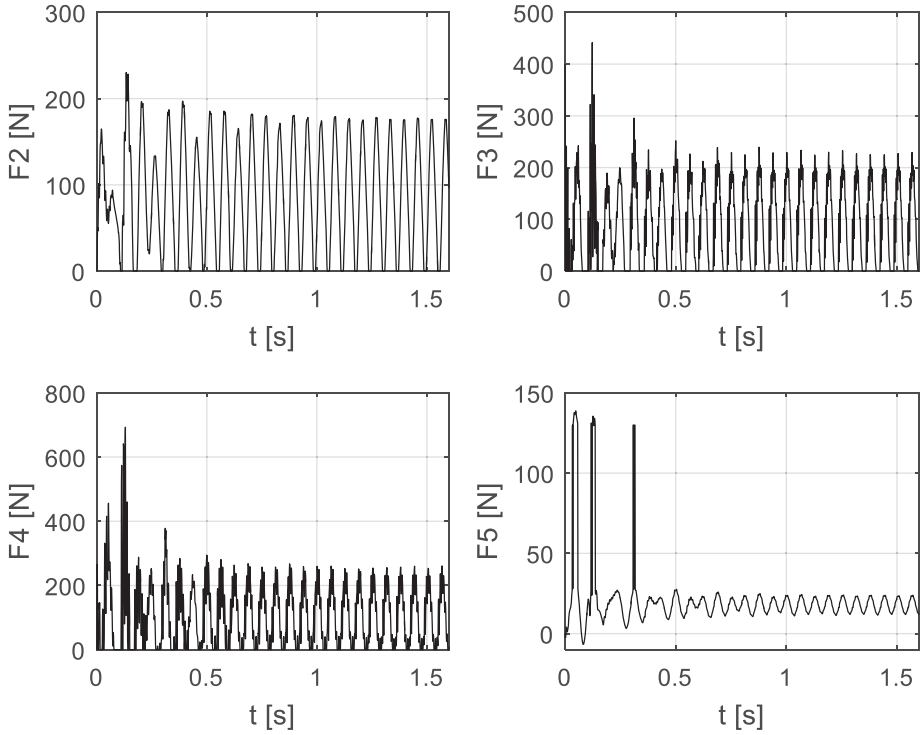

Figure 88. Rotary hammer forces

In the plot for F_5 seen in Figure 88, there are 3 peaks that reach up to 140 N, whereas, after 0.5 seconds, the force shows a periodic value of 25 N. This phenomenon happens in the beginning when the chisel chuck spring is taken to solid state, which increases the stiffness and the reaction force of the spring.

For the input parameters given, the chisel hits the ground with a force of 260 N (F_4) once vibrations have reached a steady state.

This model shows a more approximate approach to the real hammer behaviour and the complexity of impacts production.

6.3 Mathematical modelling of rotary hammer with chisel spring connection and DEV implementation (2 directions, 2 drums, 4 spheres)

The Dynamic Eliminator of Vibrations is implemented to the new rotary hammer model, to determine the possibility of damping the vibrations produced by the new rotary hammer model proposed.

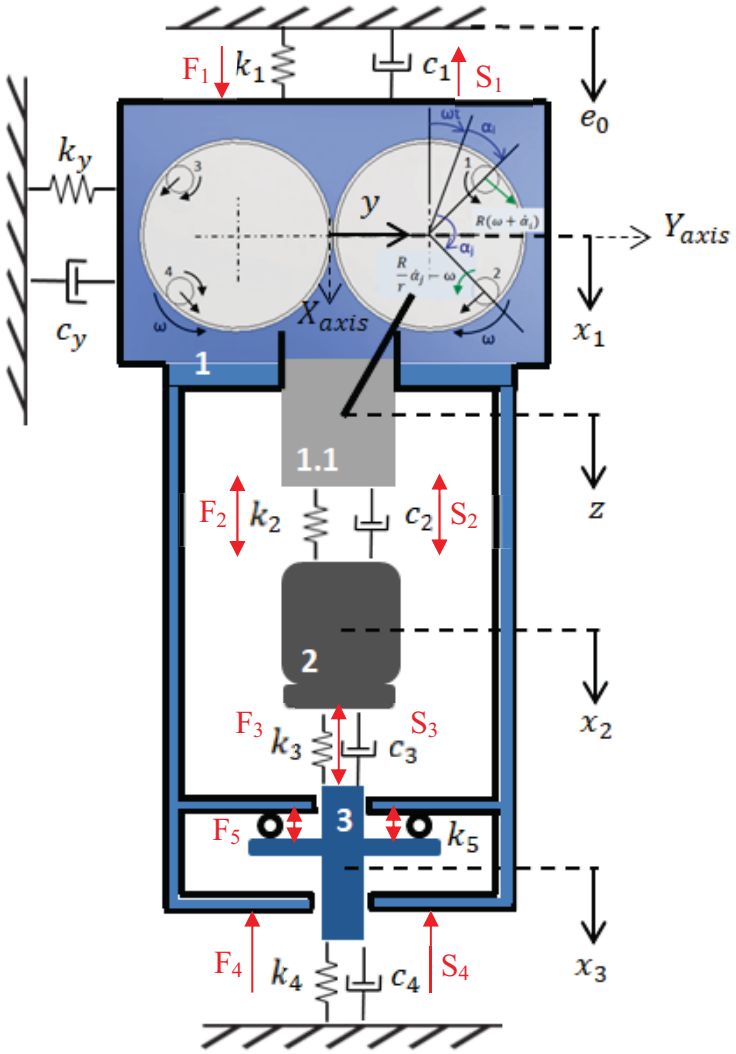

Spring force F_5

For $x_1 - x_3 < 14$

$$F_5 = k_{51}(x_1 - x_3)$$

For $14 < x_1 - x_3 < 17.5$

$$F_5 = k_{51}(x_1 - x_3) + k_{52}e^{(x_1 - x_3)}$$

Special condition

$$F_{2,3,4} = \begin{Bmatrix} F_{2,3,4}, & if\ \Delta x \geq 0 \\ 0, & if\ \Delta x < 0 \end{Bmatrix}$$

Figure 89. Rotary hammer with DEV and chuck spring

The governing equations for the system presented in Figure 89 are very similar to what it was developed on equations (5.22) - (5.27). The new F_5 only affects the equations for the main body x_1'' and for the chisel x_3''.

$$x_1'' = \frac{1}{m_1 + nm_b}\left\{-m_b R\left[\sum_{i=1}^{n}(1+\alpha_i')^2\cos(\tau+\alpha_i)\right] + \frac{F_1 - S_1\omega - F_2 - S_2\omega - F_5}{\omega^2}\right\} \quad (5.28)$$

$$y'' = \frac{1}{m_1 + nm_b}\left\{m_b R\left[\sum_{i=1}^{2}(1+\alpha_i')^2\sin(\tau+\alpha_i) - \sum_{i=3}^{4}(1+\alpha_i')^2\sin(\tau+\alpha_i)\right] - \frac{F_y}{\omega^2} - \frac{S_y}{\omega}\right\} \quad (5.29)$$

$$x_2'' = \frac{F_2 + S_2\omega - F_3\omega - S_3\omega}{m_2\omega^2} \quad (5.30)$$

$$x_3'' = \frac{F_3 + S_3\omega - F_4 - S_4\omega + F_5}{m_3\omega^2} \quad (5.31)$$

$$\alpha_i'' = \frac{mR}{meq}\left[-sin(\tau+\alpha_i)x_1'' - cos(\omega t+\alpha_i)y'' - \frac{c_r R\alpha_i'}{\omega}\right] \qquad for\ i = 1,2 \quad (5.32)$$

$$\alpha_i'' = \frac{mR}{meq}\left[-sin(\tau+\alpha_i)x_1'' + cos(\omega t+\alpha_i)y'' - \frac{c_r R\alpha_i'}{\omega}\right] \qquad for\ i = 3,4 \quad (5.33)$$

The system is solved using Matlab as it was done for previous applications. The results are presented in section 5.4.2.

6.3.1 Matlab Application

The solution for the system of equations is obtained with Matlab. The variables are assigned as it was mentioned in section 5.3.2, as well as the equations written in the Matlab code. F_5, generated by the chisel chuck spring, is added to the 1st order differential equations that define the acceleration of the main body and the chisel.

$x(1) = x_1$	$x(5) = \alpha_1$	$x(9) = \alpha_3$	$x(13) = x_2$
$x(2) = x_1'$	$x(6) = \alpha_1'$	$x(10) = \alpha_3'$	$x(14) = x_2'$
$x(3) = y$	$x(7) = \alpha_2$	$x(11) = \alpha_4$	$x(15) = x_3$
$x(4) = y'$	$x(8) = \alpha_2'$	$x(12) = \alpha_4'$	$x(16) = x_3'$

Equations for the main body:

$$D(1) = \frac{dx_1}{d\tau} = x_1' = x(2)$$

$$D(2) = \frac{d^2x_1}{d\tau^2} = x_1'' = \frac{1}{m_1 + nm_b}\left\{-m_b R\left[\sum_{i=1}^{n}(1+\alpha_i')^2\cos(\tau+\alpha_i)\right] + \frac{F_1 - S_1\omega - F_2 - S_2\omega - F_5}{\omega^2}\right\}$$

Equations for the chisel:

$$D(15) = \frac{dx_3}{d\tau} = x_3' = x(16)$$

$$D(16) = \frac{d^2x_3}{d\tau^2} = x_3'' = \frac{F_3 + S_3\omega - F_4 - S_4\omega + F_5}{m_3\omega^2}$$

The rest of the equations are identical to the ones presented in section 5.3.2. Full Matlab code is included in Appendix A.

The system is solved with the following input parameters.

n=8 DOF, m_1 = 4.175 kg, m_2 = 0.075 kg, m_3 = 0.25 kg; ω=100 rad/s; c_1 = 20 kg/s, c_2 = 5 kg/s, c_3 = 5 kg/s, c_4 = 2 kg/s, c_R = 5 rad/s; k_1=10000 N/m, k_2=10000 N/m, k_3=100000 N/m, k_4=200000 N/m; k_{51} = 2000 N/m; k_{52} = 100 Nm; z_0 = 0.01 m; e = 0.02 m; R=0.05 m; m_b= 0.1 kg.

The radius of the spheres is computed with the proposed mass and the density of the steel.

$$r = \sqrt[3]{\frac{3\ (0.1\ kg)}{4\pi(7850\frac{kg}{m^3})}} = 0.0145\ m = 14.5\ mm$$

The vibrations produced by the rotary hammer with this configuration and the implementation of a 4-ball DEV are presented in Figure 90. Moreover, the forces produced on each impact are plotted in Figure 91.

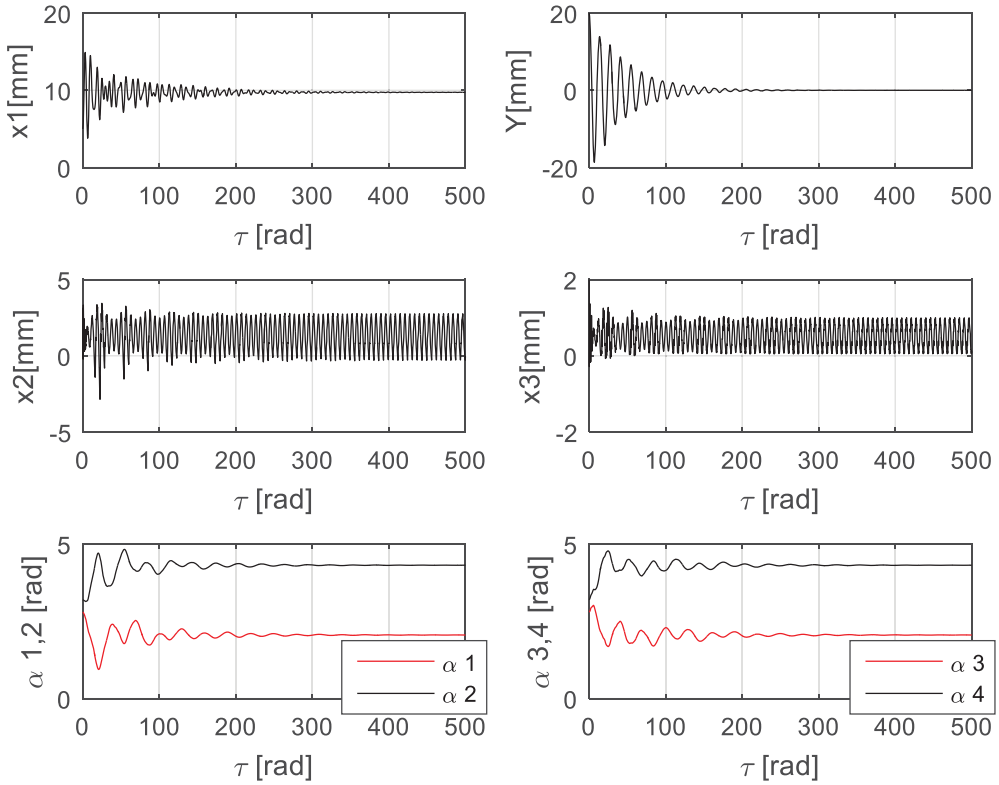

Figure 90. Rotary hammer vibrations with chuck spring and 4-ball DEV

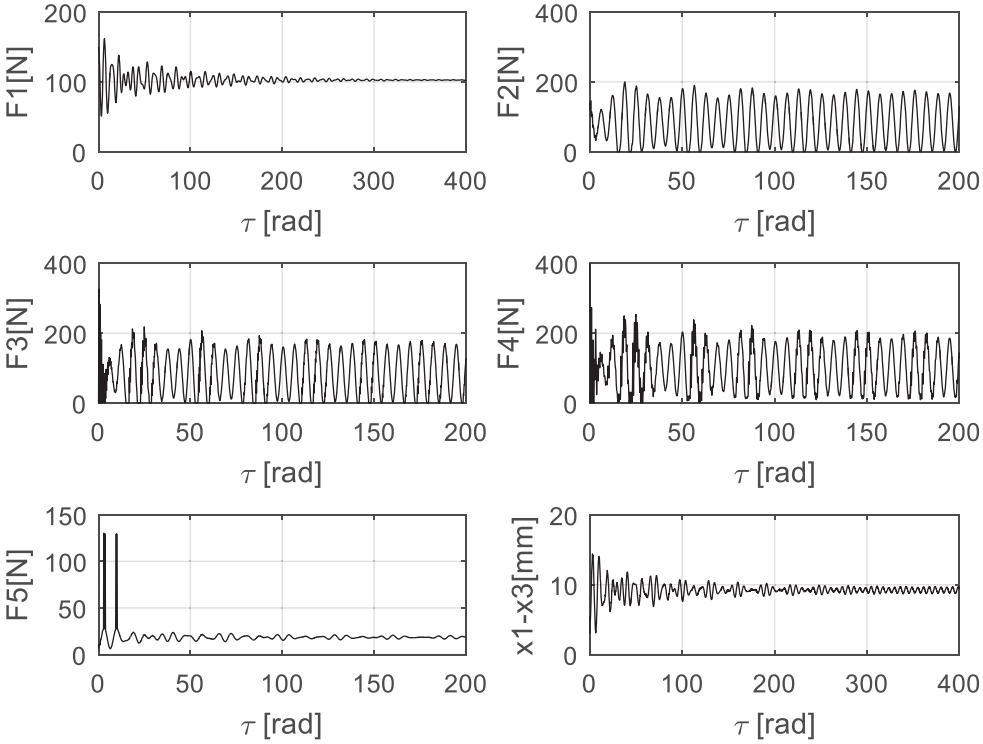

Figure 91. Forces produced by rotary hammer with chuck spring and 4-ball Dev

Vibrations are reduced from 5.5 mm of initial amplitude to 0.02 mm of amplitude in 4.5 seconds. The spheres find symmetric positions between the two drums that are shown in Table 11. The viscous damping coefficient needed is a bit higher than with the previous conditions, c_R = 5 rad/s.

Final position of free elements			
Left drum		Right drum	
α_3	2.0564 rad 117.83°	α_1	2.0562 rad 117.82°
α_4	4.3172 rad 247.37°	α_2	4.3171 rad 247.37°

Table 11. Final position of the spheres (model with chuck spring)

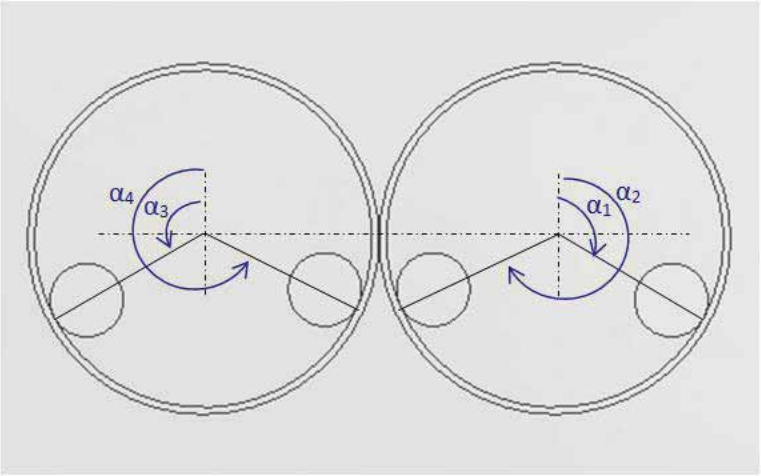

Figure 92. Equilibrium position for model with chuck spring

Again, if the angular velocity of the drums is increased to ω=365 rad/s, the spheres mass needed for damping the vibrations produced by the excitation can be strongly reduced. If the radius of the drums is left constant (R=0.05 m), the mass of the spheres can be reduced to 0.02 kg (20 grams). Moreover, it easier for the spheres to find the equilibrium position as it is seen on Figure 93 ($t = \tau/\omega = 600/365 \ = 1.65\ s$). On Figure 94 the behaviour of the chisel chuck spring can be appreciated in the plots for F_5 and (x_1 - x_3). An increase in the angular velocity of the piston results in an increase of the impact forces.

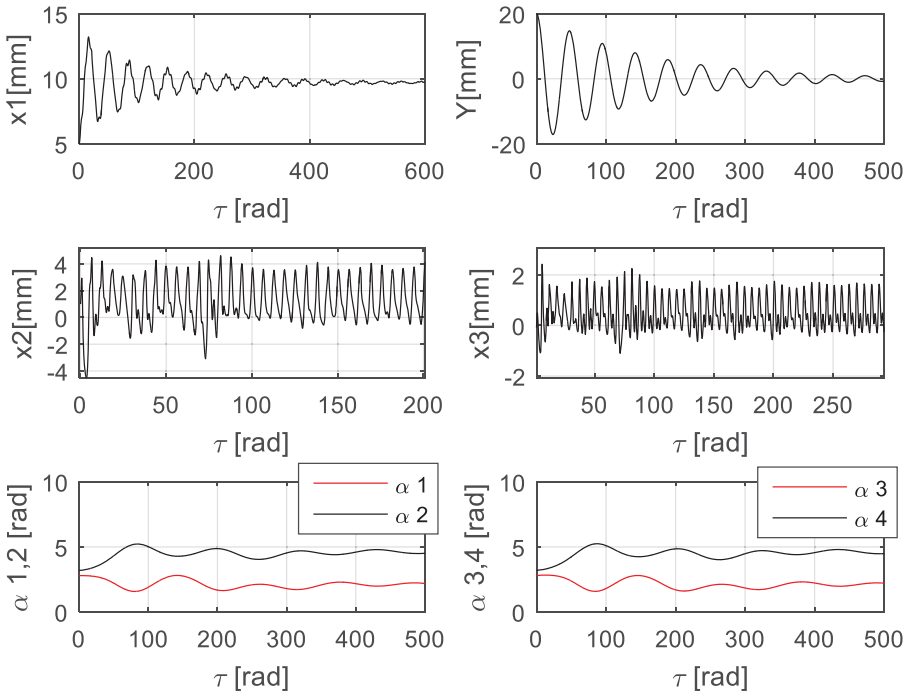

Figure 93. Vibrations of rotary hammer with DEV (ω=365 rad/s)

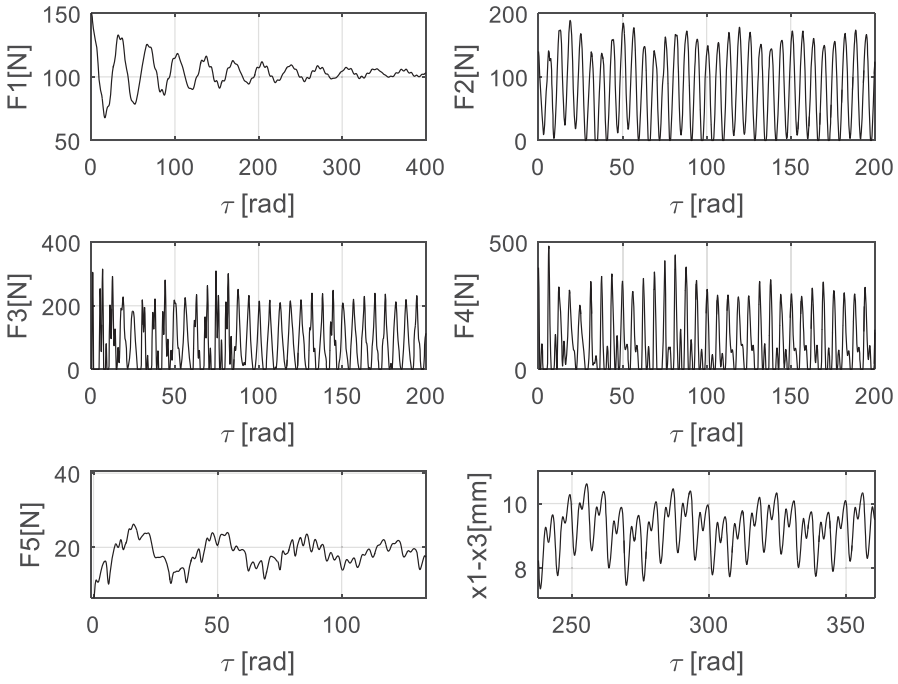

Figure 94. Rotary hammer forces with DEV (ω=365 rad/s)

This more complex model begins to challenge the possibility of damping vibrations produced by the rotary hammer as it approaches the reality; however, the results obtained show proper vibrations absorption.

CHAPTER VII - Conclusions

7.1 Conclusions

Vibrations are undesirable for most of mechanical systems and for the human body due to the adverse effects they could provoke. Particularly, the long term use of impact tools could lead to suffer disorders like the White Finger syndrome and the Dupuytren contracture. Therefore, new ideas and technologies have been designed with the objective of damping vibrations.

In this work, a rotary hammer working principle was mathematically modelled starting from a simple approach and then developing a more complex dynamic system based on Lagrange equations. This model shows amplitudes in the same order of magnitude compared to the values obtained in the experiments performed on asphalt and concrete.

Then, the Dynamic Eliminator of Vibrations model proposed was implemented to the rotary hammer and simulations were run. Even though detailed analysis was performed for a system with 2 spheres per drum, it is possible to have more free elements.

Simulation results show that vibrations produced by a rotary hammer can be damped for different parameters and conditions (ω tested from 80 rad/s to 365 rad/s) due to the presence of the inertial force. This is only possible, with the proper update on sphere mass and radius of the drums. It is important to mention that at higher angular velocities of the drums; less mass is needed for system balance due to the increase in centrifugal force, which allows space and mass optimization processes. Also, the increase in angular velocity also shortens the response time of the free elements to find their equilibrium position.

The coefficient of viscous damping of the free elements also plays an important role in the balancing process, because with the increase in this coefficient it is easier for the free elements to stay in place, due to the produced forces.

The size of the device, according to the radius of the drums and the free elements, is suitable for different applications depending on the excitation frequency of the system.

The Dynamic Eliminator of Vibrations was found to work properly only with excitation frequencies that are above the natural frequency of the system. This vibration absorber can be applied for the first harmonic of the system, which represents the mode of vibration with the highest amplitude. However if two frequencies are to be damped, 2 sets of drums need to be added to the system, each one rotating at one of the frequencies.

In general, this work served as application of all the knowledge acquired in the dynamics and vibrations courses, along with programming abilities in Matlab. The proposed objectives were accomplished leaving new ideas for future work.

7.2 Future work

Further development can be done in this project to validate the obtained results mathematically with different methods, such as computer simulation of the modes of vibration and the behaviour of the free elements. Moreover, Ideal Gas Law can be included to the system's modelling for describing the interaction between piston and striker.

Also, some other Matlab codes should be developed to investigate if a difference in excitation frequency and rotational speed of the drum is allowed and until which ratio of frequencies vibrations can still be damped.

Prototypes should be built and tested to analyze the behaviour of the system in real life. The results of the tests should be compared with those obtained in Matlab and the simulations.

APPENDICES

Appendix A - Matlab Codes

a) DEV with 2 free elements

```
clear; close all; clc;
global  n m M w R r c c1 k z0 T x meq B

n = 3; %number of DOF
w=100; % [rad/s]
m=0.054; M=4; % [kg]
R=0.05; r=0.012;% [m]
c=20; %[kg/s]
c1=4; %[kg/s]
k=5000; %[N/m]
z0=0.01; %[m]
%
B=(2/5)*m*(r^2);
meq=(R^2)*(m+B/(r^2));
%
tspan=0:0.002:400;
x0=[0; 0; 1; 0; 1; 0]; % Initial conditions
[T,x]=ode45('solvesystem_2el',tspan,x0);
%Plotting
subplot(2,2,1);
plot(T,x(:,1)*1000,'k')
xlabel('T[rad]')
ylabel('x[mm]')
grid on
subplot (2,2,2)
plot(T,x(:,2)*1000,'k')
xlabel('T[rad]')
ylabel('v[mm/rad]')
grid on
subplot (2,2,3)
plot(T,x(:,3),'k')
hold on;
plot(T,x(:,5),'r')
xlabel('T[rad]')
ylabel('\alpha 1,2 [rad]')
legend('\alpha 1','\alpha 2')
grid on
subplot (2,2,4)
plot(T,x(:,4),'k')
hold on
plot(T,x(:,6),'r')
xlabel('T[rad]')
ylabel('$\dot{\alpha}$ 1,2 [rad/rad]', 'Interpreter','latex')
legend('\alpha 1','\alpha 2')
grid on
-----------------------------------------------
```

```
function D=solvesystem_2el(T,x)

global m w R c1 z0 n M k c meq

D=zeros(n*2,1);

D(1) = x(2);
D(2) =
(1/(M+2*m))*((m*R)*(((1+x(4))^2)*cos(T+x(3))+((1+x(6))^2)*cos(T+x(5)))
-(c*(z0*w*sin(T)+w*x(2))/(w^2))-(k*x(1)/(w^2))+(k*z0*cos(T)/(w^2)));
D(3) = x(4);
D(4) = (m*R/meq)*((sin(T+x(3))*D(2))-((c1*R*x(4))/w));
D(5) = x(6);
D(6) = (m*R/meq)*((sin(T+x(5))*D(2))-((c1*R*x(6))/w));

end
```

b) DEV with 4 free elements

```
clear; close all; clc;

global  n m M w R r c c1 k z0 T x meq B

n = 5; %number of DOF
w=100; % [rad/s]
m=0.03; M=4; % [kg]
R=0.05; r=0.003; %[m]
c=20; %[kg/s]
c1=4; %[rad/s]
k=5000; %[N/m]
z0=0.01; %[m]
%
B=(2/5)*m*(r^2);
meq=(R^2)*(m+B/(r^2));
%
tspan=0:0.002:400;
x0=[0; 0; 1; 0; 2; 0; 1; 0; 2; 0]; % Initial conditions
[T,x]=ode45('solvesystem_4el',tspan,x0);
%Plotting
subplot(2,2,1);
plot(T,x(:,1)*1000,'b')
xlabel('T[rad]')
ylabel('x[mm]')
grid on
%
subplot (2,2,2)
plot(T,x(:,2)*1000,'b')
xlabel('T[rad]')
ylabel('v[mm/rad]')
grid on
%
subplot (2,2,3)
plot(T,x(:,3),'b')
hold on
plot(T,x(:,5),'r')
xlabel('T[rad]')
ylabel('\alpha 1,2 [rad]')
legend('\alpha 1','\alpha 2')
grid on
%
subplot (2,2,4)
plot(T,x(:,7),'b')
hold on
plot(T,x(:,9),'r')
xlabel('T[rad]')
ylabel('\alpha 3,4 [rad]')
legend('\alpha 3','\alpha 4')
grid on
-------------------------------------------------
```

```
function D=solvesystem_4el(T,x)

global m w R c1 z0 n M k c meq

D=zeros(n*2,1);

D(1) = x(2);
D(2) =
(1/(M+4*m))*((m*R)*(((1+x(4))^2)*cos(T+x(3))+((1+x(6))^2)*cos(T+x(5))+
((1+x(8))^2)*cos(T+x(7))+((1+x(10))^3)*cos(T+x(9)))-
(c*(z0*w*sin(T)+w*x(2))/(w^2))-(k*x(1)/(w^2))+(k*z0*cos(T)/(w^2)));
D(3) = x(4);
D(4) = (m*R/meq)*((sin(T+x(3))*D(2))-((c1*R*x(4))/w));
D(5) = x(6);
D(6) = (m*R/meq)*((sin(T+x(5))*D(2))-((c1*R*x(6))/w));
D(7) = x(8);
D(8) = (m*R/meq)*((sin(T+x(7))*D(2))-((c1*R*x(8))/w));
D(9) = x(10);
D(10) = (m*R/meq)*((sin(T+x(9))*D(2))-((c1*R*x(10))/w));
end
```

c) Inertial force

```
clear; clc; close all;
%
%Parameters
m=4.175; %[kg]
c1=10; c2=5; %[kg/s]
w=100; %[rad/s]
k1=10000; k2=10000; %[N/m]
%
%Inertial force and phase angle equations
phi=pi+atan(((c1+c2)*w)/(k1+k2-m*(w^2)))
i=1;
for alpha = -pi:0.001:3*pi/2
    F1(i,1)=-0.5*(sin(alpha+phi)+sin(phi));
    i=i+1;
end
%
alpha = -pi:0.001:3*pi/2;
plot(alpha,F1,'b')
hold on
ax = gca;
ax.XAxisLocation = 'origin';
ax.YAxisLocation = 'origin';
box off
%title ('Inertial Force Behaviour')
xlabel ('\alpha [rad]')
ylabel ('F [-]') % F=F1/amw^2
grid on
%
```

d) Kinetics description of the rotary hammer internal components

```
clear; close all; clc;
clear; close all; clc;
x0=5; % [mm] striker initial position
v0=0; % [mm/s] striker initial velocity
e=85; % [mm] striker max displacement
a=10; % [mm] piston amplitude
k1=0.7; % [-] restitution coef piston-striker
k2=0.8; % [-] restitution coef striker-chisel
w=100; %[rad/s] angular velocity of piston
tf=3; % [s] simulation time
m=0.075; % [kg] mass of the striker
dt1=0.003; % [s] duration of piston-striker collision
dt2=0.002; % [s] duration of striker-chisel collision
%% Piston displacement functions
z=@(t) a*sin(w*t);
vz=@(t) a*w*cos(w*t);
%% Functions of 1st collision with striker
t1=(1/w)*asin(x0/a); %time for 1st impact (piston-striker)
x1=x0;
v1=vz(t1)*(1+k1)-v0*k1; %speed of striker after impact
%% Functions of collision with chisel
tC=@(t1,x1,vCm) t1+(e-x1)/vCm; %time for striker-chisel col.
xC=e;
vCp=@(vCm) -k2*vCm; %striker speed after col
%% Functions of 2nd collision with piston (return of striker)
cond=@(t2,v2) t2+(0.8*(e-a)/(abs(v2))); %ecc.init.cond.
vMp=@(vz,vMm) vz*(1+k1)-vMm; %striker speed after col.
%xMp=@(t) vz(t);
numCol=1;
T=zeros(2*numCol+1,1);
X=zeros(2*numCol+1,1);
V=zeros(2*numCol+1,1);
F=zeros(2*numCol+1,1);
i=1;
T(1:3)=[0;t1;t1];
X(1:3)=[x0;x1;x1];
V(1:3)=[v0;v0;v1];
i=2;j=2;
t3=0;
while t3<tf
    t2=tC(T(i+1),X(i+1),V(i+1));   %t2 for impact with chisel
    v2=vCp(V(i+1));              %v2 after collision w/chisel
    T(i+2:i+3)=t2*[1;1];          %Assigns t2, bef&aft impact
    X(i+2:i+3)=xC*[1;1];     %Assigns pos. of impact w/chisel
    V(i+2:i+3)=[V(i+1);v2];   %Assigns striker speed b&a imp w/chisel
    F(j)=m*(V(i+1)-V(i))/(dt1*1000);
    F(j+1,1)=m*(V(i+1)-V(i+3))/(dt2*1000);
    fun=@(t3) a*sin(w*t3)-(v2*(t3-t2))-e; %t3 for 2nd impact striker-
piston
    t3=fsolve(fun,cond(t2,v2));
    T(i+4:i+5)=t3*[1;1];            %Assigns t3
```

```
    X(i+4:i+5)=z(t3)*[1;1];          %Piston position for 2nd impact
w/striker
    V(i+4:i+5)=[V(i+3);vMp(vz(t3),V(i+3))]; %Assigns speed bef&aft
col. with piston

    %Special case: double collision piston-striker
    tcruce=(pi/w)*round(t3*w/pi);
    tlim=2*tcruce+pi/w-t3;
    fun1=@(t4) a*sin(w*t4)-(V(i+5)*(t4-t3))-X(i+5);
    t4=fsolve(fun1,tlim);
    if t4 > (t3+1e-8)
        T(i+6:i+7)=t4*[1;1];
        X(i+6:i+7)=z(t4)*[1;1];
        V(i+6:i+7)=[V(i+5);vMp(vz(t4),V(i+5))];
        F(j+2)=-m*(V(i+6)-V(i+7))/(dt1*1000);
        i=i+6;
        j=j+3;
        numCol=numCol+3;
    else
        i=i+4;
        j=j+2;
        numCol=numCol+2;
    end
end
subplot (3,1,1)
plot(T,X,'k');
xlabel 't [s]'
ylabel 'X [mm]'
title('Striker Impacts')
hold on
%
Z=[]; j=1;
tv = [0:0.01:t3];
for ti=[0:0.01:t3]
    Z(j,1)=a*sin(w*ti);
    j=j+1;
end
plot (tv,Z,'r');
grid on
hold on
xlim([0 3])
%
subplot (3,1,2)
plot(T,V,'k')
xlabel 't [s]'
ylabel 'V [mm/s]'
xlim([0 3])
grid on
%
Time=zeros(numCol,1); h=1;
while h<=numCol
    Time(h)=T(2*h-1);
    h=h+1;
end
```

```
subplot(3,1,3)
scatter (Time,F,'filled','k')
xlabel 't [s]'
ylabel 'F [N]'
xlim([0 3])
grid on
```

e) Dynamic model of rotary hammer behaviour

```
clear; clc; close all;

global m1 m2 m3 k1 k2 k3 k4 z0 w n c1 c2 c3 c4 e0

n=3; %DOF
m1=4.175; m2=0.075; m3=0.25; %[kg]
k1=10000; k2=10000; k3=100000; k4=200000; %[N/m]
z0=0.01; %[m]
w=100; %[rad/s]
c1=20; c2=5; c3=5; c4=2; %[kg/s]
e0=0.02; %[m]

tspan=0:0.001:3;
x0=[0; 0; 0.004; 0; 0; 0];

[t,x]=ode45('HammerCompSolver',tspan,x0);
F=Forces(t,x);

%Plotting
% Displacement x1
subplot (3,2,1)
plot(t,x(:,1)*1000,'k')
xlabel('t[s]')
ylabel('x1[mm]')
xlim([0 3])
ylim([-10 30])
grid on
% Displacement x2
subplot (3,2,2)
plot(t,x(:,3)*1000,'k')
xlabel('t[s]')
ylabel('x2[mm]')
xlim([0 3])
ylim([-10 10])
grid on
% Displacement x3
subplot (3,2,3)
plot(t,x(:,5)*1000,'k')
xlabel('t[s]')
ylabel('x3[mm]')
xlim([0 3])
ylim([-6 4])
grid on
%Force F2
subplot (3,2,4)
plot(t,F(:,2),'k')
xlabel('t[s]')
ylabel('F2[N]')
xlim([0 3])
ylim([0 300])
grid on
%Force F3
```

```
subplot (3,2,5)
plot(t,F(:,3),'k')
xlabel('t[s]')
ylabel('F3[N]')
xlim([0 3])
ylim([0 450])
grid on
%Force F4
subplot (3,2,6)
plot(t,F(:,4),'k')
xlabel('t[s]')
ylabel('F4[N]')
xlim([0 3])
ylim([0 500])
grid on

-------------------------------------------------

function D=HammerCompSolver(t,x)

global m1 m2 m3 k1 k2 k3 k4 z0 w n c1 c2 c3 c4 e0
% x(1) = x1      x(2) = x1'
% x(3) = x2      x(4) = x2'
% x(5) = x3      x(6) = x3'
D = zeros(n*2,1);
z = z0*cos(w*t);
zprim =  -z0*w*sin(w*t);
%
F1=k1*(e0-x(1));
S1=c1*x(2);
S2=c2*(x(2)+zprim-x(4));
S3=c3*(x(4)-x(6));
S4=c4*x(6);
%
F20=k2*(x(1)+z-x(3));
if F20>0
    F2=F20;
else
    F2=0;
end
%
F30=k3*(x(3)-x(5));
S3=c3*(x(4)-x(6));
if F30>0
    F3=F30;
else
    F3=0;
end
%
F40=k4*x(5);
if F40>0
    F4=F40;
else
    F4=0;
```

```
end
%
D(1) = x(2);
D(2) = (1/m1)*(F1-S1-F2-S2);
D(3) = x(4);
D(4) = (1/m2)*(F2+S2-F3-S3);
D(5) = x(6);
D(6) = (1/m3)*(F3+S3-F4-S4);

end

------------------------------------------------

function F=Forces(t,x)

global k1 k2 k3 k4 z0 w e0
% x(:,1) = x1      x(:,2) = x1'
% x(:,3) = x2      x(:,4) = x2'
% x(:,5) = x3      x(:,6) = x3'
z = z0*sin(w*t);
%
F10=k1*(e0-x(:,1));
F10=F10.*(F10>0);
F20=k2*(x(:,1)+z-x(:,3));
F20=F20.*(F20>0);
F30=k3*(x(:,3)-x(:,5));
F30=F30.*(F30>0);
F40=k4*x(:,5);
F40=F40.*(F40>0);
F(:,1)=F10;
F(:,2)=F20;
F(:,3)=F30;
F(:,4)=F40;

End
```

f) Implementation of DEV to rotary hammer - unidirectional analysis

```
clear; close all; clc;

global  n w z0 mb m1 m2 m3 R r c1 c2 c3 c4 cR k1 k2 k3 k4 meq B T x e0
%Faltan términos de a''

n=7; %number of independent DOF
w=100; % [rad/s]
z0=0.01; %[m] Piston amplitude
e0=0.02; %[m]
mb=0.05; m1=4.175; m2=0.075; m3=0.25; % [kg]
R=0.05; r=0.0115; %[m]
c1=20; c2=5; c3=5; c4=2; %[kg/s]
cR=2; %[1/s]
k1=10000; k2=10000; k3=100000; k4=200000; %[N/m]
%
B=(2/5)*mb*(r^2);
meq=(R^2)*(mb+B/(r^2));
%
tspan=0:0.025:700;
x0=[0.005; 0; 2.8; 0; 3.2; 0; 2.8; 0; 3.2; 0; 0.004; 0; 0; 0]; % Initial
conditions
Zeta=z0*cos(tspan);
%
[T,x]=ode45('SolveSyst_X',tspan,x0);
F=Forces_X(T,x);
%
%Plotting
figure(1)
subplot(3,2,1);
plot(T,x(:,1)*1000,'k')
xlabel('T[rad]')
ylabel('x1[mm]')
xlim ([0 700])
grid on
%
subplot(3,2,2);
plot(T,x(:,11)*1000,'k')
xlabel('T[rad]')
ylabel('x2[mm]')
xlim ([0 700])
ylim ([-5 10])
grid on
%
subplot(3,2,3);
plot(T,x(:,13)*1000,'k')
xlabel('T[rad]')
ylabel('x3[mm]')
xlim ([0 700])
grid on
%
subplot (3,2,5)
plot(T,x(:,3),'r')
hold on
plot(T,x(:,5),'k')
```

```
xlabel('T[rad]')
ylabel('\alpha 1,2 [rad]')
legend('\alpha 1','\alpha 2')
xlim ([0 700])
grid on
%
subplot (3,2,6)
plot(T,x(:,7),'r')
hold on
plot(T,x(:,9),'k')
xlabel('T[rad]')
ylabel('\alpha 3,4 [rad]')
legend('\alpha 3','\alpha 4')
xlim ([0 700])
grid on
%
figure(2)
subplot (2,2,1)
plot(T,F(:,1),'k')
xlabel('T[rad]')
ylabel('F1[N]')
xlim ([0 700])
grid on
%
subplot (2,2,2)
plot(T,F(:,2),'k')
xlabel('T[rad]')
ylabel('F2[N]')
xlim ([0 700])
grid on
%
subplot (2,2,3)
plot(T,F(:,3),'k')
xlabel('T[rad]')
ylabel('F3[N]')
xlim ([0 700])
grid on
%
subplot (2,2,4)
plot(T,F(:,4),'k')
xlabel('T[rad]')
ylabel('F4[N]')
xlim ([0 700])
grid on
hold on
%
-------------------------------------------------

function D=SolveSyst_X(T,x)

global w R z0 n mb m1 m2 m3 c1 c2 c3 c4 cR meq k1 k2 k3 k4 e0
% x(1) = x1      x(2) = x1'              % x(9) = a4       x(10) = a4'
% x(3) = a1      x(4) = a1'              % x(11) = x2      x(12) = x2'
% x(5) = a2      x(6) = a2'              % x(13) = x3      x(14) = x3'
% x(7) = a3      x(8) = a3'
%
D=zeros(n*2,1);
```

```
%
z = z0*cos(T);
zprim = -z0*sin(T);
F1=k1*(e0-x(1));
S1=c1*x(2);
S2=c2*(x(2)+zprim-x(12));
S3=c3*(x(12)-x(14));
S4=c4*x(14);
%
F20=k2*(x(1)+z-x(11));
if F20>0
    F2=F20;
else
    F2=0;
end
F30=k3*(x(11)-x(13));
if F30>0
    F3=F30;
else
    F3=0;
end
F40=k4*x(13);
if F40>0
    F4=F40;
else
    F4=0;
end
%
D(1) = x(2);
D(2) = (1/(m1+4*mb))*((-mb*R*(((1+x(4))^2)*cos(T+x(3))+((1+x(6))^2)*
cos(T+x(5))+((1+x(8))^2)*cos(T+x(7))+((1+x(10))^3)*cos(T+x(9))))+(F1-
(S1*w)-F2-(S2*w))/(w^2));
D(3) = x(4);
D(4) = (mb*R/meq)*((-sin(T+x(3))*D(2))-((cR*R*x(4))/w));
D(5) = x(6);
D(6) = (mb*R/meq)*((-sin(T+x(5))*D(2))-((cR*R*x(6))/w));
D(7) = x(8);
D(8) = (mb*R/meq)*((-sin(T+x(7))*D(2))-((cR*R*x(8))/w));
D(9) = x(10);
D(10) = (mb*R/meq)*((-sin(T+x(9))*D(2))-((cR*R*x(10))/w));
D(11) = x(12);
D(12) = (1/(m2*(w^2)))*(F2+(S2*w)-F3-(S3*w));
D(13) = x(14);
D(14) = (1/(m3*(w^2)))*(F3+(S3*w)-F4-(S4*w));
end
-------------------------------------------------

function F=Forces_X(T,x)

global k1 k2 k3 k4 z0 e0
% x(:,1) = x1      x(:,2) = x1'
% x(:,11) = x2     x(:,12) = x2'
% x(:,13) = x3     x(:,14) = x3'
z = z0*cos(T);
%
F10=k1*(e0-x(:,1));
F10=F10.*(F10>0);
```

```
F20=k2*(x(:,1)+z-x(:,11));
F20=F20.*(F20>0);
F30=k3*(x(:,11)-x(:,13));
F30=F30.*(F30>0);
F40=k4*x(:,13);
F40=F40.*(F40>0);
F(:,1)=F10;
F(:,2)=F20;
F(:,3)=F30;
F(:,4)=F40;
end
```

g) Implementation of DEV to rotary hammer - bidirectional analysis

```
clear; close all; clc;

global  n w z0 mb m1 m2 m3 R r c1 c2 c3 c4 cy cR k1 k2 k3 k4 ky meq B T x
e0
n=8; %number of independent DOF
w=100; % [rad/s]
z0=0.01; %[m] Piston amplitude
e0=0.02; %[m]
mb=0.07; m1=4.175; m2=0.075; m3=0.25; % [kg]
R=0.05; r=0.0115; %[m]
c1=20; c2=5; c3=5; c4=5; cy=20; %[kg/s]
cR=2; %[1/s]
k1=10000; k2=10000; k3=100000; k4=200000; ky=10000; %[N/m]
%
B=(2/5)*mb*(r^2);
meq=(R^2)*(mb+B/(r^2));
%
tspan=0:0.005:800;
%Initial conditions
x0=[0.005; 0; 0.02; 0; 2.8; 0; 3.2; 0; 2.8; 0; 3.2; 0; 0.004; 0; 0; 0];
%
[T,x]=ode45('SolveSyst_XY',tspan,x0);
F=Forces_XY(T,x);
%Plotting
figure(1)
subplot(3,2,1);
plot(T,x(:,1)*1000,'k')
xlabel('T[rad]')
ylabel('x1[mm]')
xlim ([0 700])
ylim ([4 16])
grid on
%
subplot(3,2,2);
plot(T,x(:,3)*1000,'k')
xlabel('T[rad]')
ylabel('Y[mm]')
xlim ([0 700])
grid on
%
subplot(3,2,3);
plot(T,x(:,13)*1000,'k')
xlabel('T[rad]')
ylabel('x2[mm]')
xlim ([0 700])
ylim ([-3 5])
grid on
%
subplot(3,2,4);
plot(T,x(:,15)*1000,'k')
xlabel('T[rad]')
ylabel('x3[mm]')
xlim ([0 700])
ylim ([-1 2])
```

```
grid on
%
subplot (3,2,5)
plot(T,x(:,5),'r')
hold on
plot(T,x(:,7),'k')
xlabel('T[rad]')
ylabel('\alpha 1,2 [rad]')
legend('\alpha 1','\alpha 2')
xlim ([0 700])
ylim ([-1 5])
grid on
%
subplot (3,2,6)
plot(T,x(:,9),'r')
hold on
plot(T,x(:,11),'k')
xlabel('T[rad]')
ylabel('\alpha 3,4 [rad]')
legend('\alpha 3','\alpha 4')
xlim ([0 700])
ylim ([-1 5])
grid on
%
figure(2)
subplot (2,2,1)
plot(T,F(:,1),'k')
xlabel('T[rad]')
ylabel('F1[N]')
xlim ([0 700])
ylim ([40 160])
grid on
%
subplot (2,2,2)
plot(T,F(:,2),'k')
xlabel('T[rad]')
ylabel('F2[N]')
xlim ([0 700])
ylim ([0 250])
grid on
%
subplot (2,2,3)
plot(T,F(:,3),'k')
xlabel('T[rad]')
ylabel('F3[N]')
xlim ([0 700])
ylim ([0 400])
grid on
%
subplot (2,2,4)
plot(T,F(:,4),'k')
xlabel('T[rad]')
ylabel('F4[N]')
xlim ([0 700])
grid on
hold on
-------------------------------------------------
```

```
function D=SolveSyst_XY(T,x)

global w R z0 n mb m1 m2 m3 c1 c2 c3 c4 cR cy meq k1 k2 k3 k4 ky e0
% x(1) = x1      x(2) = x1'              % x(9) = a3       x(10) = a3'
% x(3) = y1      x(4) = y1'              % x(11) = a4      x(12) = a4'
% x(5) = a1      x(6) = a1'              % x(13) = x2      x(14) = x2'
% x(7) = a2      x(8) = a2'              % x(15) = x3      x(16) = x3'
%
D=zeros(n*2,1);
%
z = z0*cos(T);
zprim = -z0*sin(T);
%
F1=k1*(e0-x(1));
Fy=ky*x(3);
S1=c1*x(2);
S2=c2*(x(2)+zprim-x(14));
S3=c3*(x(14)-x(16));
S4=c4*x(16);
Sy=cy*x(4);
%
F20=k2*(x(1)+z-x(13));
if F20>0
    F2=F20;
else
    F2=0;
end
F30=k3*(x(13)-x(15));
if F30>0
    F3=F30;
else
    F3=0;
end
F40=k4*x(15);
if F40>0
    F4=F40;
else
    F4=0;
end
%
D(1) = x(2);
D(2) = (1/(m1+4*mb))*((-
mb*R*(((1+x(6))^2)*cos(T+x(5))+((1+x(8))^2)*cos(T+x(7))+((1+x(10))^2)*cos
(T+x(9))+((1+x(12))^3)*cos(T+x(11))))+(F1-(S1*w)-F2-(S2*w))/(w^2));
D(3) = x(4);
D(4) =
(1/(m1+4*mb))*((mb*R*(((1+x(6))^2)*sin(T+x(5))+((1+x(8))^2)*sin(T+x(7))-
((1+x(10))^2)*sin(T+x(9))-((1+x(12))^3)*sin(T+x(11))))-Fy/(w^2)-Sy/w);
D(5) = x(6);
D(6) = (mb*R/meq)*(-D(2)*sin(T+x(5))-D(4)*cos(T+x(5))-(cR*R*x(6)/w));
D(7) = x(8);
D(8) = (mb*R/meq)*(-D(2)*sin(T+x(7))-D(4)*cos(T+x(7))-(cR*R*x(8)/w));
D(9) = x(10);
D(10) = (mb*R/meq)*(-D(2)*sin(T+x(9))+D(4)*cos(T+x(9))-(cR*R*x(10)/w));
D(11) = x(12);
D(12) = (mb*R/meq)*(-D(2)*sin(T+x(11))+D(4)*cos(T+x(11))-(cR*R*x(12)/w));
D(13) = x(14);
```

```
D(14) = (1/(m2*(w^2)))*(F2+(S2*w)-F3-(S3*w));
D(15) = x(16);
D(16) = (1/(m3*(w^2)))*(F3+(S3*w)-F4-(S4*w));
end

------------------------------------------------

function F=Forces_XY(T,x)

global k1 k2 k3 k4 z0 e0
% x(:,1) = x1       x(:,2) = x1'
% x(:,13) = x2      x(:,14) = x2'
% x(:,15) = x3      x(:,16) = x3'
z = z0*cos(T);
%
F10=k1*(e0-x(:,1));
F10=F10.*(F10>0);
F20=k2*(x(:,1)+z-x(:,13));
F20=F20.*(F20>0);
F30=k3*(x(:,13)-x(:,15));
F30=F30.*(F30>0);
F40=k4*x(:,15);
F40=F40.*(F40>0);
F(:,1)=F10;
F(:,2)=F20;
F(:,3)=F30;
F(:,4)=F40;

end
```

h) Dynamic model of rotary hammer with chisel chuck spring

```
clear; clc; close all;

global m1 m2 m3 k1 k2 k3 k4 z0 w n c1 c2 c3 c4 e0 k51 k52

n=3; %DOF
m1=4.175; m2=0.075; m3=0.25; %[kg]
k1=10000; k2=10000; k3=100000; k4=200000; %[N/m]
k51=2000; k52=100; %[N/m]
z0=0.01; %[m]
w=100; %[rad/s]
c1=20; c2=5; c3=5; c4=2; %[kg/s]
e0=0.02; %[m]

tspan=0:0.001:3;
x0=[0; 0; 0.004; 0; 0; 0];

[t,x]=ode45('SolverChuck',tspan,x0);
F=ForcesChuck(t,x);

%Plotting
% Displacement x1
figure(1)
subplot (3,1,1)
plot(t,x(:,1)*1000,'k')
xlabel('t [s]')
ylabel('x1 [mm]')
xlim([0 1.6])
ylim([-10 25])
grid on
% Displacement x2
subplot (3,1,2)
plot(t,x(:,3)*1000,'k')
xlabel('t [s]')
ylabel('x2 [mm]')
xlim([0 1.6])
ylim([-15 15])
grid on
% Displacement x3
subplot (3,1,3)
plot(t,x(:,5)*1000,'k')
xlabel('t [s]')
ylabel('x3 [mm]')
xlim([0 1.6])
ylim([-10 5])
grid on
%
figure(2)
%Force F2
subplot (2,2,1)
plot(t,F(:,2),'k')
xlabel('t [s]')
ylabel('F2 [N]')
xlim([0 1.6])
```

```
grid on
%Force F3
subplot (2,2,2)
plot(t,F(:,3),'k')
xlabel('t [s]')
ylabel('F3 [N]')
xlim([0 1.6])
ylim([0 500])
grid on
%Force F4
subplot (2,2,3)
plot(t,F(:,4),'k')
xlabel('t [s]')
ylabel('F4 [N]')
xlim([0 1.6])
grid on
%
subplot (2,2,4)
plot(t,F(:,5),'k')
xlabel('t [s]')
ylabel('F5 [N]')
xlim ([0 1.6])
ylim ([-10 150])
grid on
hold on

-------------------------------------------------

function D=SolverChuck(t,x)

global m1 m2 m3 k1 k2 k3 k4 z0 w n c1 c2 c3 c4 e0 k51 k52
% x(1) = x1      x(2) = x1'
% x(3) = x2      x(4) = x2'
% x(5) = x3      x(6) = x3'
D = zeros(n*2,1);
z = z0*cos(w*t);
zprim =  -z0*w*sin(w*t);
%
F1=k1*(e0-x(1));
S1=c1*x(2);
S2=c2*(x(2)+zprim-x(4));
S3=c3*(x(4)-x(6));
S4=c4*x(6);
%
F20=k2*(x(1)+z-x(3));
if F20>0
    F2=F20;
else
    F2=0;
end
%
F30=k3*(x(3)-x(5));
S3=c3*(x(4)-x(6));
if F30>0
    F3=F30;
else
```

```
    F3=0;
end
%
F40=k4*x(5);
if F40>0
    F4=F40;
else
    F4=0;
end
%
F50=k51*(x(1)-x(5));
if (x(1)-x(5))>0.014
    F5=k51*(x(1)-x(5))+k52*(exp(x(1)-x(5)));
else
    F5=F50;
end
%
D(1) = x(2);
D(2) = (1/m1)*(F1-S1-F2-S2-F5);
D(3) = x(4);
D(4) = (1/m2)*(F2+S2-F3-S3);
D(5) = x(6);
D(6) = (1/m3)*(F3+S3-F4-S4+F5);

end

------------------------------------------------

function F=ForcesChuck(t,x)

global k1 k2 k3 k4 z0 w e0 k51 k52
% x(:,1) = x1      x(:,2) = x1'
% x(:,3) = x2      x(:,4) = x2'
% x(:,5) = x3      x(:,6) = x3'
z = z0*sin(w*t);
%
F10=k1*(e0-x(:,1));
F10=F10.*(F10>0);
F20=k2*(x(:,1)+z-x(:,3));
F20=F20.*(F20>0);
F30=k3*(x(:,3)-x(:,5));
F30=F30.*(F30>0);
F40=k4*x(:,5);
F40=F40.*(F40>0);
F(:,1)=F10;
F(:,2)=F20;
F(:,3)=F30;
F(:,4)=F40;
%
F51=k51*(x(:,1)-x(:,5));
F52=k52*(exp(x(:,1)-x(:,5)));
F52=F52.*(x(:,1)-(x(:,5))>0.014);
F(:,5)=F51+F52;
end
```

i) Implementation of DEV to the rotary hammer dynamic model with chuck spring

```
clear; close all; clc;

global  n w z0 mb m1 m2 m3 R r c1 c2 c3 c4 cy cR k1 k2 k3 k4 ky meq B T x
e0 k51 k52

n=8; %number of independent DOF
w=100; % [rad/s]
z0=0.01; %[m]
e0=0.02; %[m]
mb=0.1; m1=4.175; m2=0.075; m3=0.25; % [kg]
R=0.05; r=0.0145; %[m]
c1=20; c2=5; c3=5; c4=5; cy=20; %[kg/s]

cR=4; %[1/s]
k1=10000; k2=10000; k3=100000; k4=200000; ky=10000; %[N/m]
k51=2000; k52=100; %[N/m]
%
B=(2/5)*mb*(r^2);
meq=(R^2)*(mb+B/(r^2));
%
tspan=0:0.005:600;
x0=[0.005; 0; 0.02; 0; 2.8; 0; 3.2; 0; 2.8; 0; 3.2; 0; 0.001; 0; 0.002;
0]; % Initial conditions
%
[T,x]=ode45('SolveSyst_chuck',tspan,x0);
F=Forces_chuck(T,x);
%
%Plotting
figure(1)
subplot(3,2,1);
plot(T,x(:,1)*1000,'k')
xlabel('\tau [rad]')
ylabel('x1[mm]')
%xlim ([0 500])
%ylim ([4 16])
grid on
%
subplot(3,2,2);
plot(T,x(:,3)*1000,'k')
xlabel('\tau [rad]')
ylabel('Y[mm]')
xlim ([0 500])
grid on
%
subplot(3,2,3);
plot(T,x(:,13)*1000,'k')
xlabel('\tau [rad]')
ylabel('x2[mm]')
xlim ([0 500])
%ylim ([-3 5])
grid on
%
subplot(3,2,4);
plot(T,x(:,15)*1000,'k')
```

```
xlabel('\tau [rad]')
ylabel('x3[mm]')
xlim ([0 500])
%ylim ([-1 2])
grid on
%
subplot (3,2,5)
plot(T,x(:,5),'r')
hold on
plot(T,x(:,7),'k')
xlabel('\tau [rad]')
ylabel('\alpha 1,2 [rad]')
legend('\alpha 1','\alpha 2')
xlim ([0 500])
%ylim ([-1 5])
grid on
%
subplot (3,2,6)
plot(T,x(:,9),'r')
hold on
plot(T,x(:,11),'k')
xlabel('\tau [rad]')
ylabel('\alpha 3,4 [rad]')
legend('\alpha 3','\alpha 4')
xlim ([0 500])
%ylim ([-1 5])
grid on
%
figure(2)
subplot (3,2,1)
plot(T,F(:,1),'k')
xlabel('\tau [rad]')
ylabel('F1[N]')
xlim ([0 400])
%ylim ([40 160])
grid on
%
subplot (3,2,2)
plot(T,F(:,2),'k')
xlabel('\tau [rad]')
ylabel('F2[N]')
xlim ([0 200])
%ylim ([0 250])
grid on
%
subplot (3,2,3)
plot(T,F(:,3),'k')
xlabel('\tau [rad]')
ylabel('F3[N]')
xlim ([0 200])
%ylim ([0 400])
grid on
%
subplot (3,2,4)
plot(T,F(:,4),'k')
xlabel('\tau [rad]')
ylabel('F4[N]')
```

```
xlim ([0 200])
grid on
hold on
%
subplot (3,2,5)
plot(T,F(:,5),'k')
xlabel('\tau [rad]')
ylabel('F5[N]')
xlim ([0 200])
ylim ([0 150])
grid on
hold on
%
subplot(3,2,6)
plot(T,(x(:,1)-x(:,15))*1000,'k')
xlabel ('\tau [rad]')
ylabel ('x1-x3[mm]')
xlim ([0 400])
grid on
hold on

-------------------------------------------------

function D=SolveSyst_chuck(T,x)

global w R z0 n mb m1 m2 m3 c1 c2 c3 c4 cR cy meq k1 k2 k3 k4 ky e0 k51
k52
% x(1) = x1      x(2) = x1'              % x(9) = a3       x(10) = a3'
% x(3) = y1      x(4) = y1'              % x(11) = a4      x(12) = a4'
% x(5) = a1      x(6) = a1'              % x(13) = x2      x(14) = x2'
% x(7) = a2      x(8) = a2'              % x(15) = x3      x(16) = x3'
%
D=zeros(n*2,1);
%
z = z0*cos(T);
zprim = -z0*sin(T);
%
F1=k1*(e0-x(1));
Fy=ky*x(3);
S1=c1*x(2);
S2=c2*(x(2)+zprim-x(14));
S3=c3*(x(14)-x(16));
S4=c4*x(16);
Sy=cy*x(4);
%
F20=k2*(x(1)+z-x(13));
if F20>0
    F2=F20;
else
    F2=0;
end
F30=k3*(x(13)-x(15));
if F30>0
    F3=F30;
else
    F3=0;
```

```
end
F40=k4*x(15);
if F40>0
    F4=F40;
else
    F4=0;
end
F50=k51*(x(1)-x(15));
if (x(1)-x(15))>0.014
    F5=k51*(x(1)-x(15))+k52*(exp(x(1)-x(15)));
else
    F5=F50;
end
%
D(1) = x(2);
D(2) = (1/(m1+4*mb))*((-
mb*R*(((1+x(6))^2)*cos(T+x(5))+((1+x(8))^2)*cos(T+x(7))+((1+x(10))^2)*cos
(T+x(9))+((1+x(12))^3)*cos(T+x(11))))+(F1-(S1*w)-F2-(S2*w)-F5)/(w^2));
D(3) = x(4);
D(4) =
(1/(m1+4*mb))*((mb*R*(((1+x(6))^2)*sin(T+x(5))+((1+x(8))^2)*sin(T+x(7))-
((1+x(10))^2)*sin(T+x(9))-((1+x(12))^3)*sin(T+x(11))))-Fy/(w^2)-Sy/w);
D(5) = x(6);
D(6) = (mb*R/meq)*(-D(2)*sin(T+x(5))-D(4)*cos(T+x(5))-(cR*R*x(6)/w));
D(7) = x(8);
D(8) = (mb*R/meq)*(-D(2)*sin(T+x(7))-D(4)*cos(T+x(7))-(cR*R*x(8)/w));
D(9) = x(10);
D(10) = (mb*R/meq)*(-D(2)*sin(T+x(9))+D(4)*cos(T+x(9))-(cR*R*x(10)/w));
D(11) = x(12);
D(12) = (mb*R/meq)*(-D(2)*sin(T+x(11))+D(4)*cos(T+x(11))-(cR*R*x(12)/w));
D(13) = x(14);
D(14) = (1/(m2*(w^2)))*(F2+(S2*w)-F3-(S3*w));
D(15) = x(16);
D(16) = (1/(m3*(w^2)))*(F3+(S3*w)-F4-(S4*w)+F5);

end

-------------------------------------------------

function F=Forces_chuck(T,x)

global k1 k2 k3 k4 z0 e0 k51 k52
% x(:,13) = x2      x(:,14) = x2'
% x(:,15) = x3      x(:,16) = x3'
z = z0*cos(T);
%
F10=k1*(e0-x(:,1));
F10=F10.*(F10>0);
F20=k2*(x(:,1)+z-x(:,13));
F20=F20.*(F20>0);
F30=k3*(x(:,13)-x(:,15));
F30=F30.*(F30>0);
F40=k4*x(:,15);
F40=F40.*(F40>0);
%
F(:,1)=F10;
```

```
F(:,2)=F20;
F(:,3)=F30;
F(:,4)=F40;
%
F51=k51*(x(:,1)-x(:,15));
F52=k52*(exp(x(:,1)-x(:,15)));
F52=F52.*(x(:,1)-(x(:,15))>0.014);
F(:,5)=F51+F52;
end
```

- Experiment 5.2: Effect of viscous damping coefficient

Simulation parameters: ω=100 rad/s; z_0=0.01 m; e_0=0.02 m; m_b=0.05 kg; m_1=4.175 kg; m_2=0.075 kg; m_3=0.25 kg; R=0.05 m; r=0.0115 m; c_1=20 kg/s; c_2=5 kg/s; c_3=5 kg/s; c4=2 kg/s; c_R=8 1/s; k_1=10000 N/m; k_2=10000 N/m; k_3=100000 N/m; k_4=200000 N/m.

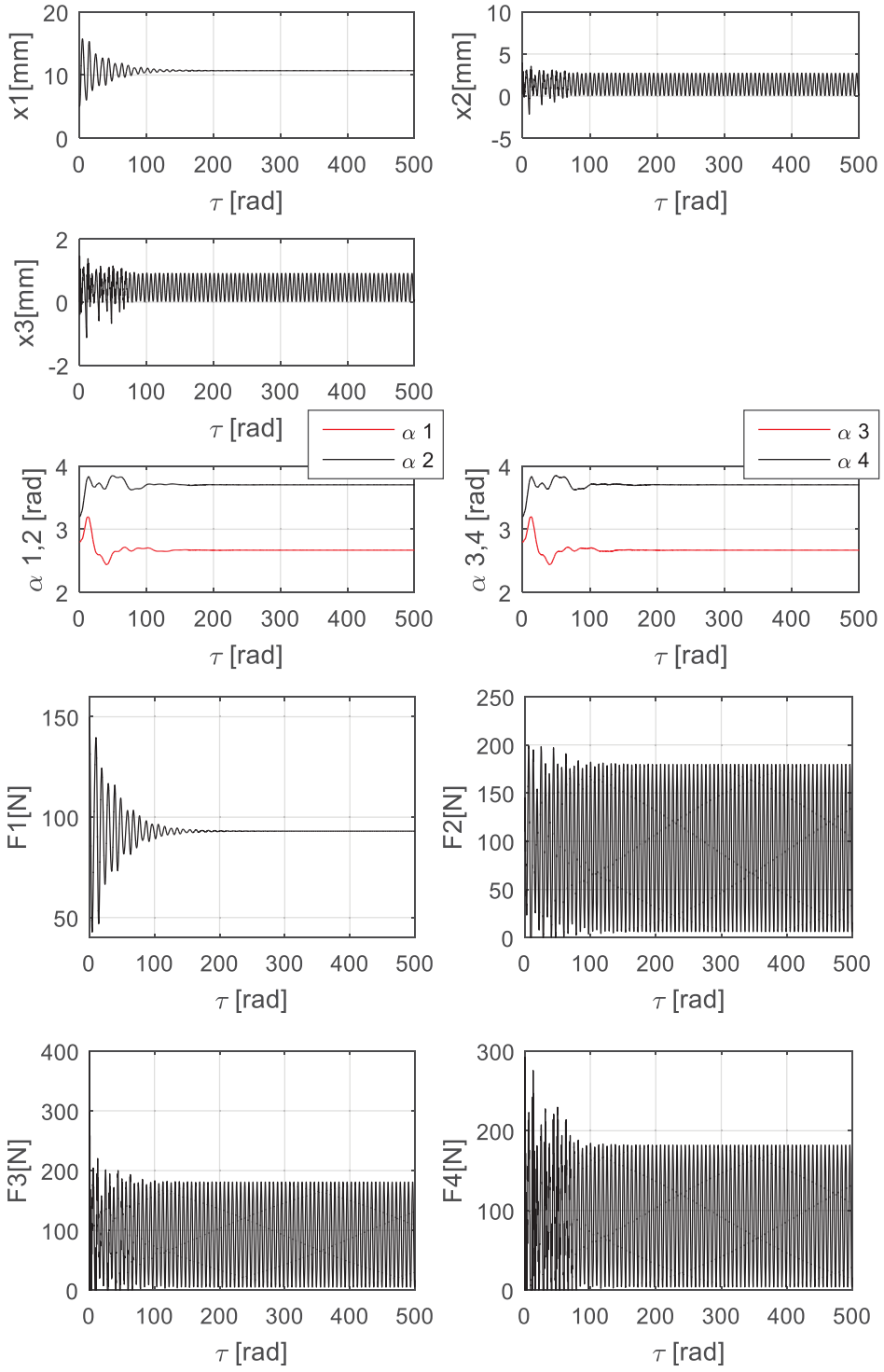

Figure 95. Experiment for cR=8 rad/s

- Experiment 5.3: Effect of viscous damping coefficient

Simulation parameters: ω=100 rad/s; z_0=0.01 m; e_0=0.02 m; m_b=0.05 kg; m_1=4.175 kg; m_2=0.075 kg; m_3=0.25 kg; R=0.05 m; r=0.0115 m; c_1=20 kg/s; c_2=5 kg/s; c_3=5 kg/s; c4=2 kg/s; c_R=0.5 1/s; k_1=10000 N/m; k_2=10000 N/m; k_3=100000 N/m; k_4=200000 N/m.

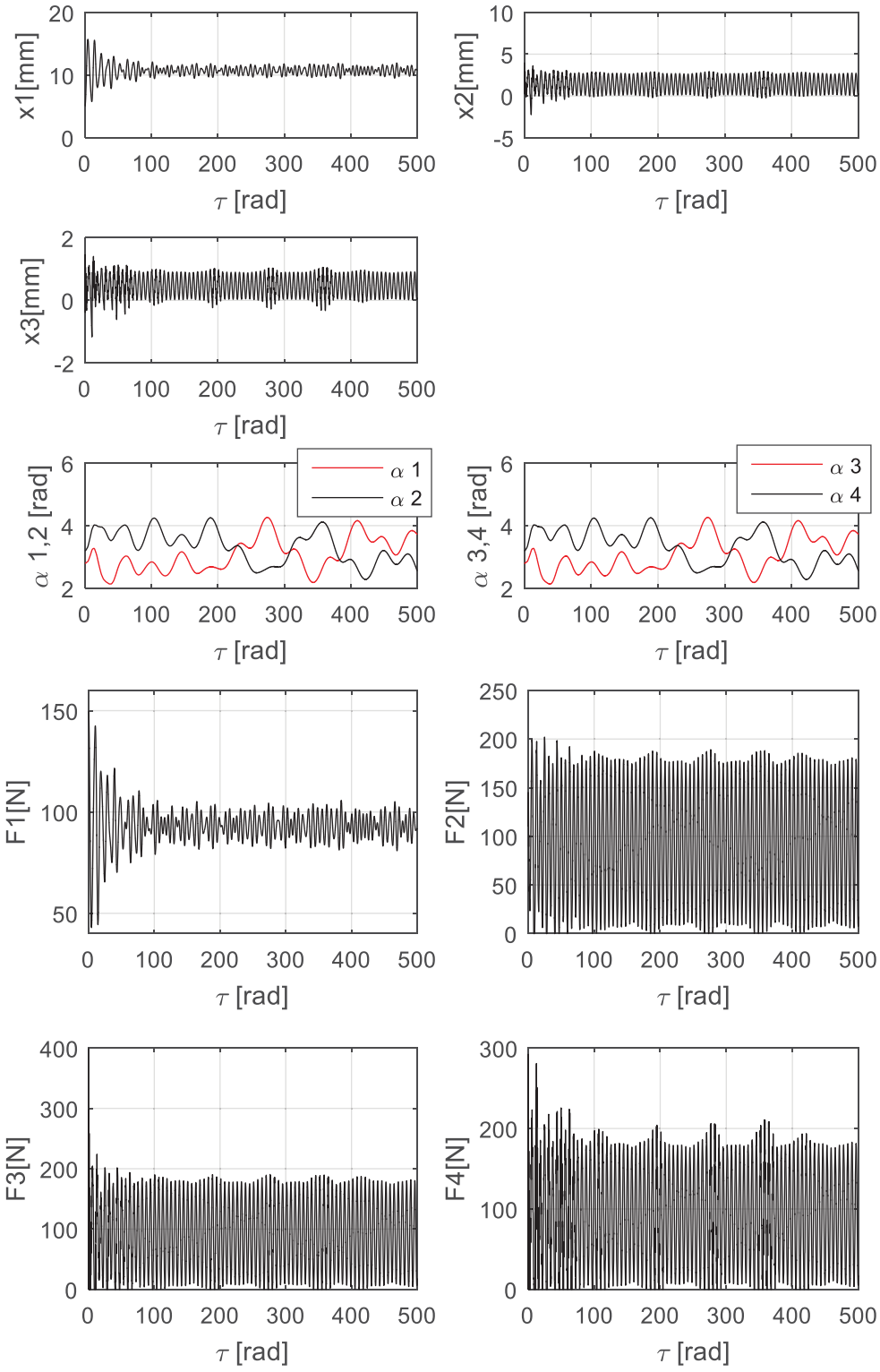

Figure 96. Experiment for cR=0.5 rad/s

Appendix C - Rotary hammer assembly diagram

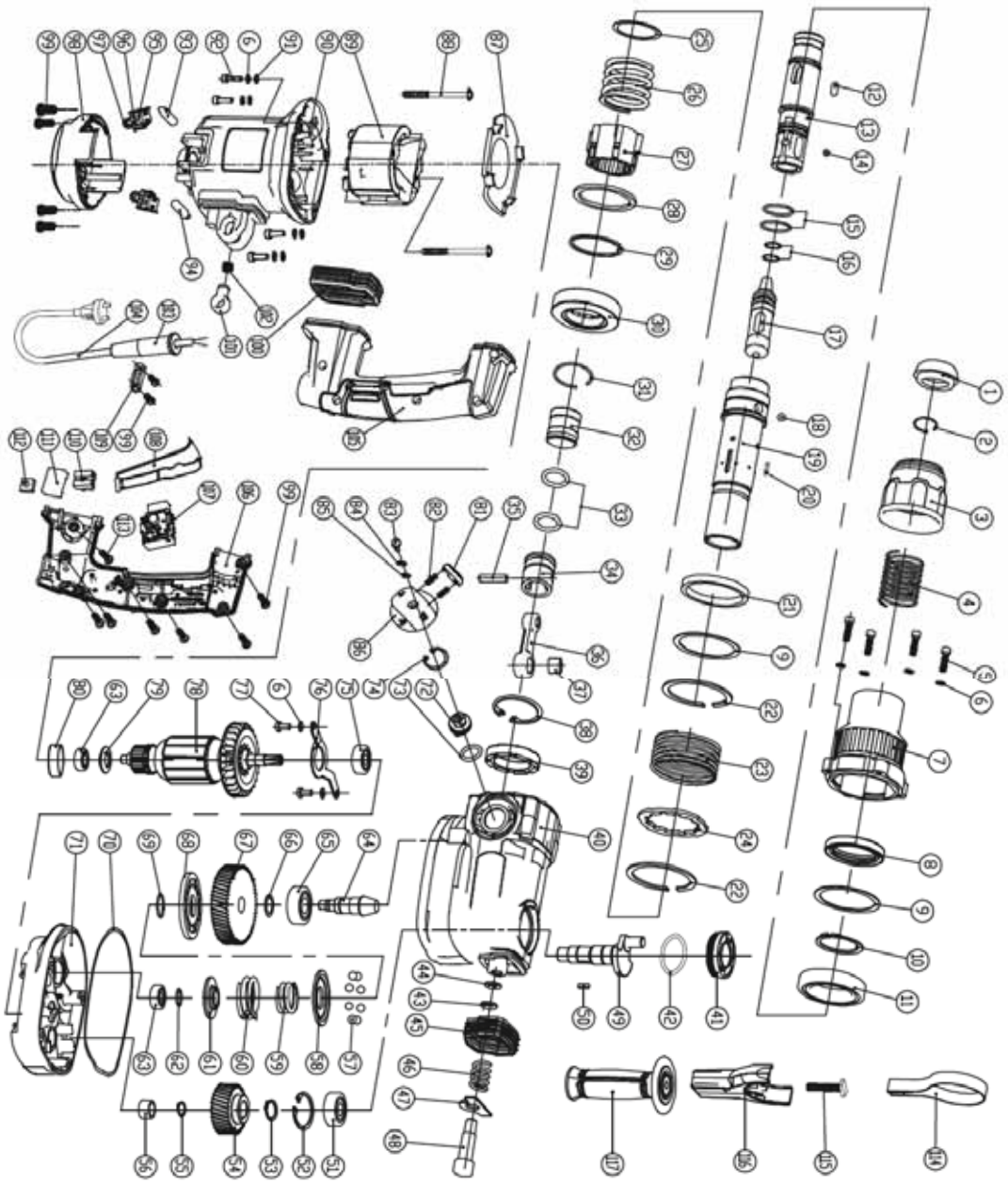

Record Product's Serial Number Here:_____

Note: If product has no serial number, record month and year of purchase instead.

Note: Some parts are listed and shown for illustration purposes only, and are not available individually as replacement parts.

Parts List and Diagram

Parts List

Part	Description	Qty
1	Front Cover	1
2	Clip Ring	1
3	Chuck	1
4	Steel Ball Rack Spring	1
5	Screw	4
6	Spring Washer	10
7	Front Housing	1
8	Oil Seal	1
9	Washer	2
10	Clip Ring	1
11	Bearing	1
12	Pulley	3
13	Rotary Sleeve	1
14	Steel Ball	3
15	O-Ring	2
16	O-Ring	2
17	Impact Hammer	1
18	Steel Ball	3
19	Cylinder	1
20	Flat Key	2
21	Rubber Ring	1
22	Circlip	2
23	Clutch Spring	1
25	Plate	1
26	Spring	1
27	Clutch	1
28	Clutch Washer	1
29	Washer	1
30	O-Ring	1
31	Circlip	1
32	Pneumatic Hammer	1
33	O-Ring	2
34	Piston	1
35	Piston Pin	1
36	Rod	1
37	Needle Bearing	1
38	Circlip	1
39	Bearing	1
40	Gear Box	1
41	Cap	1
42	O-Ring	1
43	Flat Washer	1
44	Spring Washer	1
45	Upper Damper Sleeve	1
46	Damping Spring	1
47	Damping Plate	1
48	Damping Screw	1
49	Eccentric Shaft	1
50	Flat Key	2
51	Bearing	1
52	Circlip	1
53	Circlip	1
54	First Gear	1
55	Circlip	1
56	Needle Bearing	1
57	Steel Ball	8
58	Active Plate	1
59	Inner Spring	1

Part	Description	Qty
60	Outer Spring	1
61	Spring Holder	1
62	Circlip	1
63	Bearing	2
64	Pinion	1
65	Bearing	1
66	Pinion Bearing Plate	1
67	Second Gear	1
68	Fix Block	1
69	Circlip	1
70	Intermediate Cover Plate	1
71	Intermediate Cover	1
72	Handle Knob	1
73	O-Ring	1
74	Circlip	1
75	Bearing	1
76	Bearing Clamp	1
77	Screw	2
78	Armature	1
79	Fan Guide	1
80	Bearing Cover	1
81	Release Button	1
82	Button Spring	2
84	Spring Plate	1
85	Plate	1
86	Mode Selector	1
87	Guide Ring	1
88	Screw	2
89	Stator	1
90	Housing	1
91	Washer	4
92	Screw	4
93	Long Inductance	1
94	Short Inductance	1
95	Carbon Brush Holder	2
96	Carbon Brush	2
97	Spring	2
98	Bottom Cover	1
99	Screw	12
100	Lower Damper Sleeve	1
101	Spring Holder	1
102	Damping Spring	1
103	Cord Protector	1
104	Power Cord	1
105	Left Handle	1
106	Right Handle	1
107	Switch	1
108	Trigger	1
109	Cable Clamp	1
110	Binding Post	2
111	Capacitor	1
112	Light	1
113	Screw	1
114	Band	1
115	T-Screw	1
116	Side Handle Holder	1
117	Auxiliary Handle	1

REFERENCES

Amazon Services LLC Associate Program. (2018). *The Essential List of the Different Types of Power Tools.* Retrieved June 12, 2018 from Amzaon Services: https://toolconsult.com/guides/different-power-tool-types-list#hammer-drill

Bosch. (2018). *Cordless Hammer Drill / Drivers*. Retrieved June 14, 2018, from Bosch Power Tools: https://www.boschtools.com/us/en/boschtools-ocs/hammer-drills-23516-c/

Bosch (2018). Bosch GSH 11 VC Professional Demolition hammer with SDS max. [Video]. Retrieved from https://www.youtube.com/watch?v=aO4PbdRdwqM

Brammer, A; Peterson, D. (2004). *Vibration, Mechanical, Shock, and Impact*. Chapter 10

British Standards Institution. (1987). *Measurement and Evaluation of Human Exposure to Vibration Transmitted to the Hand.* BS 6842. London: BSI.

Broch, J.T. (1972) *The Application of the Bruel & Kjaer Measuring Systems to Mechanical Vibration and Shock Measurements* (1st ed) New York: Nestle Company Inc.

Canadian Center of Ocupational Health and Safety. Government of Canada. (2018) Raynaud's Phenomenon. Accessed on July 02: https://www.ccohs.ca/oshanswers/diseases/raynaud.html

Castro, J., Palacios, M., García, G., & Moreno, L. (2014). *Salud, Ambiente y Trabajo.* México: McGraw Hill. P. 277

Centro de Acústica Aplicada, SL. (2009) *"Estudio del Nivel de Exposición a Vibraciones Mecánicas en Diferentes Puestos de Trabajo"* España: Ministerio de Trabajo e Inmigración de España. Accessed on June 15, 2018: http://www.oect.es/Observatorio/Contenidos/InformesPropios/Desarrollados/Ficheros/Resumen%20Estudio%20Exposición%20Vibraciones%20Mecánicas.pdf

Dahl, T. (2016). Impact Driver. *Popular Mechanics*. Retrieved July 21, 2018 from: https://www.popularmechanics.com/home/tools/how-to/a18931/how-to-use-an-impact-driver-diy-projects/

Dewalt. (2018). *Shocks Active Vibration Control*. Retrieved June 25, 2018, from https://www.dewalt.com/jobsite-solutions/perform-and-protect/vibration

Dewalt (2018). Impact drivers and wrenches. Retrieved June 25, 2018, from https://www.dewalt.com/products/power-tools/impact-drivers-and-wrenches?pageNum=2

Discovery Channel. (2018). Demolitore Kombihammer Bohrhammer Milwaukee Kango 950S 950 S SDS MAX [Video]. Retrieved from https://www.youtube.com/watch?v=Xd9o2D2wmhA

Dupzyk, K. (2016). Jackhammer. *Popular Mechanics*, *193*(1), 20-21.

Griffin, M. (2018). Cool Tools: Rotary Hammers. *Electrical Contractor Magazine*. Retrieved from https://www.ecmag.com/section/your-business/cool-tools-rotary-hammers

Hernández, F. G. (2012). *Tratado de Medicina del trabajo. Introducción a la salud laboral, aspectos jurídicos y técnicos.* Madrid: Ministerio de Trabajo y Asuntos Sociales. Vol I, II.

Ideara. (2014). Vibraciones Mecánicas. Factores relacionados con la fuente y medidas de control. España. Confederación de Empresarios de Pontevedra CEP. Retrieved June 16, 2018 from: https://idearainvestigacion.es/wp-content/uploads/2014/10/GUIA_ vibraciones-mecanicas_final_baixa-calidade.pdf

Inman, D. J. (2001) *Engineering Vibration* (2da ed.) New Jersey: Prentice Hall. P. 359

Majewski, T. (1987). Synchronous Vibration Eliminator for an Object Having One Degree of Freedom. *Journal of Sound and Vibration, 112*(3), 401-413.

Majewski, T. (2017). *Vibraciones en sistemas físicos* (Segunda ed.). México: Alfaomega.

Makita. (2015). *Antivibrations systems AVT* [Video]. Retrieved June 21, 2018, from https://www.youtube.com/watch?v=xmoHtY7yf2c

Makita UK. (2018). *Antivibration technology*. Retrieved June 21, 2018, from http://www.makitauk.com/anti-vibration-technology.html

Rao, S. (2011). *Mechanical Vibrations* (5th ed.). New Jersey: Prentice Hall.

The Essential List of the Different Types of Power Tools. (2018). Retrieved June 09, 2018 from https://toolconsult.com/guides/different-power-tool-types-list#hammer-drill

Thomson, William. (1988) *Theory of Vibration with Applications* (3rd ed.) New Jersey. Prentice Hall. P. 138

Walshaw, A.C. (1984) *Mechanical Vibrations with Applications* (1ra ed) New York: John Wiley and Sons. P. 108

What is a Hammer Drill vs Rotary Hammers. (2018). *Family Handyman*.

Woodford, C. (2017). *Jackhammer / Pneumatic Drill*. Retrieved June 12, 2018, from https://www.explainthatstuff.com/jackhammer.html

Yagid, R. (2009). Hammer Drill-Driver. *Fine Home Building*. Retrieved July 06, 2018 from: https://www.finehomebuilding.com/2009/11/12/hammer-drill-driver#